


8-2013

# Development of HIF-1 $\alpha$ /HIF-1 $\beta$ heterodimerization inhibitors using a novel bioluminescence reporter assay system for in vitro high throughput screening and in vivo imaging

Yun-Chen Chiang

Follow this and additional works at: [http://digitalcommons.library.tmc.edu/utgsbs\\_dissertations](http://digitalcommons.library.tmc.edu/utgsbs_dissertations)

 Part of the [Medical Biotechnology Commons](#), [Medical Molecular Biology Commons](#),  
[Pharmaceutics and Drug Design Commons](#), and the [Therapeutics Commons](#)

---

## Recommended Citation

Chiang, Yun-Chen, "Development of HIF-1 $\alpha$ /HIF-1 $\beta$  heterodimerization inhibitors using a novel bioluminescence reporter assay system for in vitro high throughput screening and in vivo imaging" (2013). *UT GSBS Dissertations and Theses (Open Access)*. Paper 383.

This Dissertation (PhD) is brought to you for free and open access by the Graduate School of Biomedical Sciences at DigitalCommons@The Texas Medical Center. It has been accepted for inclusion in UT GSBS Dissertations and Theses (Open Access) by an authorized administrator of DigitalCommons@The Texas Medical Center. For more information, please contact [laurel.sanders@library.tmc.edu](mailto:laurel.sanders@library.tmc.edu).

**Development of HIF-1 $\alpha$ /HIF-1 $\beta$  heterodimerization inhibitors using a novel  
bioluminescence reporter assay system for *in vitro* high throughput screening  
and *in vivo* imaging**

by

Yun-Chen Chiang, M.S.

APPROVED:

---

Juri Gelovani, M.D., Ph.D., Supervisory Professor

---

Victor Krasnykh, Ph.D.

---

Edward F. Jackson, Ph.D.

---

Chun Li, Ph.D.

---

David J. Yang, Ph.D.

---

APPROVED:

---

Dean, The University of Texas  
Graduate School of Biomedical Sciences at Houston

**Development of HIF-1 $\alpha$ /HIF-1 $\beta$  heterodimerization inhibitors using a novel  
bioluminescence reporter assay system for *in vitro* high throughput screening  
and *in vivo* imaging**

A

DISSERTATION

Presented to the Faculty of  
The University of Texas  
Health Science Center at Houston  
and  
The University of Texas  
MD Anderson Cancer Center  
Graduate School of Biomedical Sciences  
in Partial Fulfillment

of the Requirements

for the Degree of

DOCTOR OF PHILOSOPHY

by

Yun-Chen Chiang, M.S.

Houston, Texas

August, 2013

## **Acknowledgment**

My deepest gratitude goes to my advisor and mentor, Dr. Gelovani. I would like to thank him for his guidance, understanding, patience, and most importantly encouragement during my graduate studies at UT MD Anderson. He put his trust in me and gave me the opportunity to develop my own individuality by being allowed to work with such independence. His mentorship was invaluable in providing a well-rounded experience shaping my long-term career goals. His wisdom, knowledge and commitment to the highest standards will always inspire and motivate me.

I would also like to express my appreciation to Dr. Krasnykh, who took me under his wings during the most uncertain time of my studies. His meticulous comments and constructive criticisms for my education were thought-provoking to me. I am grateful to him for holding me to a high research standard, yet being tolerant and supportive when I made mistakes.

I would like to thank all the members of my supervisory committee. Dr. Yang, has always provided his assistance and guidance in shaping my career path. I am deeply grateful to him for all the recommendations at different aspect of personal and academic life. I would like to express my appreciation to Dr. Li for his support and practical advice. His comments and discussion on my studies helped me understand and enrich my ideas. Dr. Jackson, who is very experienced in guiding graduate students, has always provided warm encouragement and generous help during different stages of my graduate education.

I am also indebted to my lab members whom I have interacted during the course of my graduate studies. Particularly, I would like to acknowledge Dr. Nashaat Turkman, Dr. Brian Rabinovich, Dr. Andrei Volgin, Dr. Amer M Najjar, Dr. Lucia Le Roux, Dr. William Tong and Galina Mikhe for many valuable discussions and contributions to the various domains. I've

learned so much through numerous discussions with Dr. Nashaat Turkman, without whom I can't make this work complete. Special thanks to Dr. Daniel Young who is a caring teacher and created home-like atmosphere for me in laboratory environment.

I would also like to express my gratitude to my friends, who have helped me stay sane through these challenging years and inspired me despite the enormous pressures we were facing together. Their support and care helped me overcome setbacks and stay focused on my graduate study. I greatly value their friendship and I deeply appreciate their belief in me.

Finally, I would like to thank my husband Dr. Yen-Yu Shih. His support, encouragement, quiet patience and unwavering love were undeniably the bedrock of my motivation. His unyielding devotion and love allow me to be as ambitious as I wanted. Without his sacrifice and compromise, this dissertation would not have been possible. I would also like to express my gratitude to Yen-Yu's parents for all your encouragement and profound understanding. Most importantly, I owe my greatest appreciation to Chung-Ming Chaing and Mai-Chiao Ku, my parents, who have always supported, encouraged and believed in me. Their love is the inspiration and backbone for me to fearlessly pursuit my research career.

*This dissertation is dedicated to all my loving family.*

**Development of HIF-1 $\alpha$ /HIF-1 $\beta$  heterodimerization inhibitors using a novel bioluminescence reporter assay system for *in vitro* high throughput screening and *in vivo* imaging**

Publication No. \_\_\_\_\_

Yun-Chen Chiang, M.S., B.S.

Supervisory Professor: Juri Gelovani, M.D., Ph.D.

**Abstract**

Tumor growth often outpaces its vascularization, leading to development of a hypoxic tumor microenvironment. In response, an intracellular hypoxia survival pathway is initiated by heterodimerization of hypoxia-inducible factor (HIF)-1 $\alpha$  and HIF-1 $\beta$ , which subsequently upregulates the expression of several hypoxia-inducible genes, promotes cell survival and stimulates angiogenesis in the oxygen-deprived environment. Hypoxic tumor regions are often associated with resistance to various classes of radio- or chemotherapeutic agents. Therefore, development of HIF-1 $\alpha$ / $\beta$  heterodimerization inhibitors may provide a novel approach to anti-cancer therapy. To this end, a novel approach for imaging HIF-1 $\alpha$ / $\beta$  heterodimerization *in vitro* and *in vivo* was developed in this study. Using this screening platform, we identified a promising lead candidate and further chemically derivatized the lead candidate to assess the structure-activity relationship (SAR). The most effective first generation drug inhibitors were selected and their pharmacodynamics and anti-tumor efficacy *in vivo* were verified by bioluminescence imaging (BLI) of HIF-1 $\alpha$ / $\beta$  heterodimerization in the xenograft tumor model. Furthermore, the first generation drug inhibitors, M-TMCP and D-TMCP, demonstrated efficacy as monotherapies, resulting in tumor growth inhibition via disruption of HIF-1 signaling-mediated tumor stromal neoangiogenesis.

## Table of Contents

<b>Acknowledgment</b> .....	i
<b>Abstract</b> .....	v
<b>Table of Contents</b> .....	vi
<b>List of Illustrations</b> .....	x
<b>List of Tables</b> .....	xiii
<b>Abbreviations</b> .....	xiv
<b>Chapter 1: Introduction</b> .....	1
1.1 Oxygen and oxygen-dependent metabolism .....	1
1.2 Hypoxia and malignancy .....	6
1.3 Hypoxia and cancer .....	7
1.4 Hypoxia Inducible Factor - 1 (HIF-1) .....	10
1.5 Hypoxia related pathways .....	14
1.6 HIF-1 $\alpha/\beta$ related pathway in cancer .....	14
1.7 Imaging of Hypoxia .....	18
1.7.1 Bioluminescent imaging in hypoxia .....	19
1.8 HIF-1 inhibitors in cancer .....	20
A. Small molecular inhibitors of HIF-1 $\alpha$ protein levels .....	21
B. Small molecular inhibitors of HIF-1 DNA binding .....	23
C. Small molecular inhibitors of HIF-1 transcriptional activity .....	23
D. Small molecular inhibitors of HIF-1 dimerization .....	24

1.9 Specific aims of the project .....	27
<b>Chapter 2: Materials and Methods</b> .....	<b>28</b>
Cell Culture.....	28
Construction of HIF-1 Heterodimerization Imaging lentiviral Vectors.....	28
Production of Lentivirus for generating U87 HIF-1 Heterodimerization Reporter Cells .....	31
Flow Cytometry and Protein Expression Analysis of Transduced U87 Reporter Cells.....	31
Selection of Stably Transduced U87 Reporter Cells .....	32
Competitive HIF- $\alpha/\beta$ Protein-Binding Assay .....	32
Hypoxia Chamber-Induced Endogenous HIF-1 $\alpha$ Competition Assay .....	32
High-Throughput Drug Screening <i>In Vitro</i> .....	33
Chemical Reagents and Instrumentation .....	33
Chemistry Synthesis .....	34
Structure Activity Relationship of Acridine Analogs .....	37
HIF-1 transcriptional activity reporter assay .....	38
Rapamycin-regulated <i>firefly</i> luciferase complementation cell-based reporter assays .....	38
Quantitative real-time reverse-transcription PCR (qRT-PCR) .....	39
Western Blot Analysis .....	40
Tumor Xenograft and Drug Treatment .....	40
Organ Toxicity Assay .....	41
Immunohistochemistry and Immunofluorescence .....	41
Statistical Analyses .....	42



<b>Chapter 3: Development and Optimization of a Reporter System for Bioluminescence Imaging of HIF-1<math>\alpha</math>/HIF1<math>\beta</math> Heterodimerization</b> .....	43
3.1 Overview of the HIF-1 $\alpha$ / $\beta$ Heterodimerization reporter system .....	43
3.2 Optimization of HIF-1 $\alpha$ / $\beta$ heterodimerization reporter system .....	44
3.3 Validation of HIF-1 $\alpha$ / $\beta$ Dimerization Reporter System .....	50
3.3.1 Overexpressed HIF-1 $\alpha$ <sub>12-396</sub> or HIF-1 $\beta$ <sub>11-510</sub> reduces the activity of HIF-1 $\alpha$ / $\beta$ dimerization reporter .....	50
3.3.2 Hypoxia-induced upregulation of endogenous HIF-1 $\alpha$ reduces the activity of HIF-1 $\alpha$ / $\beta$ dimerization reporter .....	52
<b>Chapter 4: High-Content Screening of Inhibitors of HIF-1<math>\alpha</math>/HIF-1<math>\beta</math> Dimerization <i>in Cellulo</i></b> .....	54
<b>Chapter 5: Evaluation of Selected Agents as Inhibitors of HIF-1-mediated Transcriptional Activity</b> .....	62
5.1 M-TMCP and D-TMCP inhibit HIF-1 $\alpha$ / HIF-1 $\beta$ Dimerization, but not FLuc fragment reconstitution .....	62
5.2 M-TMCP and D-TMCP inhibit HIF-1-mediated Transcriptional Reporter Activity .....	64
5.3 M-TMCP and D-TMCP inhibit mRNA expression of HIF-1-dependent genes in hypoxia .....	67
<b>Chapter 6: Evaluation of Therapeutic Efficacy of Selected Inhibitors in Tumor Xenograft Bearing Mice</b> .....	76
6.1 Imaging Inhibition of HIF-1 $\alpha$ /HIF1- $\beta$ Heterodimerization and Antitumor Therapeutic Efficacy by M-TMCP and D-TMCP in Tumors <i>in Vivo</i> .....	76

6.2 Effects of M-TMCP and D-TMCP Treatment on Tumor Vascularization, Proliferation, and Apoptosis <i>in vivo</i> .....	83
6.3 Assessment of systemic toxicity after chronic administration of D-TMCP <i>in vivo</i> .....	92
<b>Chapter 7: Summary and Discussion</b> .....	<b>97</b>
<b>Chapter 8: Future Direction</b> .....	<b>102</b>
<b>Appendix</b> .....	<b>103</b>
<b>Bibliography</b> .....	<b>105</b>
<b>Curriculum Vitae</b> .....	<b>122</b>

## List of Illustrations

<b>Figure 1.</b> A diagram of human circulatory system and gas exchange in capillary. ....	3
<b>Figure 2.</b> A diagram of cellular respiration including glycolysis, citric acid cycle, and oxidative phosphorylation in the electron transport chain. ....	4
<b>Figure 3.</b> The role of oxygen in radiation-induced cytotoxicity. ....	9
<b>Figure 4.</b> Human HIF family HIF-1 $\alpha$ , HIF-2 $\alpha$ , HIF-3 $\alpha$ and HIF-1 $\beta$ . ....	12
<b>Figure 5.</b> Regulation of HIF-1 $\alpha$ . ....	13
<b>Figure 6.</b> HIF-1-regulated genes play essential roles in adaptive mechanisms to hypoxia. ....	17
<b>Figure 7.</b> Construction of HIF-1 $\alpha_{12-396}$ and HIF-1 $\beta_{11-510}$ reporter vectors. ....	30
<b>Figure 8.</b> Schematic of HIF-1 dimerization reporter system in drug screening. ....	43
<b>Figure 9.</b> Schematic drawing shows major features of four lentiviral vectors of HIF-1 $\alpha$ and HIF-1 $\beta$ dimerization reporters. ....	45
<b>Figure 10.</b> Bioluminescence in HEK293 cells transiently transfected with NL-1 $\alpha$ and CL-1 $\beta$ or 1 $\alpha$ -NL and 1 $\beta$ -CL vector pairs as indicated. ....	46
<b>Figure 11.</b> Result of cell cytometry to evaluate eGFP and mKate coexpression level in transduced U87 cells. ....	47
<b>Figure 12.</b> A) Highest BLI signal was observed with U87 human glioma cells transfected with NL-1 $\alpha$ + CL-1 $\beta$ vector pair. B) Subcellular co-localization of co-expressed eGFP (NL-1 $\alpha$ ) and mKate (CL-1 $\beta$ ) reporter proteins in the U87/NL1 $\alpha$ /CL1 $\beta$ cells. ....	48
<b>Figure 13.</b> The degradation half-life of enzymatically active NL-1 $\alpha$ + CL-1 $\beta$ reporter complex in U87/NL1 $\alpha$ /CL1 $\beta$ cells. ....	49
<b>Figure 14.</b> A) The overexpression of PAS domains of either HIF-1 $\alpha$ (HIF-1 $\alpha_{12-396}$ ) or HIF-1 $\beta$ (HIF-1 $\beta_{11-510}$ ) resulted in almost 25% and 50% reduction in BLI signal intensity B) No	

changes in the magnitude of expression of NL-1 $\alpha$  or CL-1 $\beta$  reporter proteins were observed.  
.....51

**Figure 15.** A) HIF-1 $\alpha$  and  $\beta$ -actin protein levels were determined by western blotting assays.  
B) Significantly decrease of BLI signals after 48 h incubation of 5% O<sub>2</sub>. C) No obvious  
reduction in cell viability between 20% O<sub>2</sub> and 5% O<sub>2</sub> incubation was observed. ....53

**Figure 16.** M-TMCP and D-TMCP inhibit HIF-1 $\alpha$ / HIF-1 $\beta$  Dimerization in a dose-dependent  
manner. ....61

**Figure 17.** No effect of ACF, M-TMCP and D-TMCP on rapamycin-induced FRB-  
NLuc/CLuc-FKBP association in HEK-293 cells. ....63

**Figure 18.** Inhibitory effect of M-TMCP, D-TMCP or ACF on HIF-1 mediated transcription. 65

**Figure 19.** Comparison of IC<sub>50</sub> of M-TMCP, D-TMCP and ACF in U87/NL1 $\alpha$ /CL1 $\beta$  reporter  
cells or C6#4/HRE-GFP/CMV-dsRed HIF-1 transcriptional activity reporter cells. ....66

**Figure 20.** mRNA expression profile of human HIF-1 related genes in normoxic U87 cells  
and hypoxic U87 cells treated with HIF-1 dimerization inhibitors. ....73

**Figure 21.** The mRNA expression of selective tumor progression and angiogenesis-related  
genes was significantly decreased in hypoxic U87 glioma cells treated with M-TMCP and D-  
TMCP. ....75

**Figure 22.** Schematic tumor growth and treatment flow. ....78

**Figure 23.** HIF-1 $\alpha$ / $\beta$  dimerization inhibition of M-TMCP and D-TMCP on U87/NL1 $\alpha$ /CL1 $\beta$   
glioma cancer xenograft model. ....79

**Figure 24.** Anti-tumor effect of M-TMCP and D-TMCP on U87/NL1 $\alpha$ /CL1 $\beta$  human glioma  
xenograft in mice. ....80

<b>Figure 25.</b> Log tumor cell kill of M-TMCP and D-TMCP on U87/NL1 $\alpha$ /CL1 $\beta$ human glioma xenograft in mice. ....	81
<b>Figure 26.</b> No loss in body weights of U87/NL1 $\alpha$ /CL1 $\beta$ xenograft-bearing mice treated with HIF-1 dimerization inhibitors. ....	82
<b>Figure 27.</b> M-TMCP and D-TMCP reduced tumor vascularization, modified metabolic micro-environment, inhibited cellular invasiveness, and induced cellular apoptosis. ....	84
<b>Figure 28.</b> Immunofluorescent staining for evaluating expression of VEGF (Green) with associated tumor vascular structure (CD34+; Red) in U87/NL1 $\alpha$ /CL1 $\beta$ tumors. ....	86
<b>Figure 29.</b> Immunofluorescent staining for evaluating expression of GLUT-1 (Green) with associated tumor vascular structure (CD34+; Red) in U87/NL1 $\alpha$ /CL1 $\beta$ tumors. ....	88
<b>Figure 30.</b> Immunofluorescent staining for evaluating expression of Annexin V (Green) with associated tumor vascular structure (CD31+; Red) in U87/NL1 $\alpha$ /CL1 $\beta$ tumor. ....	90
<b>Figure 31.</b> No physiological changes observed after repeated D-TMCP treatment, ranging from 1 to 10 mg/kg, for up to 21 days. ....	93
<b>Figure 32.</b> No abnormal cellular proliferation observed after repeated D-TMCP treatment, ranging from 1 to 10 mg/kg, for up to 21 days. ....	95

## List of Tables

<b>Table 1:</b> HIF-1 inhibitors and their mechanism of action .....	26
<b>Table 2:</b> The list of initially screened compounds .....	57
<b>Table 3:</b> SAR studies of acridine like molecules.....	58
<b>Table 4:</b> SAR studies of the homo-di-substituted-3,6-acridine amide. ....	59
<b>Table 5:</b> SAR assessment of the mono and hetero-substituted acridines and biotinylated derivatives .....	60
<b>Table 6:</b> 84 hypoxia-associated genes in human hypoxia signaling pathway array .....	69

## **Abbreviations**

18F-FAZA, fluorodeoxyglucose-fluoroazomycin arabinoside

18F-MISO, fluorodeoxyglucose-fluoromisonidazole

ATP, adenosine triphosphate

ADP, adenosine diphosphate

ARNT, aryl hydrocarbon receptor nuclear transporter

BLI, bioluminescence imaging

bHLH, basic helix-loop-helix

CL, C-terminus of firefly luciferase (residues 438-554)

C-TAD, C-terminal transactivation domain

CD34, Hematopoietic progenitor cell antigen

DMEM, Dulbecco's Modified Eagle Medium

DTT, dithiothreitol

ECM, extracellular matrix

EPO, erythropoietin

FBS, fetal bovine serum

eGFP, enhanced green fluorescent protein

HREs, HIF-responsive elements

HRP, horse-radish peroxidase

HIF-1, Hypoxia-inducible factor 1

HIF1- $\alpha$ , hypoxia induced factor 1, alpha subunit

HIF1- $\beta$ , hypoxia induced factor 1, beta subunit

HK, hexokinase

IACUC, Institutional Animal Care and Use Committee

IC<sub>50</sub>, half maximal inhibitory concentration

IGF-binding protein, insulin-like growth factor binding protein

IHC, immunohistochemistry

i.p., Intraperitoneal injection

i.v., intravenous injection

Ki67, Mki67 protein (antigen identified by monoclonal antibody Ki-67)

MRI, magnetic resonance imaging

mRNA, messenger RNA

mKate, far-red fluorescent protein TagFP635

NL, N-terminus of firefly luciferase (residues 1-437)

N-TAD, N-terminal transactivation domain

NMR, nuclear magnetic resonance



ODD, oxygen dependent degradation domain

PAS, Per-Arnt-Sim

pVHL, von Hippel-Lindau

Pro, amino proline residues

PAGE, polyacrylamide gel electrophoresis

PBS, phosphate buffered saline

PCR, polymerase chain reaction

PDK, pyruvate dehydrogenase kinase

PET, positron emission tomography

qRT-PCR, quantitative real-time reverse-transcription polymerase-chain-reaction

SDS, sodium dodecyl sulfate

SPECT, single-photon emission computed tomography

TBST, tris buffered saline with tween

VEGF, vascular endothelial growth factor

WST-1, water-soluble disulfonated tetrazolium salt

## Chapter 1: Introduction

### 1.1 Oxygen and oxygen-dependent metabolism

Oxygen, a gas that plays a vital role in all life on earth, controls respiration and metabolic processes of aerobic organisms. Under normal physiological condition, a resting adult consumes approximately 3.5 ml of oxygen per kilogram of body mass every minute. In the human body, the delivery of oxygen is accomplished by an elaborate arterial and venous circulatory network, where oxygen diffuses from areas of higher oxygen partial pressure to areas of lower oxygen partial pressure. De-oxygenated blood is circulated via venous network to the lungs while it is oxygenated again. Oxygenated blood then distributes to the body where needed. However, due to the limitations in diffusion, oxygen can only be transported to cells within 100–200  $\mu\text{m}$  from the capillary (Rouwkema et al., 2008) (**Fig.1**).

When oxygen supply is ample, living cells preferentially produce energy through aerobic respiration to convert nutrients, such as glucose, into adenosine triphosphate (ATP) (**Fig.2**). Aerobic respiration composed a set of metabolic reactions, including glycolysis, oxidative decarboxylation of pyruvate, citric acid cycle and oxidative phosphorylation. During aerobic respiration, exogenous oxygen is used in the final step of oxidative phosphorylation. In the inner mitochondrial membrane, the high-energy electrons released from coenzyme NADH produced from the citric acid cycle pass through a set of enzymes called the electron transport chain (ETC), and release the energy to pump protons across the inner membrane of mitochondria, which generates a proton gradient (chemiosmosis potential) across the intermembrane space. This proton gradient drives protons to flow back across the membrane through the ATP synthase. The flow of proton forces the rotation of a part of the enzyme, generating ATP by phosphorylation of adenosine diphosphate (ADP). Finally, the low-energy electrons passing through the electron transport chain are transferred to oxygen,

a strong oxidizing agent to accept the low-energy electrons. Oxygen then combines with a pair of electrons and two protons to form water (Lehninger et al., 2013).

In one complete cycle of aerobic respiration, a total of 38 ATP molecules are generated per each oxidized glucose molecule; whereas in the absence of oxygen, the cells are forced to switch to anaerobic respiration and use electron acceptors other than oxygen. Importantly, the anaerobic respiration is much less efficient and yields only 2 ATP molecules per each glucose molecule. Both aerobic and anaerobic respiration share the initial pathway of glycolysis to produce pyruvate, but only aerobic metabolism continues with the citric acid cycle and oxidative phosphorylation. In anaerobic respiration, cells have pyruvate oxidized with NADH, ending with the final production of ethanol or lactic acid (**Fig.2B**).

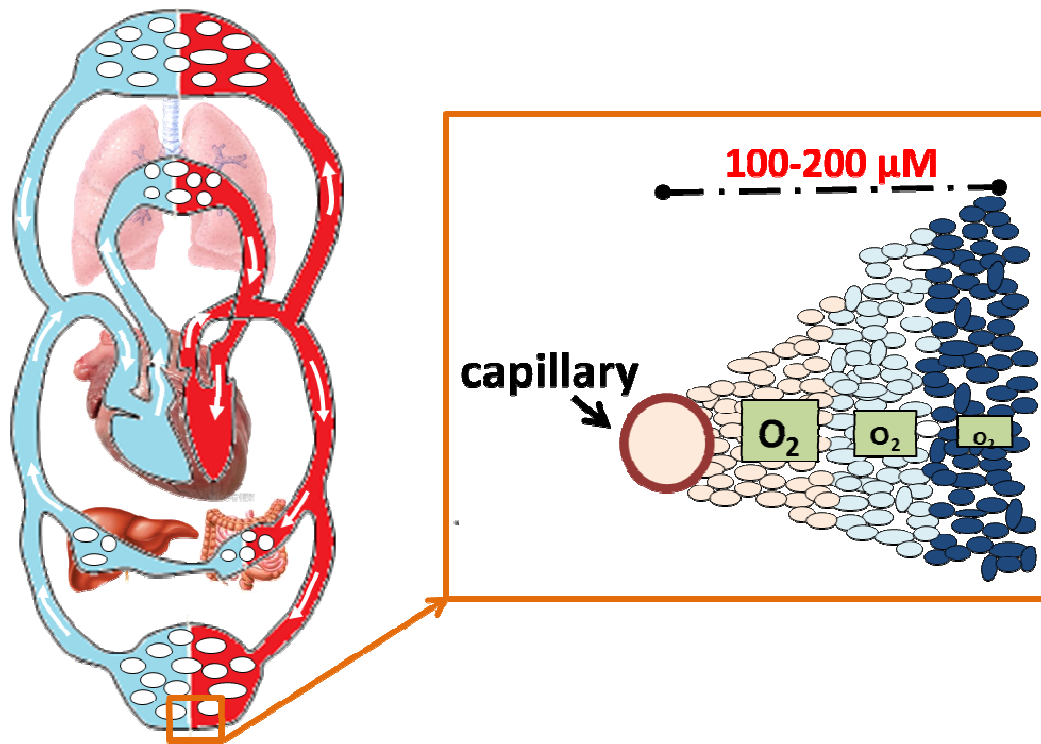
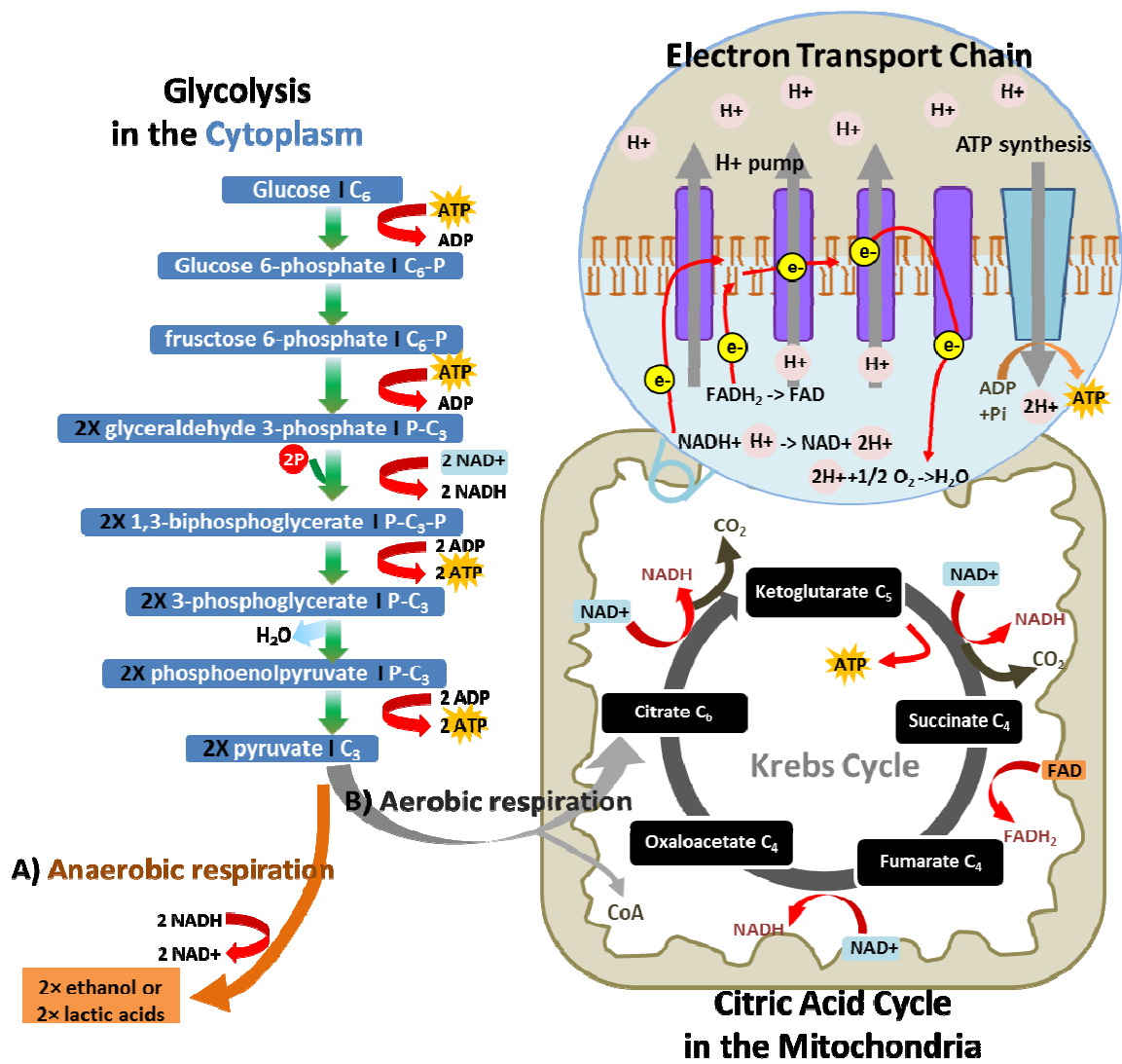


**Figure 1. A diagram of human circulatory system and gas exchange in capillary.** The human circulatory system consists of two parts: **a)** Pulmonary loop: the oxygen-depleted blood circulates from the right atrium and ventricle of the heart to the lung via pulmonary artery. The gas exchange takes place in the lung via single layer capillaries, where  $\text{CO}_2$  is released from the blood and oxygen is picked up. Then the oxygen-rich blood return to the left atrium via pulmonary vein. **b)** Systemic loop: the blood circulates to all parts of the body except the lungs. The oxygenated blood pumps from the heart through the left ventricle to all the rest of the body to supply oxygen and collect  $\text{CO}_2$  and waste via interweaving network of capillaries. The oxygen-depleted blood then returns back to the right atrium and starts a new pulmonary circulation cycle to be re-oxygenated. The capillary wall is a one-layer endothelium that allows gas and lipophilic molecules to pass through by bidirectional diffusion depending on osmotic gradients. However, due to the limitations in diffusion, oxygen can only be transported to cells within 100–200  $\mu\text{m}$  from the capillary.

**Figure 2. A diagram of cellular respiration including glycolysis, citric acid cycle, and oxidative phosphorylation in the electron transport chain.** The process of glycolysis begins with phosphorylation of glucose by hexokinase (I, II, and III) to form glucose 6-phosphate. Subsequently, fructose 1,6-disphosphate is formed by 6-phosphofructo 1-kinase at the cost of two ATP molecules. Next, the cleavage of fructose 1,6-disphosphate into two pyruvate molecules by the aldolase produces 4 ATP and 2 NADH. As a result, the entire process of glycolysis generates a net gain of 2 ATP molecules and 2 NADH.  $\text{Glucose} + 2 \text{NAD}^+ + 2 \text{Pi} + 2 \text{ADP} \rightarrow 2 \text{pyruvate} + 2 \text{NADH} + 2 \text{ATP} + 2 \text{H}^+ + 2 \text{H}_2\text{O} + \text{heat}$ . **A)** In anaerobic respiration, to convert NADH back to replenish the limited supply of  $\text{NAD}^+$ , most cells have pyruvate oxidized with NADH, ending with the final production of ethanol or lactic acids. **B)** In aerobic respiration, cells can further utilize pyruvate and  $\text{NADH} + \text{H}^+$  from glycolysis to produce additional 34 ATP molecules in the citrate acid cycle and oxidative phosphorylation pathway. First, pyruvate is oxidized to acetyl-CoA and  $\text{CO}_2$  by pyruvate dehydrogenase complex before entering to citric acid cycle within the mitochondrial matrix. Next, acetyl-CoA (2 carbons) continues to oxidize with oxaloacetate (4 carbons) to form citrate (6 carbons), which later modifies to become  $\alpha$ -ketoglutarate (5 carbons) and  $\text{CO}_2$ . When  $\alpha$ -ketoglutarate is oxidized to succinyl-CoA (4 carbons), another  $\text{CO}_2$  is released. Following production of succinate, fumarate, malate, and back to oxaloacetate, the net energy produced by one cycle is 3 NADH, 1  $\text{FADH}_2$ , and 1 GTP. Since two acetyl-CoA are generated from each glucose molecule, a total of 6 NADH, 2  $\text{FADH}_2$ , and 2 GTP are produced for one fully oxidized glucose during the citric acid cycle. The next oxidative phosphorylation occurs in the inner mitochondrial membrane, which generates the high transfer potential electrons. When released from coenzyme NADH, the high transfer potential electrons pass through a set of enzymes called the electron transport chain and release the energy to pump protons across the inner membrane of the mitochondria. The established proton gradient (chemiosmosis potential) across the intermembrane space then drives protons to flow back across the membrane via a large enzyme called ATP synthase. The flow of proton forces the rotation of a part of the enzyme, generating ATP from the phosphorylation of ADP. Finally, the low-energy electrons passing through the electron transport chain are transferred to oxygen, a strong oxidizing agent to accept the low-energy electrons. Oxygen then combines with a pair of electrons and two protons to form water. The figure was adapted from RegisFrey, [CC-BY-SA-3.0 (<http://creativecommons.org/licenses/by-sa/3.0>) (2011).



## 1.2 Hypoxia and malignancy

When oxygen consumption in the body is elevated in events such as exercise, the body can quickly adapt to the need for increased oxygen by accelerating cardiac output and increasing respiration rate to elevate blood oxygenation. However, if these adjustments are insufficient to deliver adequate supply of oxygen to the tissues, compensatory changes in oxygen delivery and utilization are initiated by adjusting arterial compliance to allow more blood flow to reach vital organs. At some point, this compensation may still fail to supply adequate oxygen, which will result in a state of reduced oxygen availability, known as hypoxia. Normally, the partial pressure of oxygen ( $PO_2$ ) in dry air at sea level is 159 mm Hg, the  $PO_2$  in arterial blood is about 100 mm Hg, the  $PO_2$  in mean capillary is about 50 mm Hg, and the  $PO_2$  in trans-capillary tissues is between 20 and 40 mm Hg. Hypoxia in tissues is defined as the  $PO_2$  below 10 mm Hg (Nunn, 1993, Loiacono and Shapiro, 2010).

During hypoxia, the activation of the hypoxia-adaptive responses triggers the production of pro-survival factors and decreases metabolic consumption via post-translational modification of existing proteins or even changes in gene transcription and protein synthesis. Nevertheless, most cells fail to survive long under chronic hypoxia, especially the oxygen-sensitive cells in the brain and heart.

A hypoxia environment has been shown to induce genome instability in cells. When genetic errors exceed the cells' capacity to repair, genetic changes and mutations would follow (Liu et al., 2012, Sung et al., 2011). Some cells may acquire resistance to hypoxia. These mutated cells with a selective growth advantage often expand much more rapidly in hypoxic environment. If overcoming restricted growth checkpoints and regulatory pathways, they may eventually manifest as malignant cells and transform into cancer (Hanahan and Weinberg, 2000, Vanderkooi et al., 1991).

### 1.3 Hypoxia and cancer

The classic hallmarks of cancer proposed by Hanahan and Weinberg listed six biological characteristics acquired during the multi-step development of human cancer, which include sustained cell proliferative signaling, evasion of growth suppressors, cell death resistance, immortal replication, induction of angiogenesis and activation of metastasis and invasion, with three emerging hallmarks added to this list: reprogramed energy metabolism, tumor-promoting inflammation and evasion of destructive immunity (Hanahan and Weinberg, 2011, Hanahan and Weinberg, 2000).

During tumor progression, rapid cellular proliferation and highly abnormal vascularization often induces inadequate oxygen supply within tumor sites. Although some of the effects of hypoxia may negatively impact cancer cell viability, in most cases hypoxia facilitates tumor growth in selective tumor microenvironment niches. The mechanisms of increased tumorigenic potential of cells exposed to hypoxia have not been fully understood, but studies have suggested a hypoxic microenvironment may provide a driving force for genomic instability, which results in resistance to apoptosis and increased invasive capacity (Bristow and Hill, 2008, Pires et al., 2010). In addition, hypoxia-driven adaptive responses trigger tumor proliferation and even resistance to anticancer therapy.

Over 55 years ago, Tomlinson and Gray first observed histological patterns of hypoxic cells residing at the edge of the oxygen diffusion limit from functional blood vessels (no more than 180  $\mu\text{m}$  diameter away) and further postulated oxygen diffusion as a major factor influencing effectiveness of radiation therapy (Tomlinson and Gray, 1955). Their finding has led to intense research on radiobiology in cancer treatment. At present, it is well-known that the intratumoral oxygen level is arguably the most important determinant of tumor response to radiation therapy. This is because radiation therapy works by causing DNA



damage in tumors through free hydroxyl radicals forming from the ionization of water. Oxygen, as a potent radiosensitizer, reacts with these free radicals and mediates radiation-induced cytotoxicity (**Fig. 3**). Therefore, a hypoxic environment decreases radiosensitivity of tumor cells and results in increased resistance to radiation damage in hypoxic tumor cells than those in normoxia (Harrison et al., 2002, Jordan and Sonveaux, 2012). Not only does oxygen level affect radiation therapy, the presence of oxygen is also associated with the efficacy of chemotherapy. Poorly developed blood vessels in intratumoral hypoxic areas limit the delivery of circulating chemotherapeutic agents to tumors. Therefore, control of tumor hypoxia by increasing the oxygenation or decreasing hypoxic fraction of tumors has great clinical implications in cancer therapeutics. One potential strategy is to target Hypoxia Inducible Factor (HIF-1), a key regulator responsible for cellular adaptation to hypoxia.

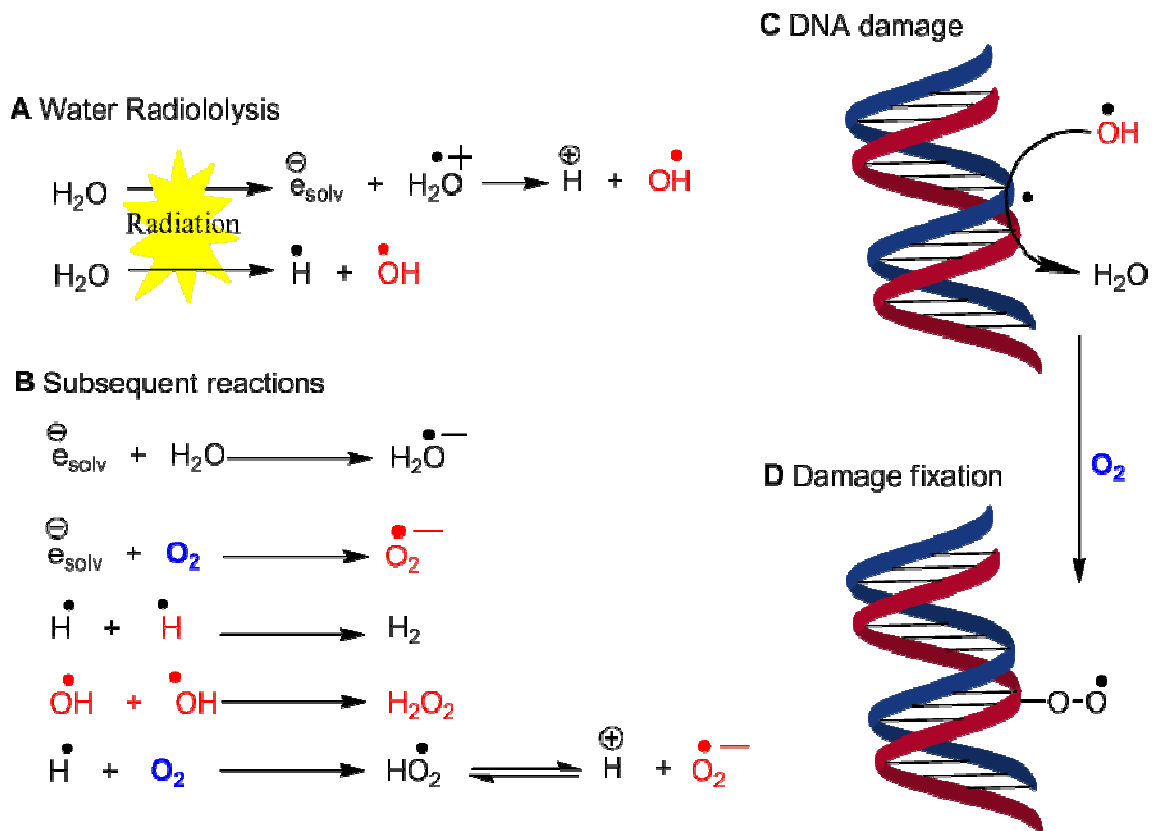


**Figure 3. The role of oxygen in radiation-induced cytotoxicity.** Hypoxic tumor areas have been found to be very resistant to radiation damage and largely influence therapeutic outcome of radiotherapy. Oxygen is involved in the stabilization of the DNA damage caused by ionizing radiations. A) Irradiation induces water ionization and destabilization, leading to the formation of reactive free radicals. B) These reactive radical species further interact with other molecules within the body and form new reactive oxygen species (ROS). C,D) Among ROS, hydroxyl radicals are the most potent mutagens to mediate DNA damage with oligonucleotide strand breaks. The initial DNA damage is readily reversible. However, the presence of oxygen can stabilize DNA damage through oxidative reaction and form DNA peroxides, which require intensive repair mechanism. This figure was adapted from Bénédicte F. Jordan and Pierre Sonveaux, *Front. Pharmacol.*, (2012). doi: 10.3389/fphar.2012.00094.

## 1.4 Hypoxia Inducible Factor - 1 (HIF-1)

The oxygen homeostasis is regulated by the transcription factor HIF-1, which was first described by Semenza and co-workers in 1992. The HIF-1 was first discovered by its induction of erythropoietin (EPO) upon hypoxia which stimulates erythrocyte proliferation and increases the O<sub>2</sub> carrying capacity of the blood (Goldberg et al., 1988, Semenza et al., 1991). Currently, there are six known members in the human HIF family, which consists of three  $\alpha$  subunits (HIF-1 $\alpha$ , HIF-2 $\alpha$  and HIF-3 $\alpha$ ) and three  $\beta$  subunits in (HIF-1 $\beta$ , HIF-2 $\beta$  and HIF-3 $\beta$ ) (**Fig. 4**). The structures of  $\alpha$  subunits share some feature domains: basic helix-loop-helix (bHLH), two internal homology Per-Arnt-Sim (PAS) domains, a von Hippel-Lindau (pVHL) oxygen dependent degradation domain (ODD), and N-terminal and C-terminal transactivation domain (N-TAD and C-TAD; except HIF-3 $\alpha$  that lacks C-TAD). In contrast, HIF's  $\beta$  subunits contain bHLH and PAS domains, but no ODD, N-TAD or C-TAD. The bHLH domain is important for mediating DNA binding and HIF- $\alpha/\beta$  heterodimerization, while two PAS domains act as secondary interfaces for HIF- $\alpha/\beta$  recognition, dimerization and stabilization (Kenneth and Rocha, 2008). **Therefore, bHLH-PAS region serves as a potential and selective target for development of small molecular disruptors of HIF- $\alpha/\beta$  heterodimerization.**

All three HIF  $\alpha$  isoforms can dimerize with HIF-1 $\beta$ , but have more limited ability to bind with HIF-2 $\beta$ . When HIF  $\alpha$  and  $\beta$  subunits dimerize, the HIF- $\alpha/\beta$  complex becomes a functional transcriptional factor. At present, the specific roles of HIF- $\alpha/\beta$  heterodimers have not been fully understood (Drutel et al., 1996, Maltepe et al., 2000, Powell and Hahn, 2002) but extensive studies have been conducted to understand the HIF-1 $\alpha/\beta$  heterodimer. These studies have demonstrated that HIF-1 $\alpha/\beta$  is a master transcription factor responsible for cellular adaptation to hypoxia and regulates the expression of several genes involved in tumor development, such as angiogenesis and glycolysis (Bardos and Ashcroft, 2005, Ziello

et al., 2007, Semenza, 2007b). Therefore, disruption of HIF-1 $\alpha$ / $\beta$  dimerization could be an effective approach to block hypoxia-induced tumorigenesis and prevent resistance to anticancer therapies. To these ends, in this dissertation, we specifically focus on developing HIF-1 $\alpha$ / $\beta$  heterodimerization inhibitors that may be utilized as anti-cancer drugs.

HIF-1 $\alpha$  is a 120 kDa bHLH-PAS protein. The stability and activity of HIF $\alpha$  are tightly regulated by oxygen-dependent degradation through its post-translational modifications such as hydroxylation, ubiquitination, acetylation, and phosphorylation. Under normoxic conditions, HIF-1 $\alpha$  is hydroxylated at conserved proline residues (Pro-402 and Pro-564) by prolyl hydroxylase, which rapidly leads to its recognition by pVHL/Elongin B and C/Cul2 ubiquitin E3 ligase for ubiquitination and further degradation by proteasome within minutes (9-11). Under hypoxic conditions, the lack of oxygen inhibits prolyl hydroxylase activity and prevents HIF-1 $\alpha$  degradation. The expression of HIF-1 $\alpha$  can usually be detected after 30 minutes of exposure to hypoxia (1-2% O<sub>2</sub>) and peaks between 4-8h under hypoxic conditions. Stabilized HIF-1 $\alpha$  then translocates into the nucleus and forms a heterodimeric transcriptional factor with HIF-1 $\beta$  (**Fig. 5**). HIF-1 $\beta$  is constitutively expressed and found abundantly in the nucleus regardless of oxygen tension. The now functional HIF-1 $\alpha$ / $\beta$  transcription factor binds to 50-base pair cis-acting hypoxia-response elements (HREs; 5'-RCGTG- 3') in cellular genome and activates the HIF-1 driven gene transcription in hypoxic cancer cells (15).

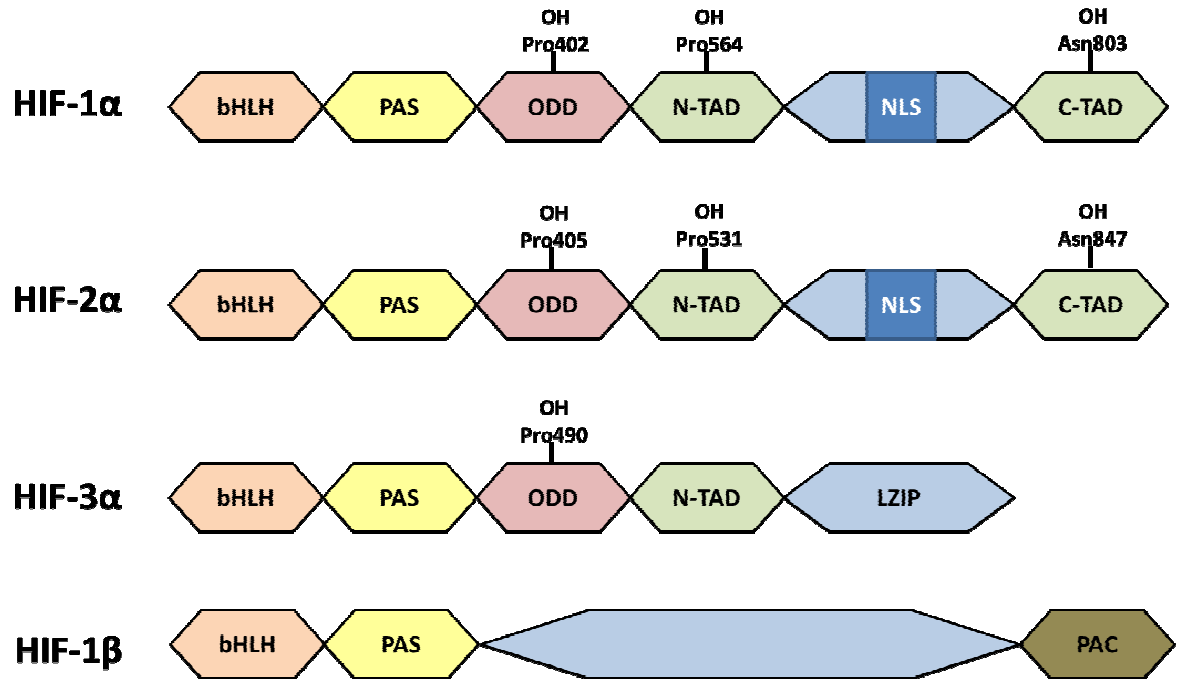


**Figure 4. Human HIF family HIF-1 $\alpha$ , HIF-2 $\alpha$ , HIF-3 $\alpha$  and HIF-1 $\beta$ .** The structure of HIF- $\alpha$  isoforms share four domains: basic helix-loop-helix (bHLH), two internal homology Per-Arnt-Sim (PAS) domains, a von Hippel-Lindau (pVHL) targeted oxygen dependent degradation domain (ODD), and N-terminal and C-terminal transactivation domain (N-TAD and C-TAD; except HIF-3 $\alpha$  without C-TAD). HIF-1 $\alpha$  and HIF-2 $\alpha$  also each contains a nucleus translocation signal (NLS) for transferring into nucleus. Meanwhile, HIF- $\beta$  contains bHLH and PAS domains, but no ODD, N-TAD and C-TAD. The figure was modified and adapted from Kenneth and S. Rocha, *Biochem. J.* (2008) 414, 19–29.

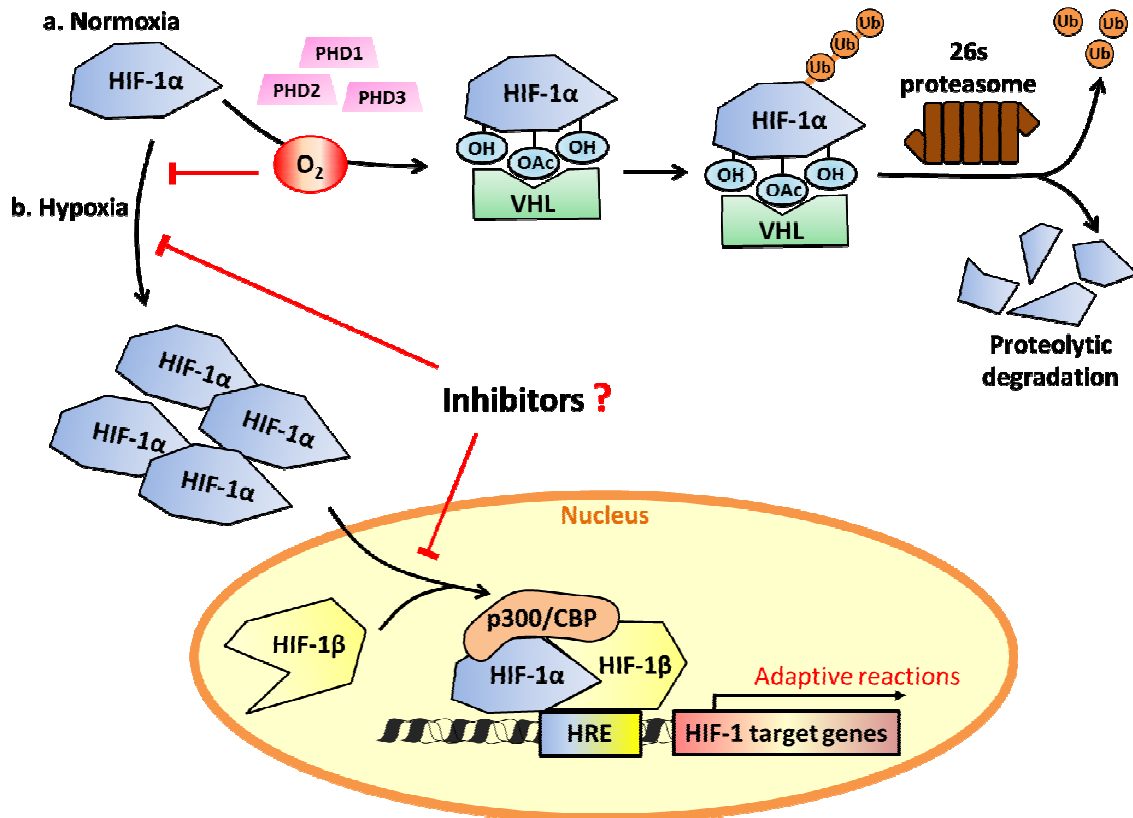


**Figure 5. Regulation of HIF-1 $\alpha$ .** In normoxia, HIF-1 $\alpha$  is hydroxylated at proline residues (Pro-402 and Pro-564) by HIF prolyl-hydroxylases, allowing recognition and ubiquitination by the pVHL/Elongin B and C/Cul2 ubiquitin E3 ligase and leading HIF-1 $\alpha$  to rapid degradation by the proteasome. Under hypoxic conditions, the lack of oxygen prevents HIF-1 $\alpha$  being hydroxylated and reduces the degradation process. In response, stabilized HIF-1 $\alpha$  then translocates into the nucleus and forms a heterodimeric with HIF-1 $\beta$ . HIF-1 $\alpha$ / $\beta$  heterodimers then served as a transcriptional activator binding to HIF-responsive elements (HREs) and regulating the expression of multiple genes involved in tumor metabolism and vascularization. The figure was modified and adapted from Veronica A. Carroll and Margaret Ashcroft, *Expert Reviews in Molecular Medicine*, (2005) Vol.7, Issue 6.

## 1.5 Hypoxia related pathways

In response to hypoxia, HIF-1 $\alpha/\beta$  serves as a master transcriptional factor, which interconnects with several essential pathways with varying functions to maintain oxygen homeostasis. Hundreds of genes are transcriptionally regulated by HIF-1 $\alpha/\beta$  via binding to the HRE consensus site in their promoter regions (Semenza et al., 1991, Elvidge et al., 2006). However, HIF-1 $\alpha/\beta$  binding is detected only in genes with increased expression. HIF-1-dependent decrease in transcription occurs via indirect mechanisms, which include HIF-1-dependent expression of transcriptional repressors and microRNAs (Yun et al., 2002, Kulshreshtha et al., 2007).

Using a comprehensive DNA microarrays analysis, it has recently been found that at least 2.6% of human genes (total 22283 genes studied) are regulated by hypoxia in a HIF-1 $\alpha/\beta$  dependent manner in arterial endothelial cells, directly or indirectly (Manalo et al., 2005). Moreover, this study also demonstrated a large group of genes regulated by hypoxia involved in cell growth/proliferation, signal transduction, oxidoreduction, mitochondrial and ribosomal biogenesis, RNA binding/metabolism, protein ubiquitination/proteasomal degradation and transcription activation (**Fig. 6**).

## 1.6 HIF-1 $\alpha/\beta$ related pathway in cancer

HIF-1 $\alpha/\beta$  is a major regulator of critical processes in malignancy such as angiogenesis, apoptosis, proliferation, invasion and metabolism. Many studies have suggested that an increased HIF-1 $\alpha/\beta$  level is highly associated with cancer progression and metastasis (Sumiyoshi et al., 2006, Volm and Koomagi, 2000, Zhong et al., 1999).

For instance, stabilized HIF-1 $\alpha$ / $\beta$  stimulates the production of vascular endothelial growth factor (VEGF) and other hypoxia-induced angiogenic cytokines (such as FGF, and TGF), that promote endothelial cell proliferation, increase vascular permeability and cell migration. The formation of new blood vessels, known as neovascularization or angiogenesis, is a critical step in the multistage process of tumor metastasis (Olenyuk et al., 2004).

HIF-1 $\alpha$ / $\beta$  is also a key mediator in many metabolism pathways, and is responsible for the upregulation of glycolytic enzymes to increase energy consumption. Expressions of glucose transporter 1 (GLUT-1), hexokinase 2 (HK2) and other glycolytic enzymes are elevated by active HIF-1 $\alpha$ / $\beta$  to promote glucose use in cancer cells during hypoxia (Song et al., 2009, Wood et al., 1998, Denko, 2008).

Moreover, HIF-1 $\alpha$ / $\beta$  is important for hypoxic stimulated epithelium-mesenchyme transition (EMT) in tumor invasion by suppressing E-cadherin expression and enhancing matrix metalloproteinase-2 (MMP2) and collagen I (Krishnamachary et al., 2006, Higgins et al., 2007, Jing et al., 2013). Many HIF-1 $\alpha$ / $\beta$  target genes, such as insulin-like growth factor 2, IGF-binding protein 1, 2 and 3, have pro-survival effects by stimulating cell proliferation under reduced oxygen availability (Vaupel, 2004). Although most of HIF-1 $\alpha$ / $\beta$  targeting genes promote cell survival, apoptosis can also be initiated by HIF-1 in certain situations like prolonged chronic hypoxia (Carmeliet et al., 1998). The HIF-1 $\alpha$ / $\beta$  regulated pro-apoptotic gene BNIP3 is found to be overexpressed in perinecrotic regions of the human tumors (Koop et al., 2009). HIF-1 $\alpha$ / $\beta$  has also been shown to induce cell cycle arrest to decrease cell proliferation rates in hypoxia, which allows cells in stressful microenvironment to slow their growth and conserve energy for survival (Koshiji et al., 2004, Goda et al., 2003).



With these essential involvements of HIF-1 $\alpha$ / $\beta$  in tumor vascularization and metabolism, HIF-1 $\alpha$ / $\beta$  has become an important target for the development of anti-cancer drugs. In fact, many researchers have suggested that inhibitors of HIF-1 $\alpha$ / $\beta$  may pose better potential to limit cancer progression than using inhibitors of its downstream gene products such as VEGF (Semenza, 2007a, Melillo, 2006, Welsh and Powis, 2003).

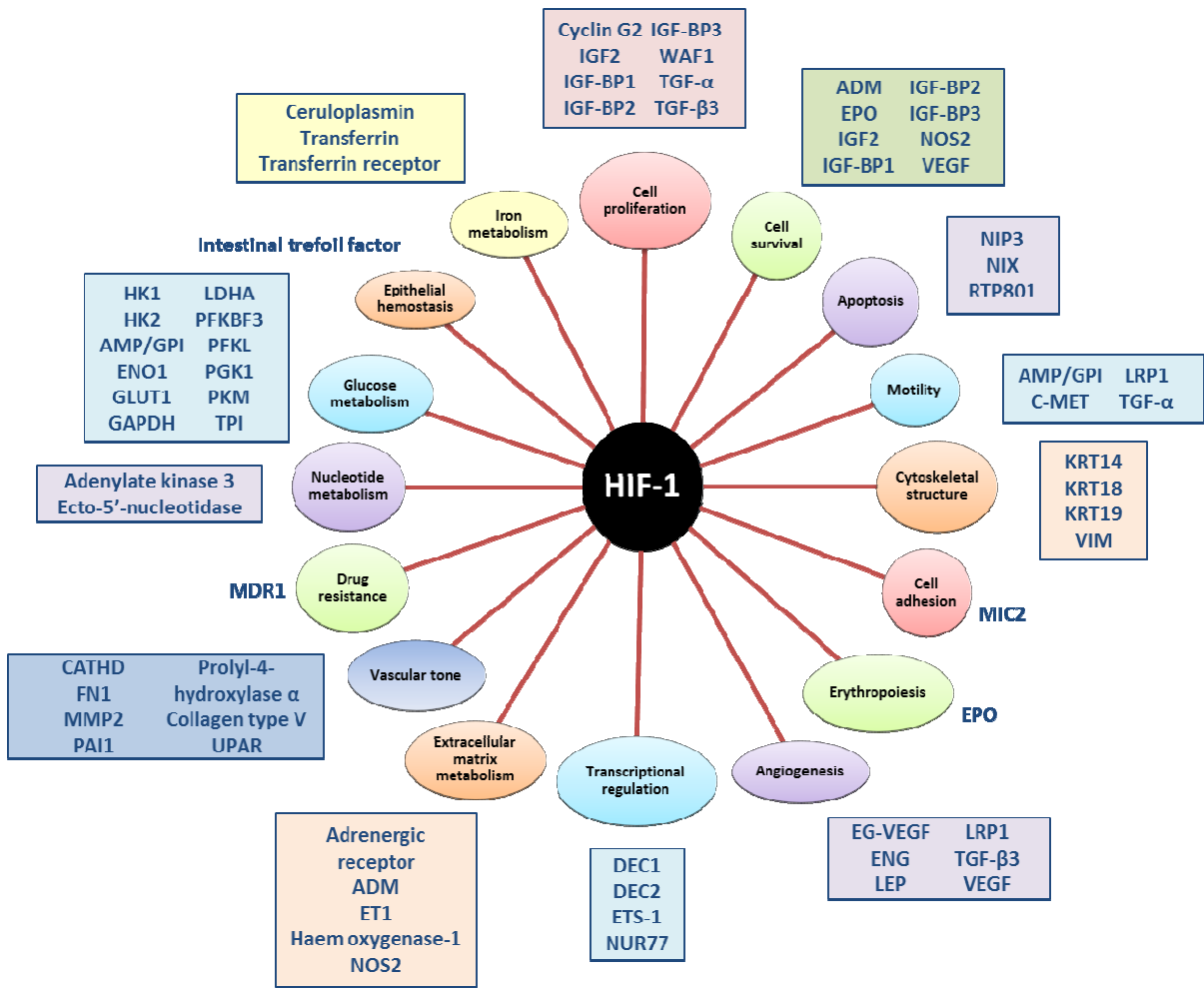


**Figure 6. HIF-1-regulated genes play essential roles in adaptive mechanisms to hypoxia.** This figure was modified and adapted from Gregg L. Semenza, Nature Reviews Cancer 3, 721-732 (October 2003). Copyright permission was obtained from Nature Publishing Group.

## 1.7 Imaging of Hypoxia

Measuring hypoxia is critical in determining the aggressiveness of tumor and assessing the effectiveness of anti-cancer treatments. As a result, numerous invasive and noninvasive approaches have been developed to measure hypoxic regions in tumors, including polarographic electrodes, magnetic resonance imaging (MRI), positron emission tomography (PET), single-photon emission computed tomography (SPECT) and optical imaging (fluorescence and bioluminescence) (Tatum et al., 2006, Sun et al., 2011).

The most promising imaging method to measure hypoxia would be using a radiolabeled probe that competes directly with intracellular  $O_2$ . PET imaging with  $^{15}O_2$  inhalation can provide accurate measurements of oxygen tension in tissues (Krohn et al., 2008, Serganova et al., 2006). However, the short half-life of  $^{15}O_2$  (about 2 minutes) and high cost hinder this approach in the clinical setting. The first clinical study to image hypoxia in PET was using 2-nitroimidazole, which is a bioreductive compound that undergoes a reduction reaction by hypoxia-induced nitroreductase and is then trapped in hypoxic tissues (Chapman, 1984, Lee and Scott, 2007). The covalent binding of a 2-nitroimidazole-protein adduct can be detected with specific antibodies or imaged by labeling PET radionuclides, such as  $^{18}F$  and  $^{124}I$ , or with single-photon emitters, such as  $^{123}I$  and  $^{99m}Tc$  for SPECT. The commonly used nitroimidazoles derivatives are EF5, pimonidazole and misonidazole (Grunbaum et al., 1987, Martin et al., 1992). So far,  $^{18}F$ -FMISO is the most robust and common radiopharmaceutical to quantify hypoxia in clinic. The other alternative PET bioreductive agent for measuring hypoxia is radioactive copper ( $^{60}Cu$ ,  $^{61}Cu$ ,  $^{62}Cu$  or  $^{64}Cu$ ) with diacetyl-bis(-methylthiosemicarbazone) (Cu-ATSM). It has been demonstrated that  $^{64}Cu$ -ATSM accumulates more rapidly than  $^{18}F$ -FMISO and has a greater hypoxic to normoxic ratio (O'Donoghue et al., 2005).

Other radiation free approaches utilize MRI to measure hypoxia. However, MRI without exogenous contrast, such as blood oxygen level dependent (BOLD) MRI or MRS for lactate or NADH/NADPH imaging, are measuring a downstream consequence of hypoxia and often cause a time delay in re-oxygenation. Some oxygen-sensitive MR reporter agents, generally based on perfluorocarbons (PFCs), have also been developed for  $^{19}\text{F}$  MR oximetry. These agents showed great potential with sequential measurements over time and provided robust detection with nanomolar (nM) sensitivities (Lemaire et al., 2013, Stoll et al., 2012, Mason et al., 2010). These MR hypoxia imaging techniques are currently developed in animal studies, but starting to be established in human tumor research.

The bioluminescent and fluorescent imaging technologies possess several strong advantages for exploring the detailed molecular mechanisms of hypoxia. Although bioluminescent and fluorescent imaging technologies are not practiced in the clinic yet, they serve as great tools for preclinical studies. In this dissertation, we utilized bioluminescence imaging as the molecular imaging modality of choice. Therefore, greater detail and more background of bioluminescence imaging will be covered in the following subsection.

### **1.7.1 Bioluminescent imaging in hypoxia**

Bioluminescence is characterized as a process of light emission from a living organism. Bioluminescence can also be utilized for noninvasive imaging studies to observe ongoing biological processes in small laboratory animals. The light-producing chemical reaction is catalyzed by the luciferase enzymes in certain insects, marine species and bacteria (*Photorhabdus luminescens* and *Vibrio fischeri*) (de Wet et al., 1987). The most commonly used luciferases in research are derived from the North American firefly (*Photinus pyralis*) and the sea pansy (*Renilla reniformis*). The luciferase enzymes start their catalytic competence immediately after being released from the ribosome, without further post-

translational processing, thus providing instantaneously enzymatic activity. Using firefly luciferase employed in this dissertation as an example, firefly luciferase catalyzes the chemical reaction through two steps:

- $D\text{-luciferin} + \text{ATP} \rightarrow \text{luciferyl adenylate} + \text{pyrophosphate}$
- $\text{luciferyl adenylate} + \text{O}_2 \rightarrow \text{oxyluciferin} + \text{AMP} + \text{light}$

The wavelengths of light emitted through firefly luciferase reaction are typically in green ( $\lambda_{\text{max}} = 550 \text{ nm}$ ) to yellow ( $\lambda_{\text{max}} = 570$ ) part of the spectrum, depending on the luciferase structure or its microenvironment (DeLuca and McElroy, 1974, Viviani et al., 2005). Researchers have utilized these luminescent proteins in genetic engineering for numerous purposes. Luciferase genes can be transferred into cells or even experimental laboratory animals and are widely used as reporters to assess transgene expression activity *in vitro* and *in vivo*. To be used as a genetic reporter, the luciferase gene is regulated by the promoter sequence of a gene of interest. Thus, the level of that gene transcription is proportional to the light intensity produced by the luciferase.

So far, a few bioluminescent imaging methods have been developed to image hypoxia via measuring HIF-1 transcriptional activity. Payen et al. first proposed the idea using HRE sequences coupled with reporter genes, such as luciferase or GFP, to enable imaging HIF-1 transcriptional activity (Payen et al., 2001). In 2004, Serganov et al. demonstrated *in vivo* small animal imaging of HIF-1 transcriptional activity using GFP/tk reporter under control of 8×HREs (Serganova et al., 2004).

## **1.8 HIF-1 inhibitors in cancer**

Hypoxia has been recognized as an essential player in tumor microenvironment and a prognosis marker to anti-cancer treatment. Since HIF-1 $\alpha$  is a master regulator in response to hypoxia, the development of HIF-1 inhibitors has become the focus of several research groups. In the following, the current discovery and characterization of small molecule inhibitors for targeting HIF-1 pathway will be covered.

To date, considerable efforts have been devoted to the development of HIF-1 inhibitors that reduce HIF-1 $\alpha$  mRNA or protein levels, HIF-1 DNA binding, or HIF-1 activation of transcription (**Table. 1**). Among them, agents that decrease HIF-1 $\alpha$  protein levels can be further classified by their ability in inhibiting the rate of HIF-1 $\alpha$  translation or promoting the rate of HIF-1 $\alpha$  degradation.

### **A. Small molecular inhibitors of HIF-1 $\alpha$ protein levels**

The PI3K/Akt/mTOR signaling pathway, which promotes cell proliferation and reduces apoptosis by regulating protein synthesis, is often overactive in many cancers. This prototypic survival pathway also plays a major role in upregulation of HIF-1 $\alpha$  protein synthesis in most human cancer cell lines. With the use of PI3K specific inhibitors: wortmannin and LY294002, they could downregulate insulin- and epidermal growth factor-induced expression of HIF-1 $\alpha$  in prostate carcinoma cell lines PC-3 and DU145 (Jiang et al., 2001). A clinically used mTOR inhibitor, rapamycin, has been proven to decrease HIF-1 $\alpha$  protein expression in cells (Hudson et al., 2002). Its chemical derivative inhibitor, RAD-001, also demonstrated attenuation of most HIF-1 target gene expressions in the prostates of AKT1 expressing mice (Majumder et al., 2004). The other mTOR inhibitor, CCI-779, showed inhibition of cell proliferation and HIF-1 $\alpha$  translation in VHL-mediated renal cell carcinoma (Thomas et al., 2006). EZN-2968 is an RNA antagonist which specifically binds to HIF-1

mRNA and inhibits the expression of HIF-1 $\alpha$  mRNA in DU-145 human prostate and glioblastoma cells (Greenberger et al., 2008).

The chaperone HSP90 interacts with HIF-1 $\alpha$  and is required for HIF-1 $\alpha$  protein stability. Inhibitors of HSP90, such as geldanamycin (GA) and its derivatives 17-allylamino-17-demethoxygeldanamycin (17-AAG) and 17-dimethylaminomethylamino-17-demethoxygeldanamycin (17-DMAG), are naturally occurring benzoquinone ansamycin antibiotics. These compounds have been demonstrated to interfere with Hsp90 function by competing with its ATP binding site, and inducing ubiquitination and proteasomal degradation of HIF-1 $\alpha$  in VHL-independent renal and prostate cancer cells (Isaacs et al., 2002, Majeesh et al., 2002, Porter et al., 2009, Drysdale et al., 2006). Of note, both 17-AAG and 17-DMAG are currently being tested in clinical trials. Other epigenetic studies have demonstrated that inhibitors of histone deacetylases (HDACi) can suppress HIF-1 $\alpha$  protein expression via increasing its acetylation-dependent degradation. The Sirtuin 1 (SIRT1) deacetylase inactivates HIF-1 $\alpha$  by blocking HIF-1 $\alpha$ -p300/HIF- $\alpha$ -CBP and consequently inhibited HIF-1 transactivation of downstream target genes (Chen and Sang, 2011). Other novel inhibitors, such as YC-1 and PX-478, have also been identified to inhibit HIF-1 $\alpha$  protein accumulation and hypoxic induced HIF-1 transcriptional activity in a variety of cancer cell lines (Semenza, 2006, Schwartz et al., 2009, Schwartz et al., 2011).

Using an engineered U251 human glioma cell-based high-throughput screen system (U251-HRE), a large chemical library was explored for the identification of agents that inhibit HIF-1 activity, three of which were closely related to camptothecin analogues and DNA topoisomerase I inhibitors (Rapisarda et al., 2002). Topotecan was one of the camptothecin analogues which showed inhibition of hypoxia induced HIF-1 $\alpha$  accumulation and HIF-1-dependent gene expression at a low nanomolar concentration in U251 cells. Although mechanisms of camptothecin analogues in suppressing HIF-1 protein expression have not

been fully delineated, two other camptothecin analogues, topotecan and irinotecan, have gone through clinical trials and are currently used in cancer therapy.

RNA interference approaches using small interfering RNA (siRNA) or short hairpin RNA (shRNA) targeting HIF-1 $\alpha$  have been developed recently. These RNA oligos were designed using the coding sequence of HIF-1 $\alpha$  for specific targeting motifs. Several studies have demonstrated that the siRNAs can effectively suppress HIF-1 $\alpha$  expression, inhibit HIF-1 related signal transduction, increase cell apoptosis, and enhance sensitivity to chemotherapeutic drug (Hanze et al., 2003, Kessler et al., 2010, Yu et al., 2004). The application of siRNA *in vivo* studies also showed potential anti-tumor efficacy *in vivo* mouse models (Liao et al., 2012, Jiang et al., 2007) Noteworthy, treatment with siRNA or antisense oligonucleotides suppressed both HIF-1 $\alpha$  expression at both mRNA and protein levels (Zhang et al., 2004).

## **B. Small molecular inhibitors of HIF-1 DNA binding**

In this category, these inhibitors prevent HIF-1 binding to HREs and suppress transactivation of HIF-1 target genes. For example, Echinomycin binds to DNA of the HIF-1 recognition sequence 5'-CGTG-3' and inhibits HRE-mediated transcriptional activity in U251 glioma cells (Van Dyke and Dervan, 1984, Kong et al., 2005). Other inhibitors of HIF-1 DNA binding include polyamides (Olenyuk et al., 2004), and DJ12 (Jones and Harris, 2006).

## **C. Small molecular inhibitors of HIF-1 transcriptional activity**

Another mechanism of HIF-1 inhibition is at the level of transactivation. Bortezomib was the first therapeutic proteasome inhibitor to be tested in humans. It elevates HIF-1 $\alpha$  protein levels by blocking its degradation and specifically inhibits HIF-1 $\alpha$  C-TAD despite the activation of HIF-1 $\alpha$  coactivators p300 (Kaluz et al., 2006). In addition, the antifungal drug



amphotericin B was found to inhibit HIF-1 transcriptional activity by promoting interaction of HIF-1 $\alpha$  C-TAD with FIH-1 (Yeo et al., 2006).

#### **D. Small molecular inhibitors of HIF-1 dimerization**

HIF-1 $\alpha$ /  $\beta$  dimerization is mediated by the bHLH and PAS domains in N-terminal end of HIF-1 $\alpha$  and HIF-1 $\beta$  (Semenza et al., 1997). Although the structural and functional map of HIF-1 has been known since 1997, the development of specific small molecular inhibitors targeting this mechanism has long been attractive, yet elusive. Recently, through the screening from a FDA approved clinical trials drug library using a cell-based split-luciferase screening assay, acriflavine (ACF) was found to act directly on the HIF-1 $\alpha$ / $\beta$  dimerization (Lee et al., 2009). ACF, a commonly used antimicrobial agent discovered almost 100 years ago, is a mixture of 3,6-diamino-10-methylacridinium chloride (trypaflavin) and 3,6-diaminoacridine (proflavine). The study showed that ACF interacts with PAS-B subdomain of HIF-1 $\alpha$  or HIF-2 $\alpha$ , thus blocking the binding with HIF-1 $\beta$ . In addition, ACF treatment suppressed HIF-1 transcriptional activity and led to inhibition of tumor growth and vascularization in mice bearing prostate cancer xenografts. However, other studies also indicated ACF works as a topoisomerase I and II inhibitor to trigger permanent DNA damage and cell death in several cancer models (Hassan et al., 2011, Salerno et al., 2010). The finding that ACF also works as a topoisomerase I and II inhibitor seems in line with its HIF-1 $\alpha$  inhibition. Topoisomerase I inhibitors, such as camptothecin mentioned above, limit DNA transcription and have strong suppressive effect on hypoxia induced HIF-1 $\alpha$  accumulation in cancer cells (Xia et al., 2012, Rapisarda et al., 2002). The study conducted by Semenza's group, however, did not observe decreased HIF-1 $\alpha$  level by ACF at the concentration used to inhibit HIF-1 dimerization. Overall, in previous preclinical models, ACF showed short pharmacokinetic half-life and reached peak plasma concentrations well above the IC<sub>50</sub> values for anti-cancer activity (Song et al., 2005, Kim et al., 1997). With this background,

further clinical development of ACF as an anti-cancer drug seems promising for its dual inhibition of HIF-1 dimerization and HIF-1 $\alpha$  expression. Nevertheless, the mechanisms of action of ACF remain to be fully elucidated.

In conclusion, none of the presently available inhibitors appears to disrupt the HIF-1 pathway as an exclusive target. The design of more specific HIF-1 targeting agents is likely to become the future research priority (Semenza, 2007a, Mooring et al., 2011, Yewalkar et al., 2010, Narita et al., 2009, Tan et al., 2005, Park et al., 2006b). Blocking the dimerization domain of HIF-1 $\alpha$ /HIF-1 $\beta$  disables its ability to form HIF-1 $\alpha$ / $\beta$  heterodimers and negates HIF-1 activated adaptive reactions involved in tumor development. Since the dimerization is essential for a fully functional HIF-1 transcriptional factor, we proposed to explore novel inhibitors of HIF-1 $\alpha$ / $\beta$  heterodimerization as the major goal of this work.

**Table 1: HIF-1 inhibitors and their mechanism of action**

<b>Mechanism and Target of HIF-1 inhibition</b>	<b>Agent</b>
<b>I. Decreased HIF-1<math>\alpha</math> mRNA levels:</b>	GL331, siRNA, shRNA
<b>II. Decreased HIF-1<math>\alpha</math> protein levels</b>	
A. PI3K-AKT-mTOR	Wortmannin, LY294002, CCI-779, rapamycin, RAD-001, EZN-2968
B. HSP90	GA, 17-AAG, 17-DMAG, apigenin
C. Histone deacetylases	SIRT1, LAQ824, FK228
D. Topoisomerases	Topoisomerase I : topotecan, irinotecan
E. Cyclin-dependent kinases	flavopiridol
F. Microtubule targeting agents	2-methoxyestradiol, epothilone B, taxotere
G. Unknown targets	YC-1, PX-478, berberine, pseudolaric acid B, bisphenol A, manassantin B1, manassantin A, 4-O-methylsaucerneol, laurediterpenol, 103D5R
<b>III. Decreased binding of HIF-1 to DNA</b>	echinomycin, polyamides, DJ12
<b>IV. Decreased HIF-1-mediated transactivation</b>	
A. Proteasome:	bortezomib
B. Histone deacetylases:	SAHA/vorinostat, trichostatin A
C. P300:	chetomin
D. Unknown:	amphotericin B
<b>V. Decreased HIF-1<math>\alpha</math> and HIF-1 <math>\beta</math> dimerization</b>	acriflavine

## **1.9 Specific aims of the project**

To initiate hypoxia adaptive responses in cancer, HIF-1 $\alpha$  and HIF-1 $\beta$  heterodimerize and serve as a transcriptional activator to hundreds of target genes involved in tumor metabolism and vascularization. In an attempt to improve hypoxia-selective cytotoxicity, disruption of HIF-1 $\alpha$ / $\beta$  dimerization using small molecules is considered to be a promising therapeutic strategy. Our ultimate goal for this dissertation was to discover selective and effective inhibitor for HIF-1 dimerization. The long-term goal of the study would be to translate our therapeutic agents into clinic and benefit cancer patients.

To achieve these goals, the following specific aims were proposed:

***Aim 1: To Develop and Optimize a Reporter System for Bioluminescence Imaging of HIF-1 $\alpha$ /HIF1 $\beta$  Heterodimerization***

***Aim 2: To Conduct High-Content Screening of Inhibitors of HIF-1 $\alpha$ /HIF1 $\beta$  Dimerization *in Cellulo* and to Explore Structure-Activity Relationships***

***Aim 3: To Assess Selected Agents as Inhibitors of HIF-1-mediated Transcriptional Activity***

***Aim 4: To Evaluate Therapeutic Efficacy of Selected Inhibitors in Tumor Xenograft Bearing Mice***

## Chapter 2: Materials and Methods

### Cell Culture

HEK293T and U87 glioma cells (American Type Culture Collection, Manassas, VA) were maintained in Dulbecco's modified Eagle's medium/F-12 medium supplemented with 10% fetal calf serum (Gibco, Carlsbad, CA) and 100  $\mu\text{g}/\text{mL}$  normaxin (InvivoGen, San Diego, CA). Cells grew in a 37°C incubator with 5%  $\text{CO}_2$ .

### Construction of HIF-1 Heterodimerization Imaging lentiviral Vectors

DNA sequences of the human bHLH-PAS domain of HIF-1 $\alpha$  (residues 12-396) and HIF-1 $\beta$  (residues 11-510), and the N-terminus (NL; residues 1-437) and C-terminus (CL; residues 438-554) of firefly luciferase were prepared using PCR. These DNA sequences were then inserted into donor vectors (pDONR222 or pDONR222) via a Gateway BP reaction (Invitrogen, Carlsbad, CA). Following a Gateway LR reaction, we obtained two different orientations of HIF-1 $\alpha_{12-396}$  linking with N- terminal halves of luciferase in pLVDL301 vector (pLVDL 301-NL-HIF-1 $\alpha_{12-396}$  and pLVDL 301-HIF-1 $\alpha_{12-396}$ -NL), and two different orientations of HIF-1 $\beta_{11-510}$  linking with C- terminal halves of luciferase in pLVDL312 vector (pLVDL 312- CL-HIF-1 $\beta_{11-510}$  and pLVDL 312 -HIF-1 $\beta_{11-510}$ - CL) (**Fig. 7**). The gateway recombination cloning technique was based on bacteriophage lambda site-specific recombination system which facilitates the integration of lambda into the E. coli chromosome and the switch between the lytic and lysogenic pathways (Arkin et al., 1998). The method prevents traditional restriction enzyme based cloning limitations, accurately shuttles target DNA inserts to our vectors, and highly facilitates the creation of our DNA vectors. Vector pLVDL301 was specifically designed to contain two gateway cassettes, attR1 and attR2

sites, with downstream IRES to control eGFP gene expression. Whereas, Vector pLVDL312 also contains two gateway cassettes with IRES controlled mKate expression. We decided to use pLVDL301 as the destination vector (eGFP) for HIF-1 $\alpha$  reporter components and pLVDL312 (mKate) for HIF-1 $\beta$  reporter components.

In the following experiment to verify its functionality, HEK293T cells were plated at 70-80% confluence on the day of transfection. Cells were transfected (1:1) with four plasmid vectors alone, two different plasmid combinations, or single plasmids with nonsense-NL/CL. Volumes of Lipofectamine 2000 (Invitrogen) were used as recommended by the manufacturer for DNA delivery. The efficiency of plasmid transfection was assayed 48 h later via fluorescence using a microplate reader (Tecan, Männedorf, Switzerland). D-luciferin was added to the cell medium to perform bioluminescent imaging (BLI) by 1 min of photon counting using an IVIS 200 Series imaging system (Caliper Life Sciences, Hopkinton, MA). All BLI measurement were performed in triplicate. Relative light-unit readings were normalized by mKate fluorescence counts.

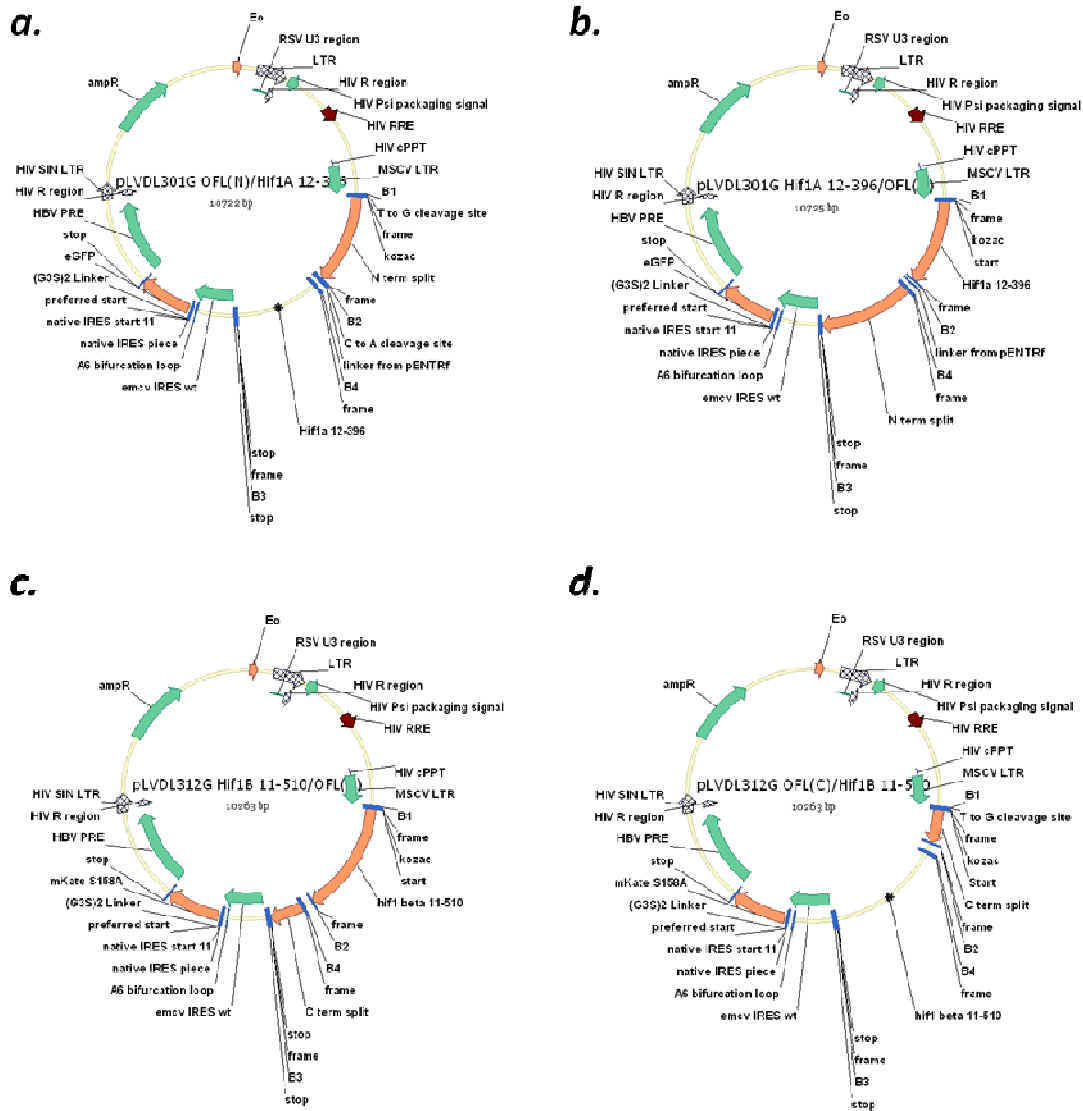


**Figure 7. Construction of HIF-1 $\alpha$ <sub>12-396</sub> and HIF-1 $\beta$ <sub>11-510</sub> reporter vectors.** Vector maps of the HIF-1 $\alpha$ <sub>12-396</sub>/N-terminal halves of luciferase (a,b) and HIF-1 $\beta$ <sub>11-510</sub>/C-terminal halves of luciferase fusion proteins(c,d). HIF-1 $\alpha$ <sub>12-396</sub> was cloned into the pLVDL 301 dual destination vector with eGFP reporter, creating pLVDL 301-NL-HIF-1 $\alpha$ <sub>12-396</sub> and pLVDL 301-HIF-1 $\alpha$ <sub>12-396</sub>-NL. HIF-1 $\beta$ <sub>11-510</sub> was cloned into the pLVDL 312 dual destination vector with mKate reporter, creating pLVDL 312- CL-HIF-1 $\beta$ <sub>11-510</sub> and pLVDL 312 -HIF-1 $\beta$ <sub>11-510</sub>-CL.

## **Production of Lentivirus for generating U87 HIF-1 Heterodimerization Reporter Cells**

Four different lentiviral stocks were produced by cotransfecting previously developed HIF-1 reporter lentiviral vectors and ViraPower Packaging Mix (Invitrogen) into HEK 293T packaging cells. The virus was harvested from the cell culture medium 24, 48, and 72 h after transfection. After filtering the collected medium through 0.22- $\mu\text{m}$  filters, the virus was concentrated via centrifugation at 3500 rpm for 30 min at 4°C. The concentrated lentiviral stocks were then stored at -80°C for later use.

After production of the lentiviral stocks, U87 cells were seeded in six-well culture dishes at 90% confluence and transduced with different pairs of HIF-1 $\alpha$  and HIF-1 $\beta$  reporters using lentivirus stocks (1:1, respectively). The culture medium was supplemented with 2  $\mu\text{g}/\text{mL}$  hexadimethrine bromide (Polybrene; Sigma, St. Louis, MO) at the time of transduction. At 24 h after transduction, the culture medium containing the virus was removed and replaced with fresh medium.

## **Flow Cytometry and Protein Expression Analysis of Transduced U87 Reporter Cells**

The transduced U87 cells were culture-expanded and analyzed for expression of the HIF-1 reporter using a FACSCalibur flow cytometer (BD Biosciences, San Jose, CA) after a week of transduction. The cells were collected via centrifugation at 1500 rpm, and resuspended into 500  $\mu\text{l}$  PBS. The coexpression of the reporter genes (eGFP and mKate) was analyzed using a 488- and 620-nm excitation laser, respectively. 100,000 events were collected each time, and the percentage of cells exhibiting dual eGFP and mKate fluorescence was determined using FlowJo X program (Ashland, OR).



### **Selection of Stably Transduced U87 Reporter Cells**

Stably expressed U87/NL1 $\alpha$ /CL1 $\beta$  reporter cells were selected using a BD FACSAria cell sorter (BD Biosciences) for future screening experiments. Only dual pLVDL 301-NL-HIF-1 $\alpha$ <sub>12-396</sub> and pLVDL 312-CL-HIF-1 $\beta$ <sub>11-510</sub> expressed cells within a narrow region spanning about 10<sup>3</sup> on the eGFP and mKate expression scale of a histogram plot were collected. The sorted U87/NL1 $\alpha$ /CL1 $\beta$  cells were replated back to 96-well plates at the concentration of 20 cells/well. After a week of growing, each well was examined for dual eGFP and mKate fluorescence under a microscope. The U87/NL1 $\alpha$ /CL1 $\beta$  cells with the most homogenous expression of dual reporters were dispersed into new 12-well plates for further expansion. These stably transduced U87/NL1 $\alpha$ /CL1 $\beta$  cells were later used in the drug screening experiments.

### **Competitive HIF- $\alpha$ / $\beta$ Protein-Binding Assay**

U87/NL1 $\alpha$ /CL1 $\beta$  cells were seeded at 5 x 10<sup>4</sup> cells per well in a 24-well plate, incubated for 12 h, and transfected with HIF-1 $\alpha$ , HIF-1 $\beta$ , or control DNA. BLI and fluorescent imaging of U87 reporter cells were performed at 24 and 48 h after transfection. Also, a WST-1 cell viability test (Cayman Chemistry, Ann Arbor, MI) was performed in each group of experiments after the imaging. All experiments were done in triplicate.

### **Hypoxia Chamber-Induced Endogenous HIF-1 $\alpha$ Competition Assay**

U87/NL1 $\alpha$ /CL1 $\beta$  cells were seeded at 5 x 10<sup>4</sup> cells per well in a 24-well plate and incubated for 12 h. To induce hypoxia, cells were placed in a modular incubator chamber (Billups-Rothenberg Inc., Del Mar, CA) and flushed with a mixture of gas consisting of 5%

O<sub>2</sub>, 5% CO<sub>2</sub>, and balance N<sub>2</sub>. The chamber was then sealed and incubated at 37°C. Cells under normal culture conditions were used as controls. BLI, fluorescent imaging, and WST-1 cell viability testing were performed 24 and 48 h after treatment. Different groups of cells were collected and lysed for later western blot analysis.

### **High-Throughput Drug Screening *In Vitro***

Stably transduced U87/NL1 $\alpha$ /CL1 $\beta$  cells were preseeded in 96-well plates at 4 x 10<sup>4</sup> cells per well. A library of 41 compounds, previously reported to inhibit HIF-1 activity, or a vehicle (0.1% dimethyl sulfoxide [DMSO]) were added to each well for 24 h. The cells were imaged and analyzed using BLI with an IVIS 200 Series system via 1-min photon counting and fluorescence with a Tecan microplate reader. All BLI results were analyzed using Living Image software program (Caliper Life Sciences, Hopkinton, MA). All the experiments were done in triplicate. If the drug treatment resulted in a significant decrease in the BLI signal, the cells were further analyzed using the WST-1 cell viability test.

### **Chemical Reagents and Instrumentation**

Reagents and solvents were purchased from Aldrich Chemical Co. (Milwaukee, WI) and used without further purification. Thin-layer chromatography was performed with precoated Kieselgel 60 F254 aluminum plates (Merck, Darmstadt, Germany). Proton, <sup>13</sup>C, and <sup>19</sup>F nuclear magnetic resonance (NMR) spectra were recorded using a Bruker 300-MHz spectrometer (Bruker, Rheinstetten, Germany) with tetramethylsilane as an internal reference at The University of Texas MD Anderson Cancer Center. High-resolution mass spectra for newly synthesized compounds were obtained with a Bruker BioTOF II mass

spectrometer (Bruker, Rheinstetten, Germany) at the University of Minnesota using electrospray ionization. Neutral proflavine was prepared from 3,6-diaminoacridine hemisulfate (Aldrich Chemical, Milwaukee, WI), which was dissolved in water, and 10%  $\text{NH}_4\text{OH}$  was added to the solution until the pH was 8 under vigorous stirring. The solution was then filtered, washed with water, and dried to afford neutral proflavine. Compounds 1, 3, 4, and 5 were purchased from Aldrich Chemical Co. and used as received. Compound 2 was prepared using a reported procedure for similar compounds. The detailed synthesis of other compounds will be covered in the following section.

## Chemistry Synthesis

**General procedure A:** reaction of proflavine with anhydrides for synthesis of compounds 6-8 as reported previously.

A solution of anhydride (3 eq.) was added dropwise to proflavine (1 mmol, 1 eq.) in pyridine (6 mL) and triethylamine (0.5 mL) at 50 °C under  $\text{N}_2$  atmosphere with vigorous stirring. Stirring was continued for 1 h at 80 °C. The mixture was then poured into water (80 mL). The obtained precipitate was filtered, washed with water, dried, and recrystallized using ethanol to yield the corresponding product.

**General procedure B:** reaction of proflavine with alkoyl chlorides for synthesis of compounds 9-15

A solution of aroyl chloride (3 eq.) in acetone (10 mL) was added dropwise to proflavine (1 mmol, 1 eq.) and  $\text{K}_2\text{CO}_3$  (10 eq.) in acetone (40 mL) at 0 °C under  $\text{N}_2$  with vigorous stirring. Stirring was continued for 15 h at room temperature. The mixture was then poured into a solution of aqueous  $\text{NaHCO}_3$  (40%, 80 mL). After cooling at 5 °C, the obtained

precipitate was filtered, washed with water, dried, and recrystallized from ethanol to yield the corresponding product.

**General procedure C:** reaction of proflavine with aroyl chlorides for synthesis of compounds 16-24 as reported previously.

A solution of aroyl chloride (3 eq.) in acetone (10 mL) was added dropwise to proflavine (1.43 mmol, 1 eq.) and  $K_2CO_3$  (10 eq.) in acetone (40 mL), at 0 °C under  $N_2$  with vigorous stirring. Stirring was continued for 15 h at room temperature. The mixture was then poured into water (30 mL) and then a satd. aq.  $NaHCO_3$  solution (20 mL). After cooling at 5 °C, the obtained precipitate was filtered, washed with water and then ether (15 mL), and dried to yield the corresponding product.

#### **Preparation of *N,N*-(Acridine-3,6-Diyl)Dicyclopropanecarboxamide (compound 10)**

General procedure B: compound 10 was obtained as yellow fluffy powder at a yield of 45%.

$^1H$  NMR: (DMSO- $d_6$ ):  $\delta$  11.43 (s, 2H, NH), 9.56 (s, 1H,  $H_9$ ), 8.85 (s, 2H,  $H_4$ ,  $H_5$ ), 8.35 (d,  $J$  = 9.0, 2H,  $H_1, H_8$ ), 7.81 (d,  $J$  = 9.0, 2H,  $H_2$ ,  $H_7$ ), 2.03 (m, 2H, CH), 0.95 (m, 8H,  $CH_2$ : cyclopropyl).

#### **Preparation of *N,N*-(Acridine-3,6-Diyl)Dicyclobutanecarboxamide (compound 11)**

General procedure B: compound 11 was obtained as yellow powder at a yield of 57%.  $^1H$

NMR: (DMSO- $d_6$ ):  $\delta$  10.45 (s, 2H, NH), 9.13 (s, 1H,  $H_9$ ), 8.67 (s, 2H,  $H_4$ ,  $H_5$ ), 8.15 (d,  $J$  = 9.0, 2H,  $H_1, H_8$ ), 7.68 (d,  $J$  = 9.0, 2H,  $H_2$ ,  $H_7$ ), 2.40-1.80 (m, 14H, CH,  $CH_2$ : cyclobutyl).

#### **Preparation of *N,N*-(Acridine-3,6-Diyl)Dicyclopentanecarboxamide (compound 12)**

General procedure B: compound 12 was obtained as yellow powder at a yield of 57%.  $^1H$

NMR: (DMSO- $d_6$ ):  $\delta$  10.91 (s, 2H, NH), 9.37 (s, 1H,  $H_9$ ), 8.80 (s, 2H,  $H_4$ ,  $H_5$ ), 8.25 (d,  $J$  = 9.0,

2H, H<sub>1</sub>,H<sub>8</sub>), 7.78 (d,  $J = 9.0$ , 2H, H<sub>2</sub>, H<sub>7</sub>), 3.00 (m, 2H, CH: cyclopentyl), 2.00-1.50 (m, 16H, CH<sub>2</sub>: cyclopentyl).

#### **Preparation of *N,N*-(Acridine-3,6-Diyl)Dicyclohexanecarboxamide (compound 13)**

General procedure B: compound 13 was obtained as yellow powder at a yield of 57%. <sup>1</sup>H NMR: (DMSO-d<sub>6</sub>):  $\delta$  11.06 (s, 2H, NH), 9.56 (s, 1H, H<sub>9</sub>), 8.91 (s, 2H, H<sub>4</sub>, H<sub>5</sub>), 8.33 (d,  $J = 9.0$ , 2H, H<sub>1</sub>,H<sub>8</sub>), 7.82 (d,  $J = 9.0$ , 2H, H<sub>2</sub>, H<sub>7</sub>), 2.55 (m, 2H, CH: cyclohexyl), 2.00-1.62 (m, 11H, CH<sub>2</sub>: cyclohexyl), 1.55-1.18 (m, 11H, CH<sub>2</sub>: cyclohexyl).

#### **Preparation of *N,N*-(Acridine-3,6-Diyl)Bis(Adamantanecarboxamide) (compound 14)**

General procedure B: compound 13 was obtained as yellow powder at a yield of 57%. <sup>1</sup>H NMR: (DMSO-d<sub>6</sub>):  $\delta$  11.06 (s, 2H, NH), 9.56 (s, 1H, H<sub>9</sub>), 8.91 (s, 2H, H<sub>4</sub>, H<sub>5</sub>), 8.33 (d,  $J = 9.0$ , 2H, H<sub>1</sub>,H<sub>8</sub>), 7.82 (d,  $J = 9.0$ , 2H, H<sub>2</sub>, H<sub>7</sub>), 2.55 (m, 2H, CH: cyclohexyl), 2.00-1.62 (m, 11H, CH<sub>2</sub>: cyclohexyl), 1.55-1.18 (m, 11H, CH<sub>2</sub>: cyclohexyl).

#### **Preparation of *N,N*-(Acridine-3,6-Diyl)Bis(2,2,3,3-Tetramethylcyclopropanecarboxamide) (compound 15)**

General procedure B: compound 15 was obtained as yellow powder at a yield of 65%. <sup>1</sup>H NMR: (DMSO-d<sub>6</sub>):  $\delta$  11.06 (s, 2H, NH), 9.56 (s, 1H, H<sub>9</sub>), 8.91 (s, 2H, H<sub>4</sub>, H<sub>5</sub>), 8.33 (d,  $J = 9.0$ , 2H, H<sub>1</sub>,H<sub>8</sub>), 7.82 (d,  $J = 9.0$ , 2H, H<sub>2</sub>, H<sub>7</sub>), 2.55 (m, 2H, CH: cyclohexyl), 2.00-1.62 (m, 11H, CH<sub>2</sub>: cyclohexyl), 1.55-1.18 (m, 11H, CH<sub>2</sub>: cyclohexyl).

#### **Preparation of *N,N*-(Acridine-3,6-Diyl)Dibenzenesulfonamide (compound 17)**

General procedure C: compound 17 was obtained as yellow powder at a yield of 30%. <sup>1</sup>H NMR: (DMSO-d<sub>6</sub>):  $\delta$  11.06 (s, 2H, NH), 9.56 (s, 1H, H<sub>9</sub>), 8.91 (s, 2H, H<sub>4</sub>, H<sub>5</sub>), 8.33 (d,  $J = 9.0$ ,

2H, H<sub>1</sub>,H<sub>8</sub>), 7.82 (d, *J* = 9.0, 2H, H<sub>2</sub>, H<sub>7</sub>), 2.55 (m, 2H, CH: cyclohexyl), 2.00-1.62 (m, 11H, CH<sub>2</sub>: cyclohexyl), 1.55-1.18 (m, 11H, CH<sub>2</sub>: cyclohexyl).

### **Preparation of *N,N*-(Acridine-3,6-Diyl)Bis(4-(Trifluoromethyl)Benzamide) (compound 19)**

General procedure C: compound 19 was obtained as yellow powder at a yield of 65%. <sup>1</sup>H NMR: (DMSO-d<sub>6</sub>): δ 11.44 (s, 2H, NH), 9.50 (s, 1H, H<sub>9</sub>), 9.01 (s, 2H, H<sub>4</sub>, H<sub>5</sub>), 8.31 (d, *J* = 9.0, 2H, H<sub>1</sub>,H<sub>8</sub>), 8.24 (d, *J* = 8.1, 4H, Ph), 8.08 (d, *J* = 9.0, 2H, H<sub>2</sub>, H<sub>7</sub>), 7.92 (d, *J* = 8.1, 4H, Ph).

### **Preparation of *N,N*-(Acridine-3,6-Diyl)Bis(4-*Tert*-Butylbenzamide) (compound 20)**

General procedure C: compound 20 was obtained as yellow powder at a yield of 60%. <sup>1</sup>H NMR: (DMSO-d<sub>6</sub>): δ 10.73 (s, 2H, NH), 9.06 (s, 1H, H<sub>9</sub>), 8.78 (s, 2H, H<sub>4</sub>, H<sub>5</sub>), 8.16 (d, *J* = 9.0, 2H, H<sub>1</sub>,H<sub>8</sub>), 7.99 (d, *J* = 8.7, 2H, Ph), 7.95 (d, *J* = 9.0, 2H, H<sub>2</sub>, H<sub>7</sub>), 7.60 (d, *J* = 8.7, 2H, Ph), 1.35 (s, 18H, *t*-Bu).

### **Preparation of *N,N*-(Acridine-3,6-Diyl)Bis(3,4-Dimethoxybenzamide) (compound 21)**

General procedure C: compound 20 was obtained as yellow powder at a yield of 60%. <sup>1</sup>H NMR: (DMSO-d<sub>6</sub>): δ 11.22 (s, 2H, NH), 9.55 (s, 1H, H<sub>9</sub>), 9.01 (s, 2H, H<sub>4</sub>, H<sub>5</sub>), 8.41 (d, *J* = 8.1, 2H, Ph), 8.22 (d, *J* = 9.0, 2H, H<sub>1</sub>,H<sub>8</sub>), 7.88 (d, *J* = 9.0, 2H, H<sub>2</sub>, H<sub>7</sub>), 7.65 (s, 2H, Ph), 7.16 (d, *J* = 8.1, 2H, Ph).

## **Structure Activity Relationship of Acridine Analogs**

U87/NL1α/CL1β reporter cells were preseeded in 96-well plates at 4 x 10<sup>4</sup> cells per well. A list of our developed acridine analogs with side chain derivatization, ACF (10μM, positive control) or a vehicle (0.1% dimethyl sulfoxide [DMSO]) were added to each well for

24 h incubation. The cells were analyzed by BLI with an IVIS 200 Series system via 1-min photon counting and fluorescence imaging with a Tecan microplate reader, and tested for the WST-1 cell viability assay. All the experiments were done in triplicate.

### **HIF-1 transcriptional activity reporter assay**

C6#4 reporter cells previously developed in our lab were seeded at  $1 \times 10^4$  per well in a 96-well plate, incubated for 12 h, and changed new medium with supplement of 100  $\mu$ M  $\text{CoCl}_2$ , producing chemically-induced hypoxia (Serganova et al., 2004). After 4 h, the cells were treated with different concentrations of vehicle, ACF, M-TMCP and D-TMCP for additional 24 h incubation. Fluorescent imaging was performed with a Tecan microplate reader to analyze GFP versus DsRed expression. All the experiments were done in triplicate. The WST-1 cell viability test (Cayman Chemistry, Ann Arbor, MI) was performed in each treatment group after the fluorescent imaging.

### **Rapamycin-regulated *firefly* luciferase complementation cell-based reporter assays**

This reporter assay utilized the rapamycin-binding domain (FRB) of the kinase mammalian target of rapamycin and FK506-binding protein 12 (FKBP) fused with firefly luciferase halves, respectively, to develop rapamycin-regulated firefly luciferase complementation assay (Luker et al., 2004). HEK293T cells were plated to 70-80% confluence on the day of transfection. HEK-293 cells transfected with (1:1) FRB-NLuc/CLuc-FKBP (DNA vectors were obtained from Dr. David Piwnica-Worms's lab at Washington University School of Medicine). Volumes of Lipofectamine 2000 (Invitrogen) were used as recommended by the manufacturer for DNA delivery. In this firefly complementation

construct design, rapamycin induced FRB/FKBP association and reconstituted luciferase activity in cells. Therefore, the efficiency of plasmid transfection was assayed via BLI 48 h later after incubation of 50 nM rapamycin for 6 h. Transfected cells were then transferred into a 12 well plate at  $5 \times 10^4$  per well, incubated for 6 h, and changed with new medium. For the first group of experiments, the transfected cells were first incubated with 50 nM rapamycin for 6 h to reconstitute luciferase, and then treated with or without 10  $\mu$ M ACF, N-3-(2,2,3,3-tetramethylcyclopropane-carboxamide)-6-aminoacridine hydrochloric acid salt (M-TMCP) and N,N'-(acridine-3,6-diyl)bis(2,2,3,3-tetramethyl-cyclopropanecarboxamide) (D-TMCP) for 24 h to examine the effect of these inhibitors in disrupting luciferase pairs. For the second group, 10  $\mu$ M vehicles ACF, M-TMCP and D-TMCP were first added to the cell medium for 24 h incubation. Then the cells were treated with 50 nM rapamycin for additional 6 h. All BLI were performed by 1 min of photon counting using an IVIS 200 Series imaging system (Caliper Life Sciences, Hopkinton, MA).

### **Quantitative real-time reverse-transcription PCR (qRT-PCR)**

U87 WT cells were incubated under normoxia or hypoxia in the absence or presence of ACF, M-TMCP and D-TMCP (0 or 10  $\mu$ M) for 24 hours. Total RNA isolated from  $1 \times 10^5$  cells (RNeasy mini kit; Qiagen, Valencia, CA) was reversely transcribed to cDNA by using RT<sup>2</sup> First Strand Kit (Qiagen, Valencia, CA). First-strand cDNA equivalent to 5  $\mu$ g RNA was applied in real-time PCR using RT<sup>2</sup> SYBR Green Mastermix and RT<sup>2</sup> Profiler Hypoxia Signaling Pathway PCR Arrays (Qiagen, Valencia, CA) following the manufacturer's protocol. qPCR conditions were 95°C for 10 min, followed by 40 cycles of 95°C for 15 sec, annealing at 60°C for 1 min. Fluorescence was collected at 60°C step. Data was normalized to the housekeeping gene beta-actin (ACTB). Controls were also included on each array for



genomic DNA contamination, RNA quality, and general PCR performance. The experiments were carried out in three independent experiments and analyzed using Applied Biosystems 7500 Fast Real-Time PCR System and RT<sup>2</sup> Profiler PCR Array Data Analysis v3.5 (Qiagen, Valencia, CA).

### **Western Blot Analysis**

U87 cells were lysed with urea lysis buffer. Cell lysates (50 µg) were separated on 4-12% Bis-Tris sodium dodecyl sulfate-polyacrylamide gel electrophoresis gels (Invitrogen) and transferred onto nitrocellulose membranes. The membranes were blocked for 3 h in phosphate-buffered saline containing 5% nonfat dry milk and incubated in the same blocking buffer at 4°C overnight with primary antibodies against HIF-1α (1:500 dilution; Novus Biologicals, Littleton, CO) and β-actin (1:1000 dilution; Thermo Fisher Scientific, Waltham, MA). After incubation of corresponding secondary antibodies, proteins were detected using ECL chemiluminescence (Pierce, Rockford, IL).

### **Tumor Xenograft and Drug Treatment**

Nude mice (NCR nu/nu) were purchased at 4 weeks of age from Taconic Farms (Hudson, NY). Stably transduced U87/NL1α/CL1β reporter cells ( $5 \times 10^6$  cells in 0.2 mL of Dulbecco's modified Eagle's medium) were injected subcutaneously into the right thigh of each mouse. The animals' tumor growth patterns and physical conditions were monitored throughout the whole study. Tumor volume (V) was calculated using the following formula:  $V = \text{length} \times \text{width} \times \text{height} \times 0.52$ . Once their tumor volumes reached approximately 100 mm<sup>3</sup>, the tumor-bearing mice were randomly categorized into four groups (8/group). They were

then intraperitoneally (*i.p.*) administered 150  $\mu$ L of M-TMCP (2 mg/kg in 3%DMSO in saline; per *i.p.* injection), D-TMCP (2 mg/kg in 3%DMSO in saline; per *i.p.* injection), ACF (2 mg/kg in 3%DMSO in saline; per *i.p.* injection), or saline in each groups of mice over 14 days. The animals' physiological parameters (weights, food intake, organ weights and motor activity), tumor volumes, and BLI were longitudinally monitored 3 h after each injection. On day 14 of treatment, BLI was performed before and 3 h after drug injection. All animals were handled in accordance with The University of Texas MD Anderson Institutional Animal Care and Use Committee guidelines. Statistical analyses were performed and fitted using with the Prism software program (GraphPad Software, La Jolla, CA).

### **Organ Toxicity Assay**

After 21 daily treatments of D-TMCP (doses of 0, 1, 2, 5, 10 mg/kg in 3%DMSO in saline; 150  $\mu$ l per *i.p.* injection), the mice were sacrificed. The animals' physiological parameters (weights, food intake, organ weights and motor activity) were longitudinally monitored. Their organ samples, such as brain, heart, liver and kidney, were obtained and fixed in 10% formalin, embedded in paraffin, and sectioned into 5- $\mu$ m slices for hematoxylin and eosin staining (H&E) or immunochemical staining of Ki67 (1:100 dilution; Thermo Fisher Scientific, Waltham, MA).

### **Immunohistochemistry and Immunofluorescence**

The U87/NL1 $\alpha$ /CL1 $\beta$  tumor bearing mice were sacrificed after the 14th day of treatment. Tumor samples were obtained and fixed in 10% formalin, embedded in paraffin, and sectioned into 5- $\mu$ m slices first for immunochemical staining. The primary antibodies

used in immunochemical staining were those against CD34, GLUT-1, VEGF, Ki67 and Annexin V. According to the host of the primary antibody, compatible secondary antibodies (Vectastain ABC Kit; Vector Labs, Burlingame, CA) were applied. The tumor sections were then visualized by adding diaminobenzidine (Dako, Carpinteria, CA) and counterstained with hematoxylin in IHC or hoechst in immunofluorescent staining. Four representative regions (10-20× objectives) in each tumor were photographed. The areas of CD34, Ki67 and Annexin V staining were quantified under × 400 magnifications with a position pixel algorithm using the ImageJ software program (National Institutes of Health, Bethesda, MD).

### **Statistical Analyses**

Statistical analyses were performed using built-in statistical software programs from Prism software program (GraphPad Software, La Jolla, CA). The specific test and significant level of each experiment were showed in the each figure legend.

## Chapter 3: Development and Optimization of a Reporter System for Bioluminescence Imaging of HIF-1 $\alpha$ /HIF1 $\beta$ Heterodimerization

### 3.1 Overview of the HIF-1 $\alpha$ / $\beta$ Heterodimerization reporter system

The first aim of this study was to develop a split *firefly* luciferase (FLuc) fragment complementation-based approach for quantitative bioluminescence imaging of HIF-1 $\alpha$ / $\beta$  heterodimerization *in vitro* and *in vivo*. In this reporter system, physical interactions of two HIF-1 $\alpha$ / $\beta$  proteins bring the N- and C-terminal fragments of FLuc close enough to reconstitute the luciferase activity and result in photon emission (luminescence) in the presence of the luciferase substrate. Reciprocally, the addition of inhibitor of HIF-1 $\alpha$ / $\beta$  dimerization can disrupt the interaction and results in loss of luciferase activity. Thus, this reporter system can be used as a drug screening tool for HIF-1 dimerization inhibitors. The schematic illustration of the split luciferase complementation system is summarized in Figure 8.

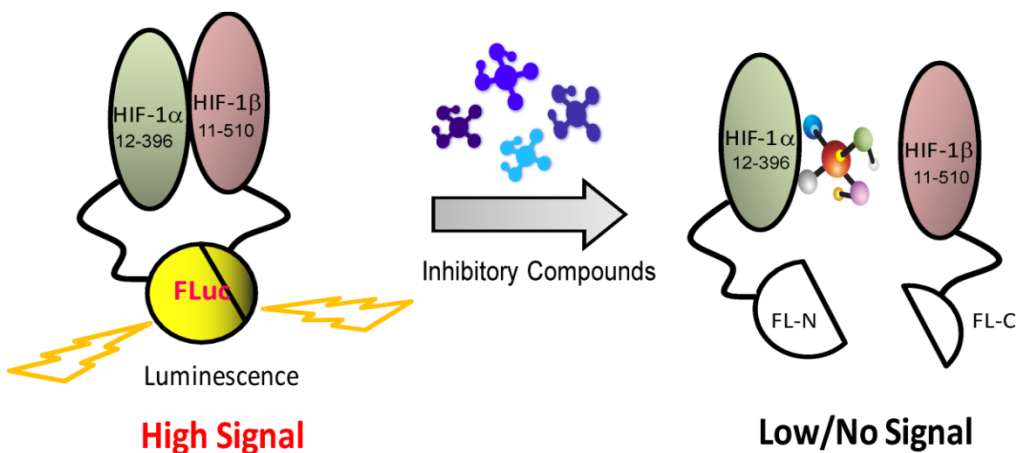


**Figure 8. Schematic of HIF-1 dimerization reporter system in drug screening.** Spontaneous association of HIF-1 $\alpha$ <sub>12-396</sub> and HIF-1 $\beta$ <sub>11-510</sub> brings inactive fragments of firefly luciferase into close proximity to reconstitute bioluminescence activity. Disruption of HIF-1 $\alpha$ <sub>12-396</sub> and HIF-1 $\beta$ <sub>11-510</sub> dimerization results in no bioluminescence activity.

### 3.2 Optimization of HIF-1 $\alpha$ / $\beta$ heterodimerization reporter system

Using four lentiviral vector constructs with different positions of individual FLuc fragments in relation to HIF-1 $\alpha$  and HIF-1 $\beta$  (N- or C-terminal fusions through a linker; major features showed in **Fig. 9**), the highest constitutive bioluminescence signal was observed from the HEK293 cells transiently transfected with NL-1 $\alpha$  and CL-1 $\beta$  or 1 $\alpha$ -NL and 1 $\beta$ -CL vector pairs (**Fig. 10**), whereas no Fluc activity was observed in HEK293 cells transfected with either one of the vectors or with negative control vectors containing a nonsense sequence in place of the PAS domains of HIF-1 $\alpha$  and HIF-1 $\beta$  (NL-non or non-CL).

In consistent, similar results were also observed in U87 human glioma cells, which were stably transduced with different pairs or individual lentiviral vectors. The magnitude of expression of individual reporter constructs in stably transduced U87 cells was very similar, based on co-expression levels of eGFP and mKate fluorescent proteins measured by dual-color FACS (**Fig. 11**). The highest BLI signal was observed with NL-1 $\alpha$  + CL-1 $\beta$  vector pair (**Fig. 12A**). Overall, we found that a *head-to-head* or *tail-to-tail* combination of the fusion proteins produced better BLI signals than *head-to-tail* combination did. U87 cells stably transduced with NL-1 $\alpha$  + CL-1 $\beta$  vector pairs (U87/NL1 $\alpha$ /CL1 $\beta$  cells) were chosen to establish a HIF-1 $\alpha$ / $\beta$  heterodimerization reporter system in the following experiments. The subcellular co-localization of co-expressed eGFP and mKate reporter proteins in the U87/NL1 $\alpha$ /CL1 $\beta$  cells was also confirmed by fluorescence confocal microscopy (**Fig. 12B**).

In addition, the degradation half-life of the enzymatically active NL-1 $\alpha$  + CL-1 $\beta$  reporter complex in U87/NL1 $\alpha$ /CL1 $\beta$  cells was about 34.12 min, as measured by BLI after cycloheximide block (**Fig. 13**). In subsequent *in vitro* experiments, for the assessment of inhibitors of HIF-1 $\alpha$  and HIF-1 $\beta$  heterodimerization in U87/NL1 $\alpha$ /CL1 $\beta$  cells, BLI was performed no earlier than 24h post initiation of incubation.

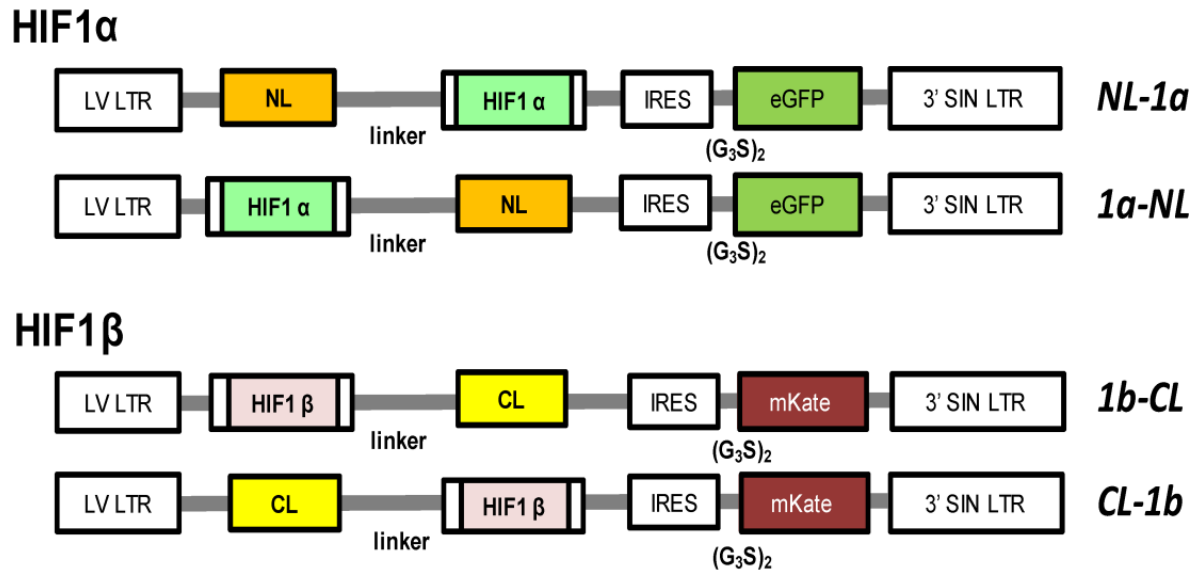


**Figure 9. Schematic drawing shows major features of four lentiviral vectors of HIF-1 $\alpha$  and HIF-1 $\beta$  dimerization reporters.** Four developed lentiviral vector constructs with different positions of individual N- or C-terminal Fluc fragments (NL or CL) in relation to HIF-1 $\alpha$  and HIF-1 $\beta$  subdomains, fused through a flexible linker. Two different orientations of HIF-1 $\alpha$ <sub>12-396</sub> linking with NL in pLVDL301 vector (pLVDL 301-NL-HIF-1 $\alpha$ <sub>12-396</sub> and pLVDL 301-HIF-1 $\alpha$ <sub>12-396</sub>-NL) co-expressed eGFP fluorescent protein, and another two orientations of HIF-1 $\beta$ <sub>11-510</sub> linking with CL in pLVDL312 vector (pLVDL 312- CL-HIF-1 $\beta$ <sub>11-510</sub> and pLVDL 312 -HIF-1 $\beta$ <sub>11-510</sub>- CL) co-expressed mKate fluorescent protein.

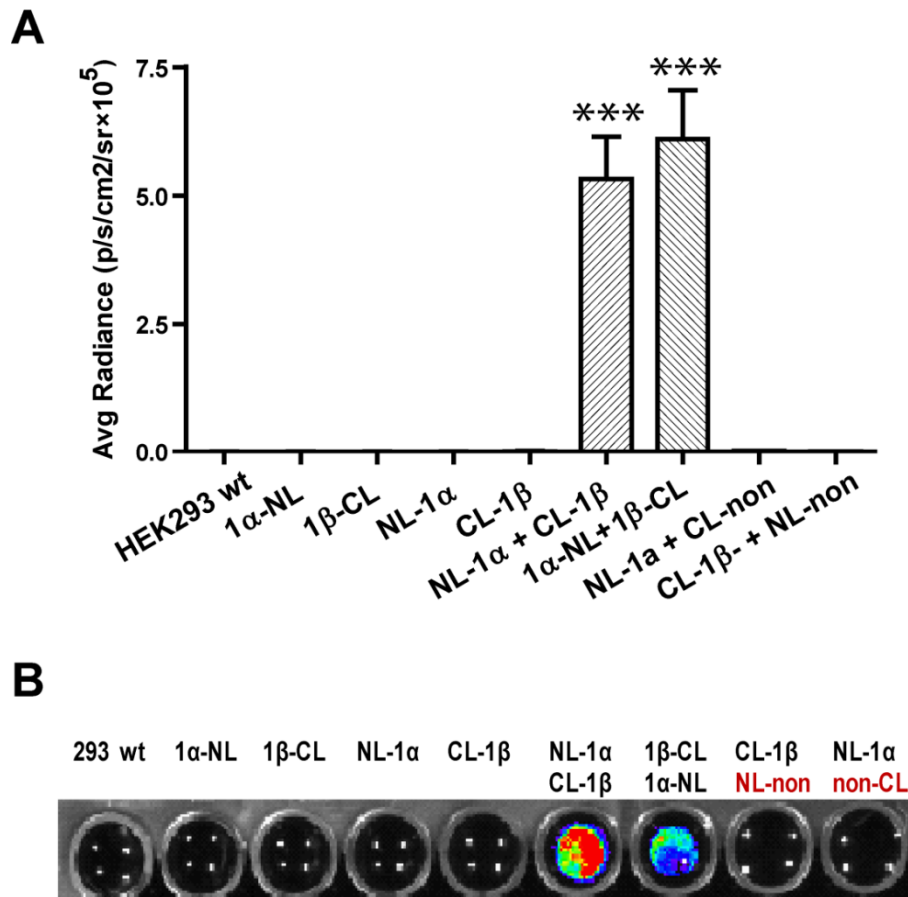


**Figure 10. Bioluminescence in HEK293 cells transiently transfected with NL-1α and CL-1β or 1α-NL and 1β-CL vector pairs as indicated.** The highest constitutive bioluminescence signal was observed from the HEK293 cells transiently transfected with NL-1α and CL-1β or 1α-NL and 1β-CL vector pairs, whereas no Fluc activity was observed in HEK293 cells transfected with either one of the vectors or with negative control vectors containing a nonsense sequence in place of the PAS domains of HIF-1α and HIF-1β (NL-non or non-CL). Data are expressed as average photon radiance ± SEM of quadruplicate wells. (\*,  $P < 0.05$ ; \*\*,  $P < 0.01$ ; \*\*\*,  $P < 0.005$ )

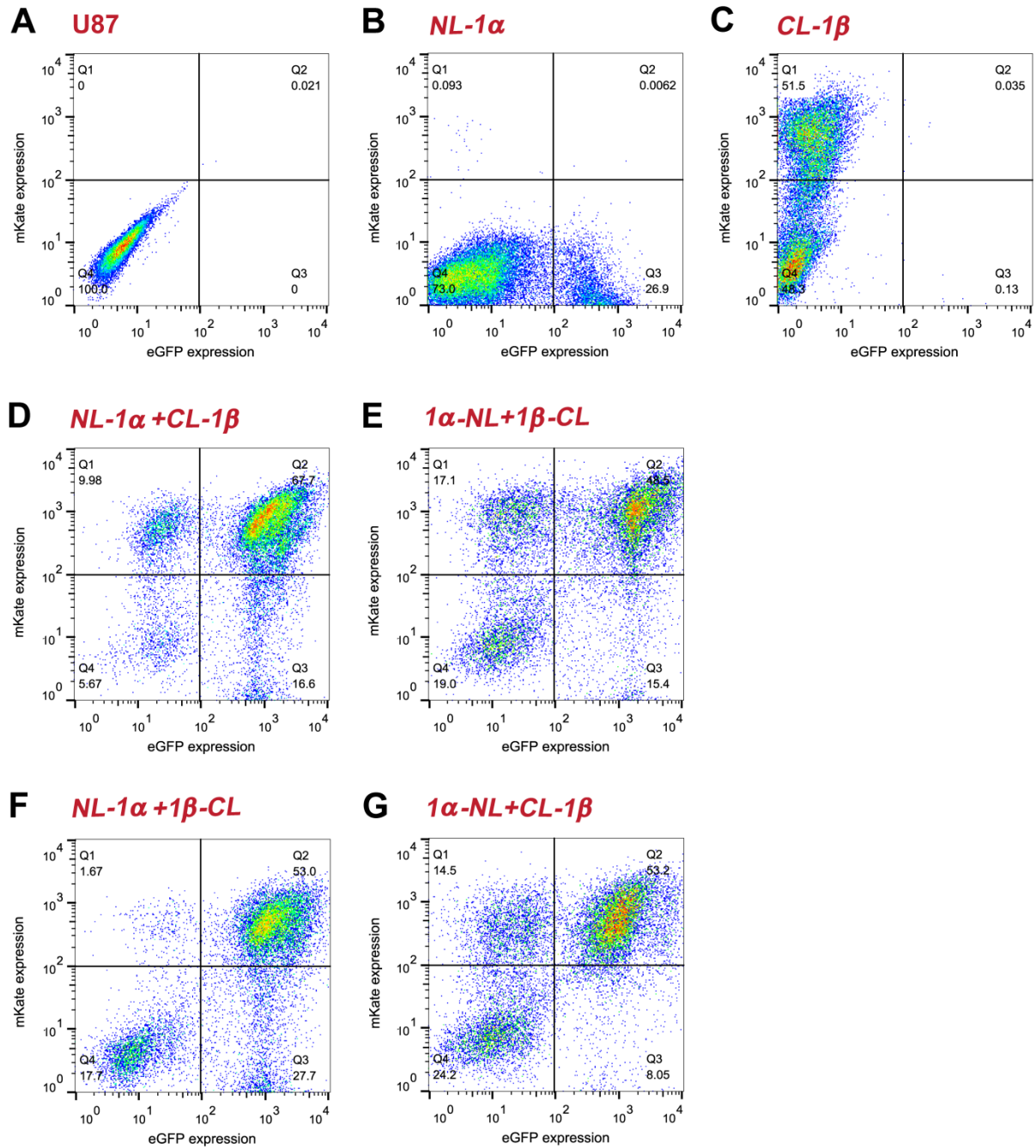


**Figure 11. Result of cell cytometry to evaluate eGFP and mKate coexpression level in transduced U87 cells.** A) Wt U87 cells. B, C) Single transfection of NL-1 $\alpha$  or CL-1 $\beta$  in U87 cells. D,E,F,G) Dual transduction of four different complementary reporter combinations in U87 cells.



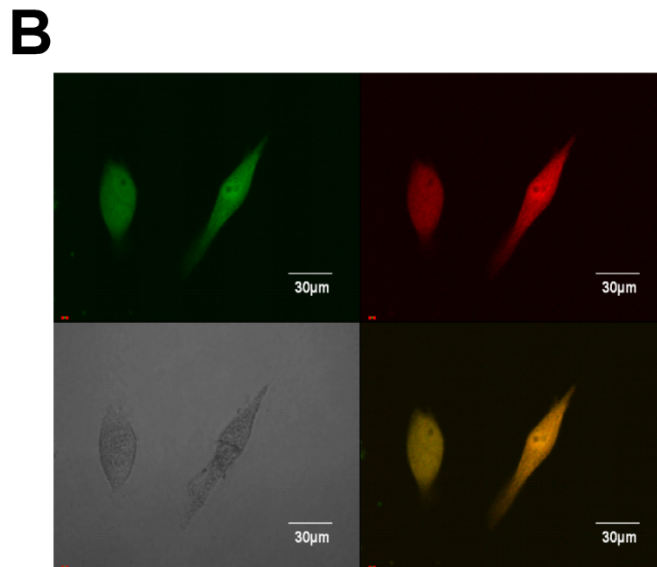
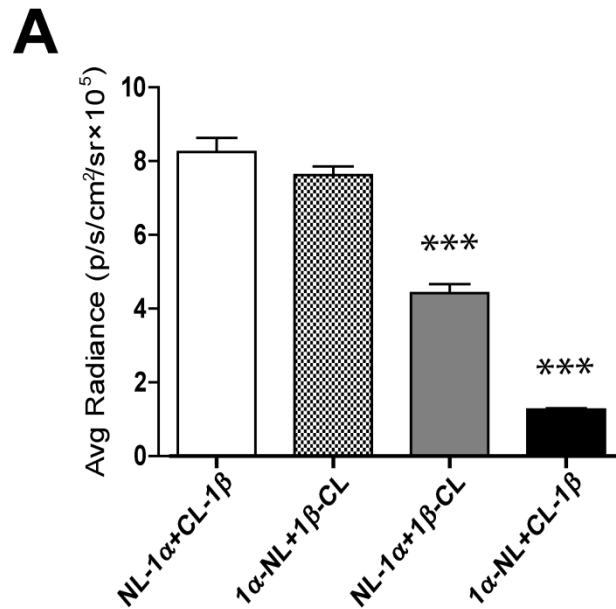


**Figure 12.** A) Highest BLI signal was observed with U87 human glioma cells transfected with NL-1α + CL-1β vector pair, following by 1α-NL + 1β-CL (*head-to-head* or *tail-to-tail* position), NL-1α + 1β-CL and 1α-NL + CL-1β (*head-to-tail* position). Result of quantitative BLI signal measurement indicated *head-to-head* or *tail-to-tail* HIF-1 complementation pairs demonstrated higher Fluc activity than *head-to-tail* pairs. B) Subcellular co-localization of co-expressed eGFP (NL-1α) and mKate (CL-1β) reporter proteins in the U87/NL1α/CL1β cells was confirmed by fluorescence confocal microscopy. The merged panel in lower-right shows colocalization (yellow) of NL-1α and CL-1β in cytoplasm. Fluorescence data are shown in comparison with the corresponding bright-field image.

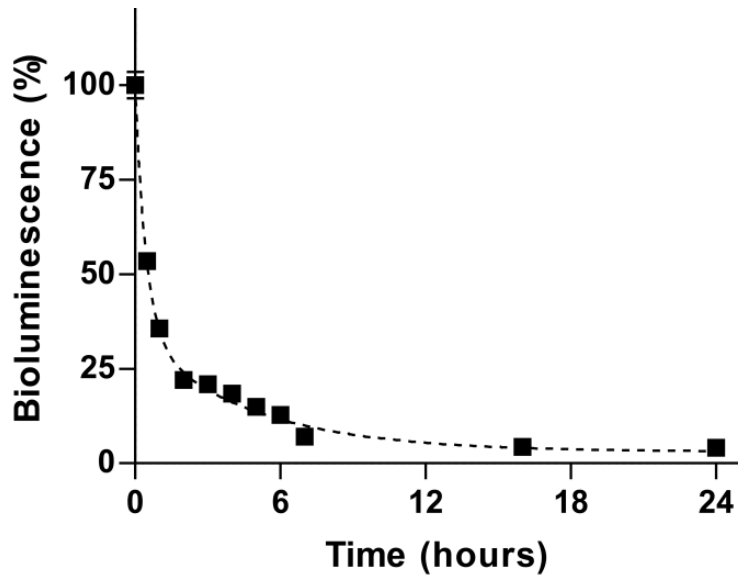


**Figure 13. The degradation half-life of enzymatically active NL-1 $\alpha$  + CL-1 $\beta$  reporter complex in U87/NL1 $\alpha$ /CL1 $\beta$  cells.** The cells were plated into a 96 well plate for 4 hours. Cycloheximide was then mixed with culture media to block protein synthesis. The cells were imaged for BLI by IVIS, and fluorescence using a plate reader after the addition of cycloheximide for 0.5, 1, 2, 3, 4, 5, 6, 7, 16 and 24 hours. The half-life was calculated as 34.12 min, with a 95% confidence interval of 29.72 to 40.4 min.

### 3.3 Validation of HIF-1 $\alpha$ / $\beta$ Dimerization Reporter System

#### 3.3.1 Overexpressed HIF-1 $\alpha$ <sub>12-396</sub> or HIF-1 $\beta$ <sub>11-510</sub> reduces the activity of HIF-1 $\alpha$ / $\beta$ dimerization reporter

To validate the specificity of this reporter system, we transfected U87/NL1 $\alpha$ /CL1 $\beta$  reporter cells with HIF-1 $\alpha$ <sub>12-396</sub> or HIF-1 $\beta$ <sub>11-510</sub> DNA plasmids for 24 and 48 h. The overexpression of PAS domains of either HIF-1 $\alpha$  or HIF-1 $\beta$  without FLuc fragments (which acts as competitive inhibitors of FLuc fragment-containing interacting PAS domains), resulted in almost 25% and 50% reduction in BLI signal intensity at 24h and 48h, respectively (**Fig. 14A**); no changes in the magnitude of expression of NL-1 $\alpha$  or CL-1 $\beta$  reporter proteins were observed, based on the fluorescence levels of co-expressed eGFP and mKate, respectively (**Fig. 14B**).

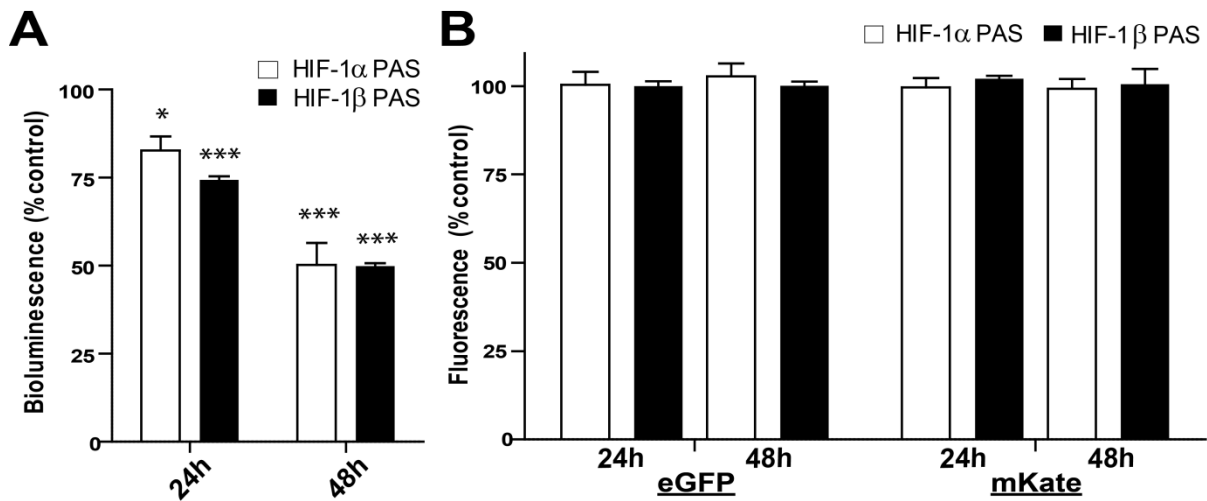


**Figure 14.** A) In U87/NL1 $\alpha$ /CL1 $\beta$  cells, the overexpression of PAS domains of either HIF-1 $\alpha$  (HIF-1 $\alpha$ <sub>12-396</sub>) or HIF-1 $\beta$  (HIF-1 $\beta$ <sub>11-510</sub>), competing with PAS domain-binding sites of reporter protein, resulted in almost 25% and 50% reduction in BLI signal intensity at 24h and 48h, respectively. Representative data are expressed as percentage changes of photon radiance vs. vehicle at 24 or 48h. (\*,  $P < 0.05$ ; \*\*,  $P < 0.01$ ; \*\*\*,  $P < 0.005$  vs. vehicle 24h; two-way ANOVA with Bonferroni correction) B) No changes in the magnitude of expression of NL-1 $\alpha$  or CL-1 $\beta$  reporter proteins were observed based on the fluorescence levels of co-expressed eGFP and mKate. Data was calculated as the relative changes of fluorescence level vs. vehicle at 24 or 48h.

### 3.3.2 Hypoxia-induced upregulation of endogenous HIF-1 $\alpha$ reduces the activity of HIF-1 $\alpha$ / $\beta$ dimerization reporter

We induced low oxygen condition (5% O<sub>2</sub>) to create hypoxia using a modular incubator chamber. Lack of oxygen stabilizes endogenous HIF-1 $\alpha$  in U87/NL1 $\alpha$ /CL1 $\beta$  cells and allows endogenous HIF-1 $\alpha$  to compete with the reporter protein binding sites. The result of western blotting showed that incubation of U87/NL1 $\alpha$ /CL1 $\beta$  cells in a hypoxic atmosphere after 24h induced the upregulation of endogenous HIF-1 $\alpha$  protein levels (**Fig. 15A**). Upregulated HIF-1 $\alpha$  acted as a competitive inhibitor of this reporter system and caused a significant decrease (85%,  $p < 0.005$ ) in BLI signal at 48h of incubation (**Fig. 15B**) as compared to control (20% O<sub>2</sub>), without reduction in cell viability (**Fig. 15C**). These results proved that this U87/NL1 $\alpha$ /CL1 $\beta$  reporter system was able to reflect the interaction between HIF-1 $\alpha$ <sub>12-396</sub> and HIF-1 $\beta$ <sub>11-510</sub> and can confidently be used as a platform for identifying inhibitors of HIF-1 dimerization.

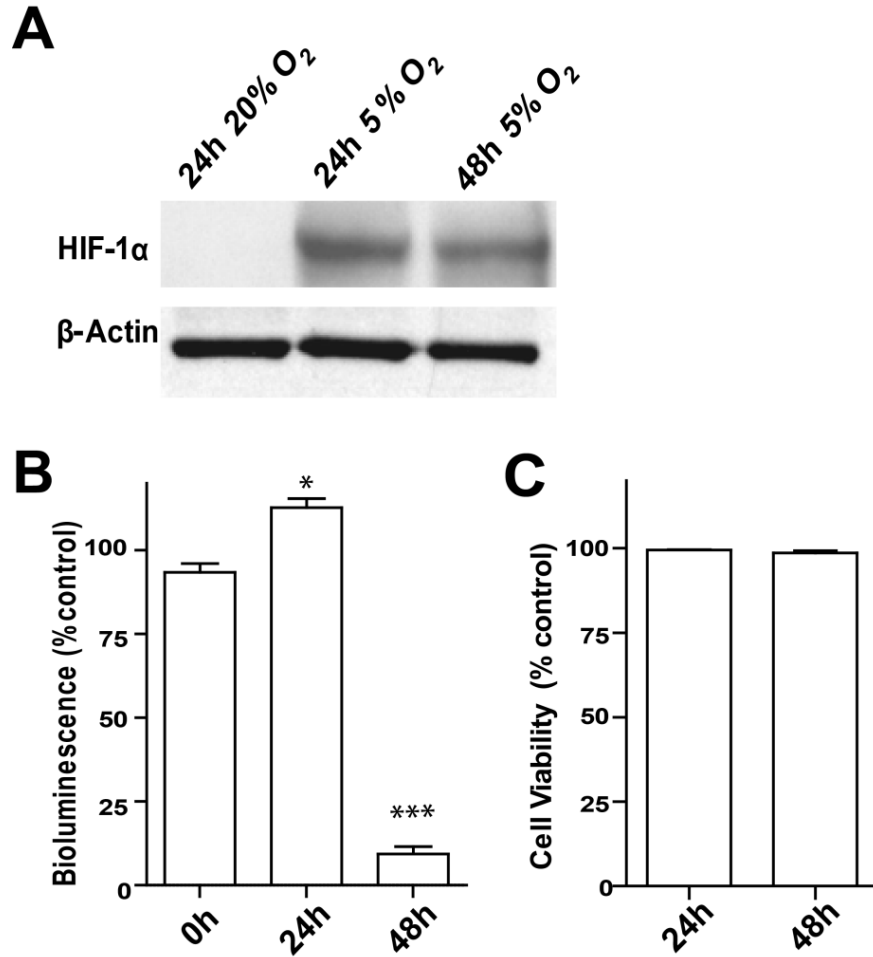


**Figure 15.** A) HIF-1 $\alpha$  and  $\beta$ -actin protein levels were determined by Western blotting assays. Endogenous HIF-1 $\alpha$  increased after 24h incubation in 5% O<sub>2</sub>, but no difference in  $\beta$ -actin protein expression was noted. B) Low oxygen induced endogenous HIF-1 $\alpha$  stabilization also allows HIF-1 $\alpha$  to compete with NL-HIF-1 $\alpha_{12-396}$  for dimerization with CL-HIF-1 $\beta_{11-510}$ , which causes significantly decreased BLI signals after 48 h incubation of 5% O<sub>2</sub>. (\*\*,  $P < 0.01$ ; \*\*\*,  $P < 0.005$  vs. 20% O<sub>2</sub> at each time point; two-way ANOVA with Bonferroni correction) C) No obvious reduction in cell viability between 20% O<sub>2</sub> and 5% O<sub>2</sub> incubation was observed at 24 or 48h.

## Chapter 4: High-Content Screening of Inhibitors of HIF-1 $\alpha$ /HIF-1 $\beta$ Dimerization in Cellulo

As part of the initial screen for novel inhibitors of HIF-1 $\alpha$ /HIF-1 $\beta$  dimerization, 41 compounds were tested at 10  $\mu$ M concentration. Twelve out of 41 compounds demonstrated various degrees of inhibition of HIF-1 $\alpha$ /HIF-1 $\beta$  heterodimerization in U87/NL1 $\alpha$ /CL1 $\beta$  reporter cells, but without significant inhibition of cellular viability (**Table. 2**). The most potent compound identified was acriflavine (ACF; compounds **7**), a known inhibitor of HIF-1 $\alpha$ / $\beta$  heterodimerization (Lee et al., 2009), which confirmed the efficacy of this screening system.

As indicated by Dr. Semanza's group, ACF is likely to bind to HIF-1 $\alpha$ , not HIF-1 $\beta$ . In order to optimize its inhibitory effect, a systematic approach was designed to understand the structure-activity relationships (SAR) between ACF and HIF-1 $\alpha$  using side-chain derivatization. The half-maximal inhibitory concentration (IC<sub>50</sub>) and cytotoxicity of each compound were determined using the newly developed cell-based HIF-1 $\alpha$ / $\beta$  dimerization reporter system and WST-1 cell viability assay, respectively.

As shown in **Table 3**, the studies were initiated by evaluating compounds (**1-4**), which are structurally related to ACF. Although these compounds showed some efficacy, the inhibition is several folds lower than ACF. We also compared the neutral and salt forms of 3,6-diaminoacridine (**5**) which demonstrated that salt forms ( compounds **6** and **7**) were more potent than the neutral form, which may be explained by the significantly improved solubility of salts compared to the neutral form. The observation was also supported by comparing compounds **3** and **4**. Furthermore, the data in Table 3 shows that the elimination of the 3,6-amino groups (compound **3** relative to **6**) demonstrates the importance of the 3,6-amino moiety to the efficacy of the compound. The dimethylation of the 3,6-amino groups (compound **10** relative to **5**) showed little change in efficacy, which could lead to the

conclusion that hydrogen bonding either does not exist or does not contribute to the efficacy of the molecule. In addition, compound **10** is not a good lead since an extended functionalization is blocked by the unreactive nature dimethyl groups. As a result, 3,6-diaminoacridine was selected for further functionalization at the amino groups to assess the SAR in the next step. The alkyl amide variation revealed an interesting pattern, the efficacy of the molecule was significantly enhanced by increasing the bulkiness of the alkyl group (*t*-butyl > isopropyl > ethyl). The same pattern was shown using a variation of ring size and bulkiness. The three-membered ring system showed the lowest efficacy, and then the efficacy was gradually enhanced by increasing the ring size (cyclopropyl < cyclobutyl < cyclopentyl < cyclohexyl). Also, the bulkiness of the ring system has a profound impact on the efficacy. The adamantyl and the tetra-methylcyclopropyl moieties showed the highest efficacy among all molecules.

In **Table 4**, the amide aromatic moieties in a variety of substituents on the benzene ring such as electron releasing groups (e.g. methyl and *t*-butyl) and electron withdrawing groups (e.g. trifluoromethyl), which could negatively impacted the efficacy. Interestingly, the heteroaromatic thiophene showed an improved efficacy compared to benzene (thiophene > benzene > furan > isoxazole). On the other hand, the di-thiophene (compound **26**) moiety showed the highest toxicity among all molecules. It is also worth noting that increased lipophilicity of the molecule positively impacted the efficacy. This was illustrated by the fact that the best compounds (tetramethylcyclopropyl, adamantyl, BOC, benzyl, thiophene) in this series share a relatively higher logD value (> 5.0) with the exception of benzene-substituted molecules, which showed lower efficacy regardless of the lipophilicity.

The SAR of the mono and the hetero-di substituted acridines were assessed for their efficacy as shown in Table 5. *N*-3-(2,2,3,3-tetramethylcyclopropanecarboxamide)-6-aminoacridine hydrochloric acid salt (**29**) was the best compound in the entire series. These



results revealed a very interesting pattern in compounds that contain the *N*-3-(2,2,3,3-tetramethylcyclopropanecarboxamide) moiety, they showed an improved efficacy (compounds **28** vs. **27** and **31** vs. **32** or **30**). This conclusion demonstrates the significance and validates the importance of the *N*-3-(2,2,3,3-tetramethylcyclopropanecarboxamide) moiety on the efficacy of the molecule.

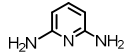
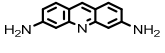
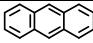
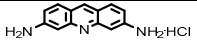
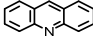
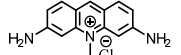
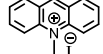
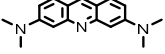
In **Table 5**, compounds **30-32** are the biotinylated derivatives of ACF (compound **5**), and compounds **27** and **29**, respectively. These compounds were synthesized to determine the binding target (HIF-1 $\alpha$  or HIF1- $\beta$  PAS domain) in pull-down assays. The efficacy of biotinylated mono *N*-3-acridine-(2,2,3,3-tetramethylcyclopropanecarboxamide) **31** was comparable to that of the ACF. However, the inhibitory activity of the biotinylated compounds **30-32** was uniformly reduced by only about two-fold as compared to the corresponding non-biotinylated compounds, which may result from interference of biotin group in binding to HIF-1. These results confirmed that the biotinylated compounds **30-32** still bind to their targets and could be used for the pull-down assay.

Based on the results of SAR studies, the *N,N'*-(acridine-3,6-diyl)bis(2,2,3,3-tetramethyl-cyclopropanecarboxamide) (compound **18**, **D-TMCP**) and *N*-3-(2,2,3,3-tetramethylcyclopropane-carboxamide)-6-aminoacridine hydrochloric acid salt (compound **29**, **M-TMCP**) exhibited the most potent inhibitory activities against HIF-1 $\alpha$ /HIF-1 $\beta$  heterodimerization ( $IC_{50}$  = 1.0 and 0.9  $\mu$ M, respectively; **Fig. 16A,B**) that were about 10-fold more potent than that of the ACF ( $IC_{50}$  = 11.19  $\mu$ M). Cellular toxicity from D-TMCP (**18**) and M-TMCP (**29**) was observed at 80 and 50-fold higher concentrations ( $IC_{50}$  = 80.5 and 49.04  $\mu$ M, respectively; **Fig. 16C**), which provides a fairly broad therapeutic window. Although the BOC group showed comparable efficacy ( $IC_{50}$  = 1.6  $\mu$ M), the compound was relatively toxic (toxicity  $IC_{50}$  = 23.9  $\mu$ M). These SAR observations may provide valuable perspectives to the future development of HIF-1 $\alpha$ / $\beta$  disruptors.

**Table 2: The list of initially screened compounds**

Chemical Names
Acrflavine (ACF)
Proflavine hemisulfate salt hydrate
3,4,9,10-perylenetetracarboxylic diimide
2-(4,5,6-TRIHYDROXY-3-OXO-3H-XANTHEN-9-YL)-BENZOIC ACID
Methylene Blue hydrate
Anthracene
BIX-01338 HYDRATE
Acridine Orange 10-nonyl bromide
1,9-PYRAZOLOANTHRONE
BIX 01294 TRIHYDROCHLORIDE HYDRATE
Dibenzothiophene
3,4,9,10-perylenetetracarboxylic 3,4,9,10-dianhydride
5-AZA-2'-DEOXYCYTIDINE
Valproic acid
5-Methylfuran-2-carbonyl chloride
trans-2-Phenyl-1-cyclopropanecarbonyl chloride
NSC-609699
N,N-DIMETHYL-10H-INDOLO(3,2-B)QUINOLIN-11-AMINE HYDROCHLORIDE
Bortezomib
3,3'-Diindolylmethane
6-Formylindolo(3,2-b)carbazole
KC7F2
AC1-004
2-Methoxyestradiol
FG-4592
IOX2
Berberine
KF58333
S409995
N-Methoxycarbonylmaleimide
RG108
Hydralazine hydrochloride
SAHA
Bis(dibenzylideneacetone)palladium(0)
Ethynyltributylstannane
Silver <i>p</i> -toluenesulfonate
ATTO-465
ATTO-495
ATTO-520 thio-12
methyl-acridine orange
2-amino-3-(1,2-dihydro-2-oxoquinoline-4-yl)propionic acid

**Table 3: SAR studies of acridine like molecules**

#	R	IC <sub>50</sub> (μM)	Toxicity IC <sub>50</sub> (μM)	logP	M.WT	#	R	IC <sub>50</sub> (μM)	Toxicity IC <sub>50</sub> (μM)	logP	M.WT
1		31.48	>50	0.52	109.1	5		17.31	>50	1.93	297.2
2		54.93	139	4.0	178.1	6		20.20	21.5		245.7
3		53.0	>100	3.5	179.2	7		11.19	>50	1.93	209.2
4		27.46	>100	0.34 <sup>a</sup>	321	8		20.80	15.40	4.11	265.4

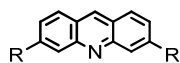


**Table 4: SAR studies of the homo-di-substituted-3,6-acridine amide.**

#	R	IC <sub>50</sub> (μM)	Toxicity IC <sub>50</sub> (μM)	logP	M.WT	#	R	IC <sub>50</sub> (μM)	Toxicity IC <sub>50</sub> (μM)	logP	M.WT
9		1.57	23.90	5.48	409.5	18		1.01	80.57	6.58	457.6
10		39.48	>50	3.16	321.4	19		4.064	9.39	5.15	417.5
11		44.42	>50	3.86	349.4	20		10.44	>50	6.12	445.5
12		10.90	26.76	4.69	377.5	21		62.55	>50	7.00	553.5
13		42.66	>50	2.92	345.4	22		29.71	42.11	8.56	529.6
14		19.98	31.71	3.97	373.4	23		47.12	117.4	4.64	537.6
15		9.01	>50	5.03	401.5	24		7.719	>100	2.38	397.4
16		4.15	6.54	6.0	429.6	25		20.08	19.28	1.61	399.4
17		4.121	32.87	7.8	533.7	26		2.172	3.497	5.11	429.5

**Table 5: SAR assessment of the mono and hetero-substituted acridines and biotinylated derivatives**

#	Structure	IC <sub>50</sub> (μM)	Toxicity IC <sub>50</sub> (μM)	logP	M.WT
27		5.17	53.12	5.48	409.5
28		2.894	>50	5.14	433.6
29		0.91	49.04	5.15	417.5
30		9.797	98.85	3.0	535.7
32		36.40	50.80	1.83	435.6
31		7.847	62.93	3.86	559.7

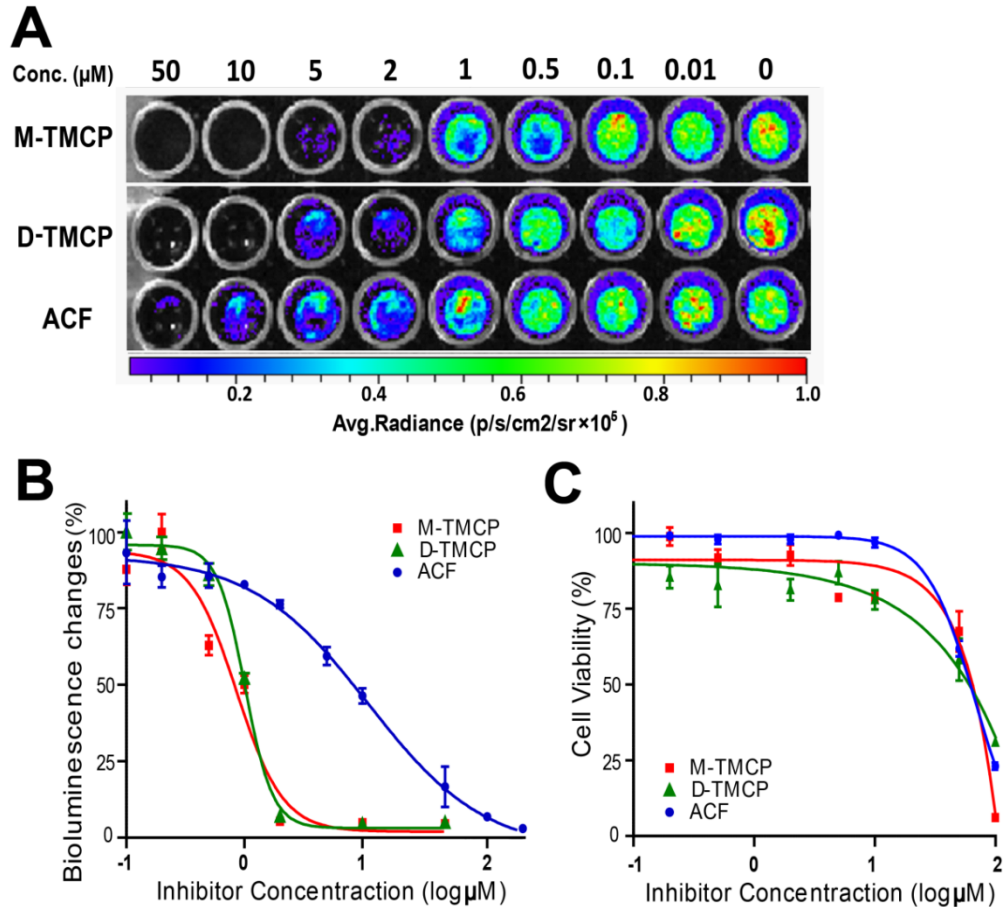


**Figure 16. M-TMCP and D-TMCP inhibit HIF-1 $\alpha$ / HIF-1 $\beta$  Dimerization in a dose-dependent manner. A, B)** BLI of U87 reporter cells treated with different dose of M-TMCP, D-TMCP or ACF. The  $\text{IC}_{50}$  was determined by constructing a non-linear dose response curve. D-TMCP or M-TMCP exhibited significantly higher inhibitory activities against HIF-1 $\alpha$ /HIF-1 $\beta$  heterodimerization ( $\text{IC}_{50} = 1.0$  and  $0.9 \mu\text{M}$ , respectively) than ACF ( $\text{IC}_{50} = 11.19 \mu\text{M}$ ) ( $P < 0.005$ ). Representative data are expressed as percentage change of photon radiance vs. un-treated control. Data were obtained from quadruplicate wells of three independent experiments. **C)** Cell viability of different doses of M-TMCP, D-TMCP or ACF treatments was also determined using WST-1 assay. Cellular toxicity from D-TMCP and M-TMCP was observed at 80 and 50-fold higher concentrations ( $\text{IC}_{50} = 80.5$  and  $49.04 \mu\text{M}$ , respectively), which provides a fairly broad therapeutic window.

## **Chapter 5: Evaluation of Selected Agents as Inhibitors of HIF-1-mediated Transcriptional Activity**

### **5.1 M-TMCP and D-TMCP inhibit HIF-1 $\alpha$ / HIF-1 $\beta$ Dimerization, but not FLuc fragment reconstitution**

Both M-TMCP and D-TMCP were equally ineffective at 10  $\mu$ M when tested in HEK293 cells transfected with an alternative well characterized rapamycin-inducible FRB-NLuc/CLuc-FKBP protein-protein interaction reporter system (Luker et al., 2004). The magnitude of bioluminescent signals from HEK293/FRB-NLuc/CLuc-FKBP cells was unaffected by the sequence of incubation with M-TMCP or D-TMCP compounds, either before or after reporter induction with rapamycin. Thus, this study confirmed that both M-TMCP and D-TMCP do not inhibit the trans-complementation of FLuc N- and C-terminal fragments, or enzymatic activity of reconstituted FLuc, or generation of BLI signal (**Fig. 17**).

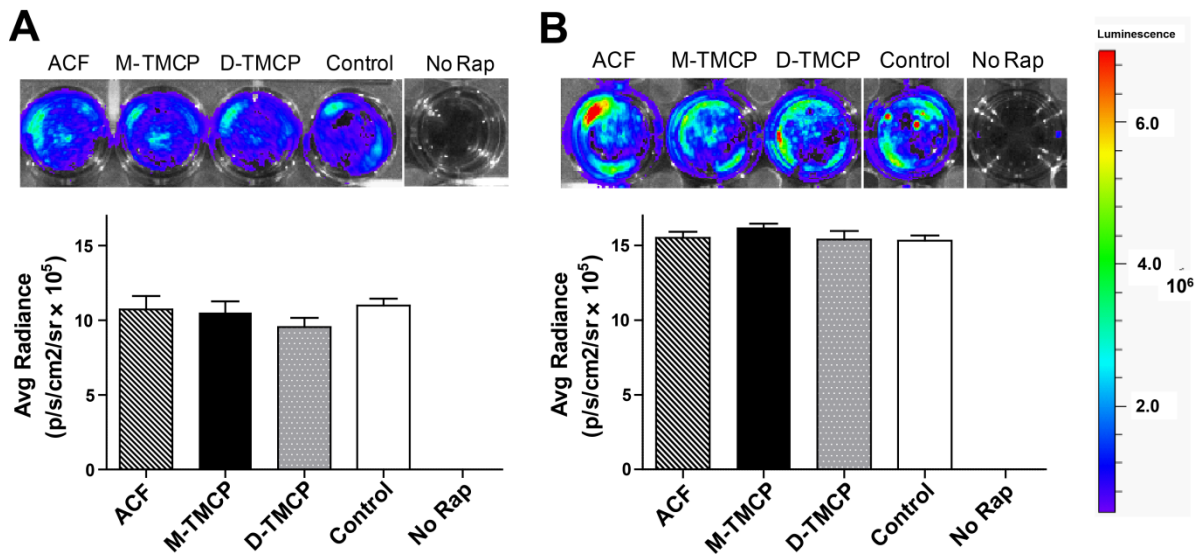


**Figure 17. No effect of ACF, M-TMCP and D-TMCP on rapamycin-induced FRB-NLuc/CLuc-FKBP association in HEK-293 cells.** ACF, M-TMCP and D-TMCP do not disrupt the association of two FLuc fragment pairs. HEK-293 cells transfected with FRB-NLuc/CLuc-FKBP were incubated A) with 50 nM rapamycin and treated with or without 10  $\mu$ M ACF, M-TMCP and D-TMCP, or B) 10  $\mu$ M vehicle or inhibitors first for 24 h and then followed by the addition of 50 nM rapamycin. The representative bioluminescence images of live cells in a 12-well plate are shown. Data expressed as average photon radiance  $\pm$  SEM from three independent experiments.



## 5.2 M-TMCP and D-TMCP inhibit HIF-1-mediated Transcriptional Reporter

### Activity

To directly assess the contribution of our inhibitors in disrupting HIF-1 $\alpha/\beta$  heterodimers and suppressing HIF-1-mediated transcriptional activity via HRE, a hypoxia-inducible C6#4/HRE-GFP/CMV-dsRed cell reporter system with 8 $\times$ HRE driven TKGFP expression was used to examine the efficacy of selected inhibitors (Serganova et al., 2004). In C6#4/HRE-GFP/CMV-dsRed reporter cells, both M-TMCP and D-TMCP exhibited similar efficacy for inhibition of HIF-1-mediated transcriptional activity ( $IC_{50}$  = 3.88 and 2.17  $\mu$ M, respectively), which was about 2-fold better than that of the ACF ( $IC_{50}$  = 7.01  $\mu$ M) (**Fig. 18A**). Cellular toxicity from D-TMCP and M-TMCP in the C6#4/HRE-GFP/CMV-dsRed reporter cells was observed at more than 100-fold higher concentrations and revealed no contribution to inhibitory effect (**Fig. 18B**). A comparison of  $IC_{50}$  for both HIF-1 dimerization and transcriptional activity of each inhibitor is presented in **Figure. 19**. Overall, M-TMCP and D-TMCP showed about a log order of HIF-1 inhibitory activity as compared to ACF.

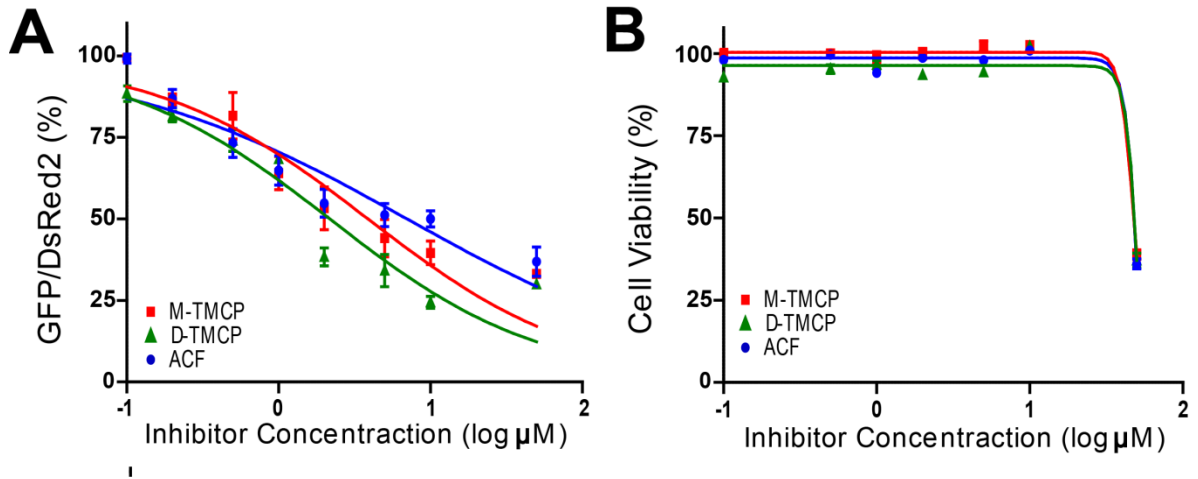


**Figure 18. Inhibitory effect of M-TMCP, D-TMCP or ACF on HIF-1 mediated transcription.** **A)** M-TMCP, D-TMCP or ACF inhibits HRE-driven transcription under hypoxia in C6#4/HRE-GFP/CMV-dsRed reporter cells. The reporter cells were incubated with different concentrations of M-TMCP, D-TMCP or ACF for 24 h. Constitutively expressed DsRed fluorescent protein in C6#4/HRE-GFP/CMV-dsRed cells were used as reference. The relative changes of GFP/DsRed expression vs. control was calculated as an indication of HRE-driven transcription levels in cells treated with inhibitors at each concentration. The result showed that  $IC_{50}$  of HIF-1 transcriptional activity in the cells treated with M-TMCP, D-TMCP or ACF is  $3.88 \mu\text{M}$ ,  $2.17 \mu\text{M}$  and  $7.01 \mu\text{M}$ , respectively. Data were obtained from quadruplicate wells of three independent experiments. **B)**  $IC_{50}$  of cellular toxicity of C6#4/HRE-GFP/CMV-dsRed cells treated with M-TMCP, D-TMCP or ACF is almost 10 times higher than the  $IC_{50}$  of HIF-1 transcriptional activity. (\*,  $P < 0.05$ ; \*\*,  $P < 0.01$ ; \*\*\*,  $P < 0.005$ ; two-way ANOVA with Bonferroni correction)

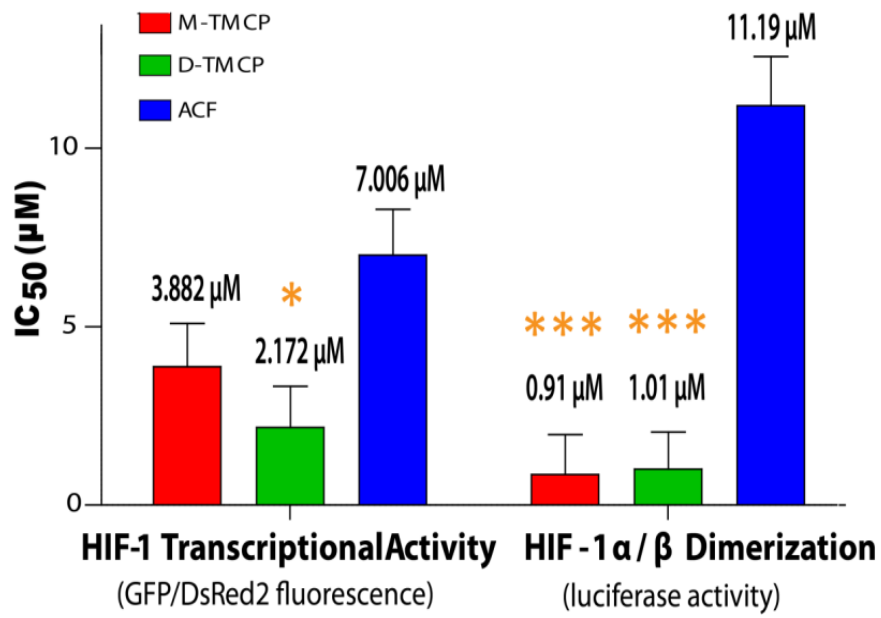


**Figure 19. Comparison of IC<sub>50</sub> of M-TMCP, D-TMCP and ACF in U87/NL1α/CL1β reporter cells or C6#4/HRE-GFP/CMV-dsRed HIF-1 transcriptional activity reporter cells. (\*, P < 0.05; \*\*, P < 0.01; \*\*\*, P < 0.005; two-way ANOVA with Bonferroni correction)**

### **5.3 M-TMCP and D-TMCP inhibit mRNA expression of HIF-1-dependent genes in hypoxia**

To further investigate whether the selected inhibitors were effective in transcriptionally regulating hypoxia-induced genes in tumorigenesis, the human hypoxia signaling pathway array was used to profile the expression of 84 hypoxia-associated genes (**Tab. 6**), including genes related to stress response, angiogenesis, metabolism, DNA damage and repair, HIF signaling transcription factors and HIF interacting proteins. First, non-supervised hierarchical clustering analysis of our entire qRT-PCR data was displayed as a heat map with dendrograms to indicate co-regulated genes across groups (**Fig. 20**). Comparison of gene expression patterns in wild-type U87 cells cultured under conditions of normoxic, hypoxic conditions or hypoxic U87 cells treated with M-TMCP or D-TMCP demonstrated significant differences in the magnitudes of expression of multiple HIF1-dependent genes. The hierarchical cluster analysis also revealed that the gene expression pattern in treatment group were more similar to that of the normoxic group, rather than hypoxic groups. This finding confirmed the assertion that M-TMCP and D-TMCP intervene with the expression of hypoxia-responsive genes.

Furthermore, hierarchical cluster analysis revealed that several clusters of genes upregulated by hypoxia have been significantly inhibited by 24h treatment with ACF, M-TMCP or D-TMCP (cluster 3.2.1.2 in **Figure. 20**). Disruption of hypoxia-induced HIF-1 transcriptional activity by ACF, M-TMCP or D-TMCP treatment resulted in a more profound inhibition in one sub-cluster of genes (i.e., 3.2.1.2.1) as compared to other sub-clusters (i.e., 3.2.1.2.2), suggesting the genes in 3.2.1.2.2 may not be directly or solely regulated through HIF-1 complex but other pathways. The subset of data including representative genes from these two clusters is presented in Figure 21. Notably, several genes which are upregulated in hypoxia and promote tumorigenesis (Hirota and Semenza, 2006, Semenza, 2001, Zhang

et al., 2012, Tacchini et al., 2001, Zou et al., 2013, Iyer et al., 1998, Garayoa et al., 2000, Cormier-Regard et al., 1998, Riddle et al., 2000, Ryan et al., 1998, Manalo et al., 2005, Bhattacharyya and Tobacman, 2012, Semenza et al., 1994) were significantly down-regulated by ACF, M-TMCP or D-TMCP treatment, including: vascular endothelial growth factor A (VEGFA); facilitated glucose transporter member 1 (GLUT-1); hexokinase 2 (HK2), enolase 1 (ENO1), notch 1 (NOTCH1), plasminogen activator (PLAU), collagen type I alpha (COL1A1), procollagen-lysine, 2-oxoglutarate 5-dioxygenase 3 (PLOD3); whereas lesser extend of downregulation was observed for: glucose-6-phosphate isomerase (GPI); angiopoietin-like 4 (ANGPTL4), including adrenomedullin (ADM), and insulin-like growth factor binding protein 1 (IGFBP1). These results confirmed that M-TMCP and D-TMCP can suppress the expression of pro-tumorigenic genes and disrupt hypoxia adaptive cascade in tumor by inhibiting HIF-1 $\alpha$ / $\beta$  complex.

**Table 6: 84 hypoxia-associated genes in human hypoxia signaling pathway array**

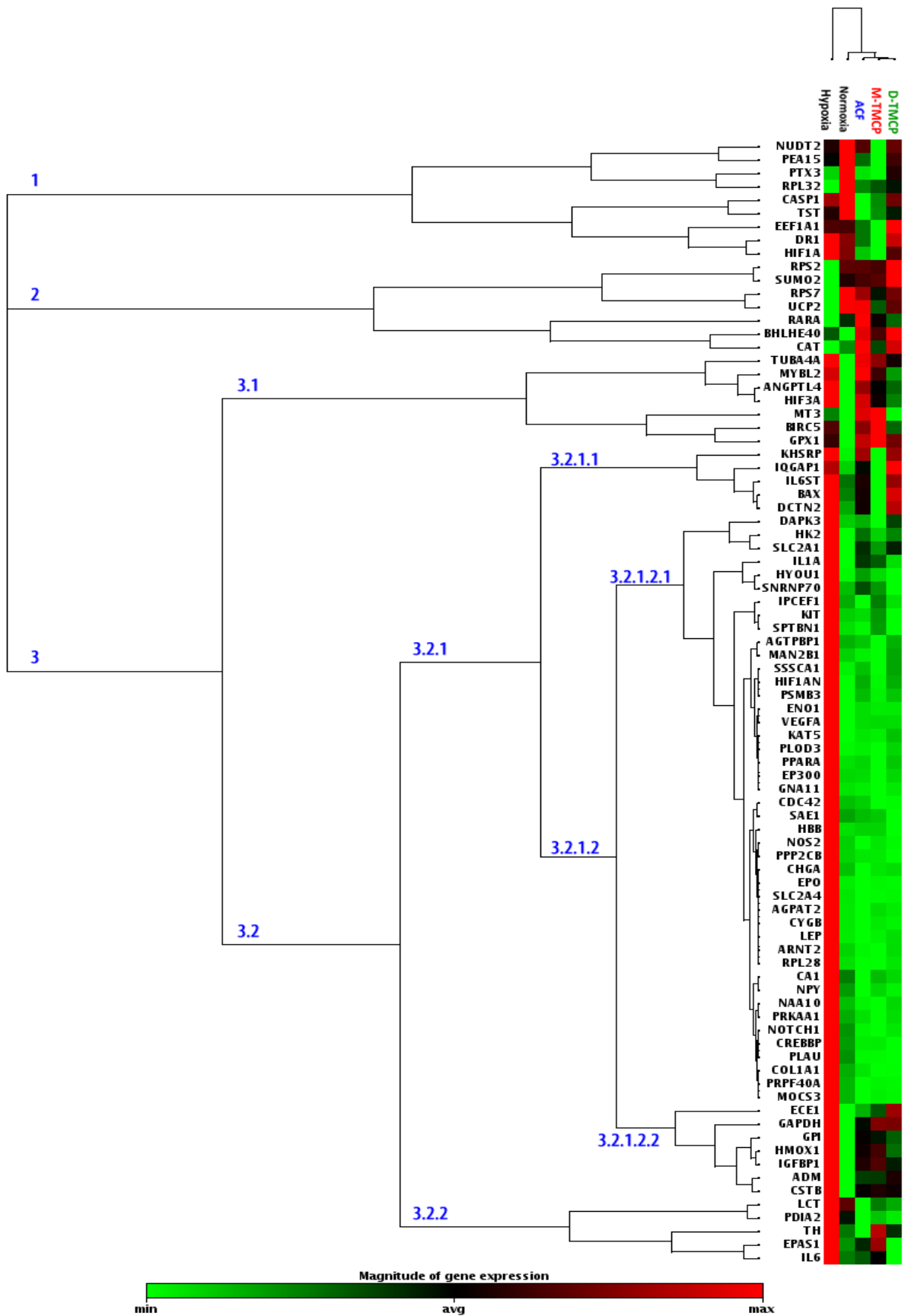
Position	Unigene	Refseq	Symbol	Description
A01	Hs.441047	NM_001124	ADM	Adrenomedullin
A02	Hs.320151	NM_006412	AGPAT2	1-acylglycerol-3-phosphate O-acyltransferase 2
A03	Hs.494321	NM_015239	AGTPBP1	ATP/GTP binding protein 1
A04	Hs.9613	NM_001039667	ANGPTL4	Angiopietin-like 4
A05	Hs.433291	NM_003491	NAA10	N(alpha)-acetyltransferase 10, NatA catalytic subunit
A06	Hs.459070	NM_014862	ARNT2	Aryl-hydrocarbon receptor nuclear translocator 2
A07	Hs.624291	NM_004324	BAX	BCL2-associated X protein
A08	Hs.728782	NM_003670	BHLHE40	Basic helix-loop-helix family, member e40
A09	Hs.728893	NM_001168	BIRC5	Baculoviral IAP repeat containing 5
A10	Hs.23118	NM_001738	CA1	Carbonic anhydrase I
A11	Hs.2490	NM_033292	CASP1	Caspase 1, apoptosis-related cysteine peptidase (interleukin 1, beta, convertase)
A12	Hs.502302	NM_001752	CAT	Catalase
B01	Hs.690198	NM_001791	CDC42	Cell division cycle 42 (GTP binding protein, 25kDa)
B02	Hs.150793	NM_001275	CHGA	Chromogranin A (parathyroid secretory protein 1)
B03	Hs.172928	NM_000088	COL1A1	Collagen, type I, alpha 1
B04	Hs.459759	NM_004380	CREBBP	CREB binding protein
B05	Hs.695	NM_000100	CSTB	Cystatin B (stefin B)
B06	Hs.95120	NM_134268	CYGB	Cytoglobin
B07	Hs.631844	NM_001348	DAPK3	Death-associated protein kinase 3
B08	Hs.289123	NM_006400	DCTN2	Dynactin 2 (p50)
B09	Hs.348418	NM_001938	DR1	Down-regulator of transcription 1, TBP-binding (negative cofactor 2)
B10	Hs.195080	NM_001397	ECE1	Endothelin converting enzyme 1
B11	Hs.520703	NM_001402	EEF1A1	Eukaryotic translation elongation factor 1 alpha 1
B12	Hs.517145	NM_001428	ENO1	Enolase 1, (alpha)
C01	Hs.517517	NM_001429	EP300	E1A binding protein p300
C02	Hs.468410	NM_001430	EPAS1	Endothelial PAS domain protein 1
C03	Hs.2303	NM_000799	EPO	Erythropoietin
C04	Hs.643580	NM_017892	PRPF40A	PRP40 pre-mRNA processing factor 40 homolog A ( <i>S. cerevisiae</i> )
C05	Hs.654784	NM_002067	GNA11	Guanine nucleotide binding protein (G protein), alpha 11 (Gq class)
C06	Hs.466471	NM_000175	GPI	Glucose-6-phosphate isomerase
C07	Hs.76686	NM_000581	GPX1	Glutathione peroxidase 1
C08	Hs.523443	NM_000518	HBB	Hemoglobin, beta
C09	Hs.597216	NM_001530	HIF1A	Hypoxia inducible factor 1, alpha subunit
C10	Hs.500788	NM_017902	HIF1AN	Hypoxia inducible factor 1, alpha subunit inhibitor
C11	Hs.420830	NM_152794	HIF3A	Hypoxia inducible factor 3, alpha subunit
C12	Hs.406266	NM_000189	HK2	Hexokinase 2
D01	Hs.517581	NM_002133	HMOX1	Heme oxygenase (decycling) 1
D02	Hs.528299	NM_006388	KAT5	K(lysine) acetyltransferase 5
D03	Hs.277704	NM_006389	HYOU1	Hypoxia up-regulated 1
D04	Hs.523414	NM_000612	IGF2	Insulin-like growth factor 2 (somatomedin A)
D05	Hs.642938	NM_000596	IGFBP1	Insulin-like growth factor binding protein 1
D06	Hs.1722	NM_000575	IL1A	Interleukin 1, alpha
D07	Hs.654458	NM_000600	IL6	Interleukin 6 (interferon, beta 2)
D08	Hs.532082	NM_002184	IL6ST	Interleukin 6 signal transducer (gp130, oncostatin M receptor)
D09	Hs.430551	NM_003870	IQGAP1	IQ motif containing GTPase activating protein 1

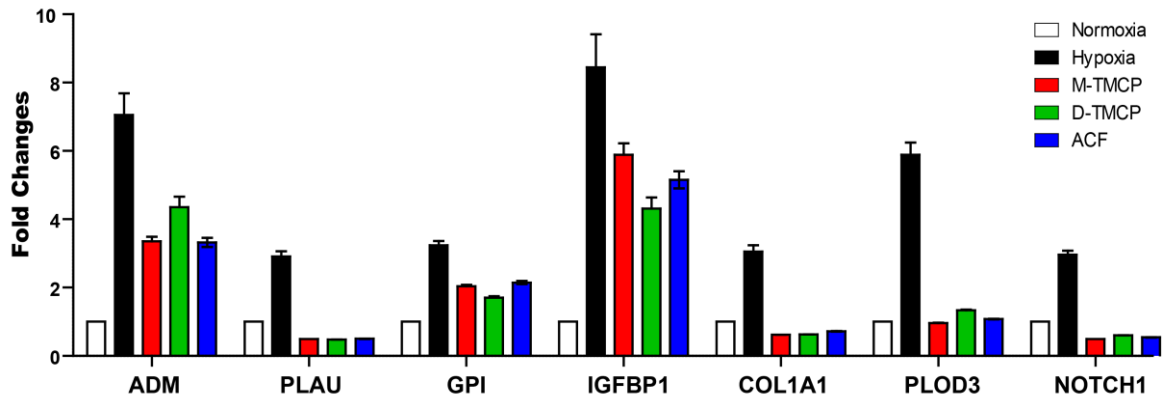
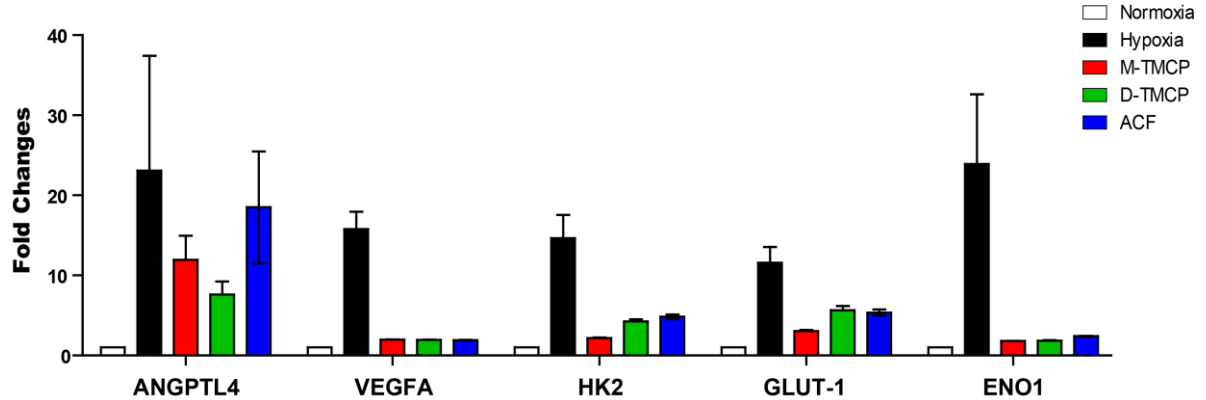
Position	Unigene	Refseq	Symbol	Description
D10	Hs.708128	NM_003685	KHSRP	KH-type splicing regulatory protein
D11	Hs.479754	NM_000222	KIT	V-kit Hardy-Zuckerman 4 feline sarcoma viral oncogene homolog
D12	Hs.551506	NM_002299	LCT	Lactase
E01	Hs.194236	NM_000230	LEP	Leptin
E02	Hs.356769	NM_000528	MAN2B1	Mannosidase, alpha, class 2B, member 1
E03	Hs.159410	NM_014484	MOCS3	Molybdenum cofactor synthesis 3
E04	Hs.73133	NM_005954	MT3	Metallothionein 3
E05	Hs.179718	NM_002466	MYBL2	V-myb myeloblastosis viral oncogene homolog (avian)-like 2
E06	Hs.709191	NM_000625	NOS2	Nitric oxide synthase 2, inducible
E07	Hs.495473	NM_017617	NOTCH1	Notch 1
E08	Hs.1832	NM_000905	NPY	Neuropeptide Y
E09	Hs.493767	NM_001161	NUDT2	Nudix (nucleoside diphosphate linked moiety X)-type motif 2
E10	Hs.66581	NM_006849	PDIA2	Protein disulfide isomerase family A, member 2
E11	Hs.517216	NM_003768	PEA15	Phosphoprotein enriched in astrocytes 15
E12	Hs.146100	NM_015553	IPCEF1	Interaction protein for cytohesin exchange factors 1
F01	Hs.77274	NM_002658	PLAU	Plasminogen activator, urokinase
F02	Hs.153357	NM_001084	PLOD3	Procollagen-lysine, 2-oxoglutarate 5-dioxygenase 3
F03	Hs.103110	NM_005036	PPARA	Peroxisome proliferator-activated receptor alpha
F04	Hs.491440	NM_001009552	PPP2CB	Protein phosphatase 2, catalytic subunit, beta isozyme
F05	Hs.43322	NM_006251	PRKAA1	Protein kinase, AMP-activated, alpha 1 catalytic subunit
F06	Hs.82793	NM_002795	PSMB3	Proteasome (prosome, macropain) subunit, beta type, 3
F07	Hs.591286	NM_002852	PTX3	Pentraxin 3, long
F08	Hs.654583	NM_000964	RARA	Retinoic acid receptor, alpha
F09	Hs.652114	NM_000991	RPL28	Ribosomal protein L28
F10	Hs.265174	NM_000994	RPL32	Ribosomal protein L32
F11	Hs.498569	NM_002952	RPS2	Ribosomal protein S2
F12	Hs.546287	NM_001011	RPS7	Ribosomal protein S7
G01	Hs.515500	NM_005500	SAE1	SUMO1 activating enzyme subunit 1
G02	Hs.473721	NM_006516	GLUT-1	Facilitated glucose transporter, member 1
G03	Hs.380691	NM_001042	GLUT-4	Facilitated glucose transporter, member 4
G04	Hs.467097	NM_003089	SNRNP70	Small nuclear ribonucleoprotein 70kDa (U1)
G05	Hs.503178	NM_003128	SPTBN1	Spectrin, beta, non-erythrocytic 1
G06	Hs.25723	NM_006396	SSSCA1	Sjogren syndrome/scleroderma autoantigen 1
G07	Hs.380973	NM_006937	SUMO2	SMT3 suppressor of mif two 3 homolog 2 (S. cerevisiae)
G08	Hs.435609	NM_000360	TH	Tyrosine hydroxylase
G09	Hs.474783	NM_003312	TST	Thiosulfate sulfurtransferase (rhodanese)
G10	Hs.75318	NM_006000	TUBA4A	Tubulin, alpha 4a
G11	Hs.80658	NM_003355	UCP2	Uncoupling protein 2 (mitochondrial, proton carrier)
G12	Hs.73793	NM_003376	VEGFA	Vascular endothelial growth factor A
H01	Hs.534255	NM_004048	B2M	Beta-2-microglobulin
H02	Hs.412707	NM_000194	HPRT1	Hypoxanthine phosphoribosyltransferase 1
H03	Hs.728776	NM_012423	RPL13A	Ribosomal protein L13a
H04	Hs.592355	NM_002046	GAPDH	Glyceraldehyde-3-phosphate dehydrogenase
H05	Hs.520640	NM_001101	ACTB	Actin, beta
H06	N/A	SA_00105	HGDC	Human Genomic DNA Contamination
H07	N/A	SA_00104	RTC	Reverse Transcription Control
H08	N/A	SA_00104	RTC	Reverse Transcription Control
H09	N/A	SA_00104	RTC	Reverse Transcription Control



H10	N/A	SA_00103	PPC	Positive PCR Control
H11	N/A	SA_00103	PPC	Positive PCR Control
H12	N/A	SA_00103	PPC	Positive PCR Control

**Figure 20. mRNA expression profile of human HIF-1 related genes in normoxic U87 cells and hypoxic U87 cells treated with HIF-1 dimerization inhibitors.** Two-dimensional hierarchical clustering of the data matrix consisting of 84 genes by five different treatment groups, normoxia, hypoxia, hypoxia and treated with ACF, M-TMCP and D-TMCP, respectively. Genes (rows) and groups (columns) were clustered independently by hierarchical clustering. Three main clusters are numbered. The gene expression in the subcluster of 3.2.1.2.1 was down-regulated in all three inhibitor groups compared to hypoxia and relatively closer to the expression in normoxia. In cluster of 3.2.1.2.2, the gene expression was also decreased in the inhibitor treated groups, but not as dramatically as the genes in cluster of 3.2.1.2.1. This indicates that the genes in 3.2.1.2.2 may not be strictly controlled by HIF-1 but also other signaling pathways. Data shown are averages of triplicate qRT-PCR measurements.



**A****B**

**Figure 21. The mRNA expression of selective tumor progression and angiogenesis-related genes was significantly decreased in hypoxic U87 glioma cells treated with M-TMCP and D-TMCP.** U87 cells were incubated under normoxia or hypoxia in absence or presence of the inhibitors at concentration of 10  $\mu$ M for 24 hours. Total RNA was isolated from the whole-cell lysates for profiling of hypoxia-related genes by qRT-PCR. Fold changes of mRNA levels relative to normoxia were calculated as  $2^{(-\text{Avg.}(\Delta\text{Ct}))}$ . Mean  $\pm$  SEM (n=3). Note the scales of fold changes in two plots are different.

## Chapter 6: Evaluation of Therapeutic Efficacy of Selected Inhibitors in Tumor Xenograft Bearing Mice

### 6.1 Imaging Inhibition of HIF-1 $\alpha$ /HIF1- $\beta$ Heterodimerization and Antitumor Therapeutic Efficacy by M-TMCP and D-TMCP in Tumors *in Vivo*

The anti-tumor efficacy of selected HIF-1 inhibitors was evaluated in nude mice bearing subcutaneous (s.c.) tumor xenografts developed from the U87/NL1 $\alpha$ /CL1 $\beta$  reporter cells. Vehicle, M-TMCP, D-TMCP or ACF was administered by daily intraperitoneal (i.p.) injection to tumor xenograft mouse. Treatment was initiated 14 days after implantation, at which time the tumors had grown to an average of approximately 100 mm<sup>3</sup> in all groups, and continued for another 14 days (**Fig. 22**). Daily administration of either M-TMCP or D-TMCP (2 mg/kg in 3%DMSO in saline; 150  $\mu$ l i.p.) in mice, resulted in a significant inhibition of bioluminescence signals from the reporter tumors as early as 3 days post treatment (**Fig. 23**) and significant inhibition of tumor growth, which was manifested by prolongation of tumor doubling times - 4.86 and 5.19 days, respectively, when compared to vehicle-treated control mice (doubling time of 3.88 days) (**Fig. 24**). Daily treatment of mice with ACF (2 mg/kg in 3% DMSO in saline; 150  $\mu$ l i.p.) resulted in a less dramatic inhibition of the reporter activity (**Fig. 23A**) and tumor growth (**Fig. 24**) (doubling time of 4.42 days), as compared to M-TMCP or D-TMCP-treated mice. In addition, treatments of M-TMCP or D-TMCP at the dosage of 2 mg/kg demonstrated more significant log<sub>10</sub> tumor cell kill (0.453 and 0.45, respectively), as compared to ACF (0.387) (Bissery et al., 1991) in **Figure 25**. Statistically significant differences in average tumor sizes between groups of mice treated with either M-TMCP or D-TMCP versus the ACF-treated group were observed starting from the 9th day of treatment ( $P < 0.05$  and  $P < 0.001$ , respectively). Noteworthy, there were no differences between the

treated and control groups in the dynamics of body weight during treatment (**Fig. 26**), indicating a low systemic toxicity of the treatment doses used.



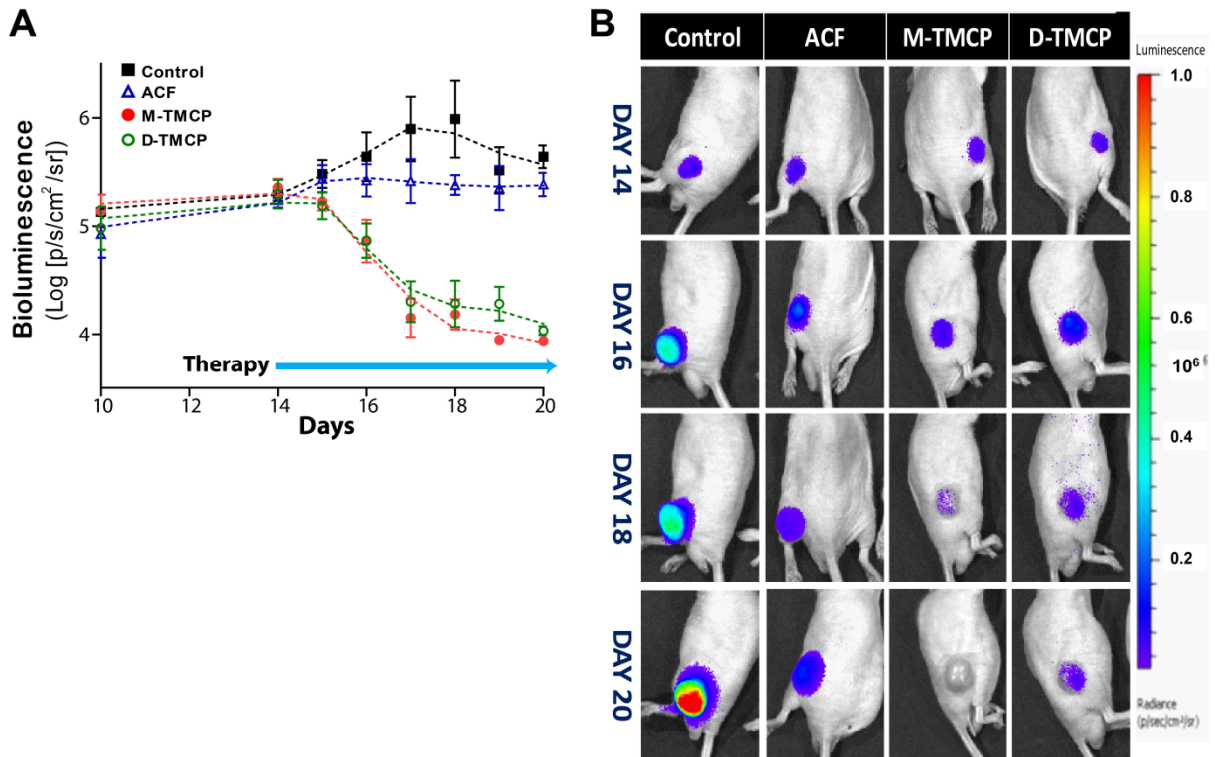


**Figure 23. HIF-1 $\alpha$ / $\beta$  dimerization inhibition of M-TMCP and D-TMCP on U87/NL1 $\alpha$ /CL1 $\beta$  glioma cancer xenograft model.** A) Monitoring HIF-1 disruption in mice by BLI. The BL signal decrease significantly in M-TMCP and D-TMCP group only after 4 day of repeated treatment. Data are presented as log (total photon radiance)  $\pm$  SEM of six mice in each group imaged repeatedly over the course of the experiment. B) Bioluminescent imaging of four representative Nu/Nu mice with different treatments. The BLI images were taken 4 h after daily treatment.



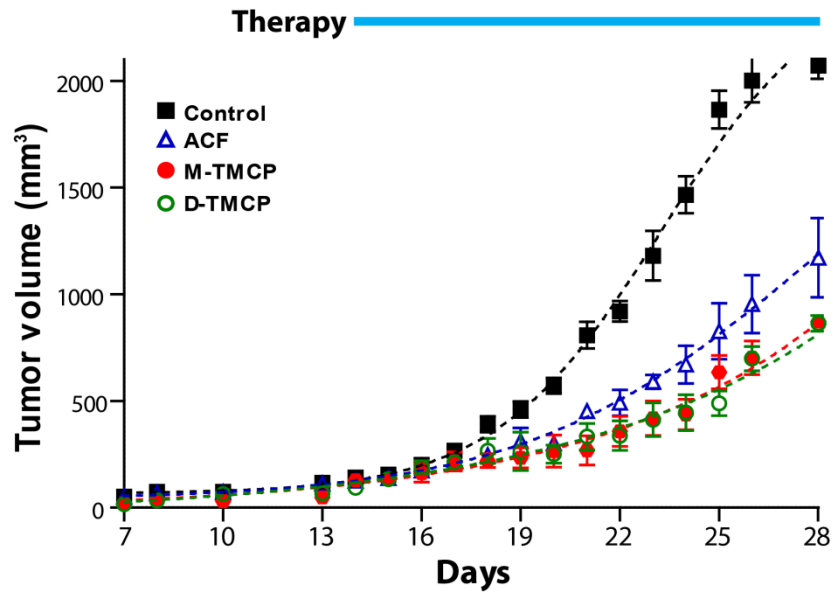
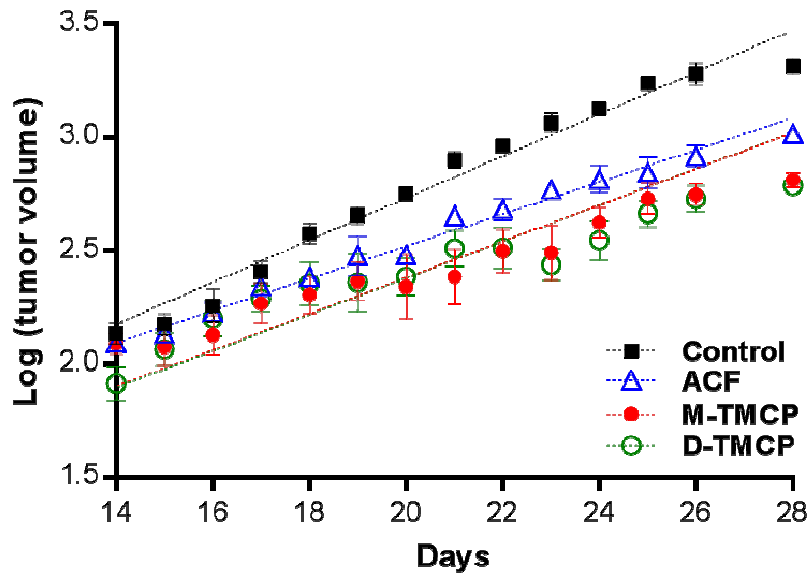


**Figure 24. Anti-tumor effect of M-TMCP and D-TMCP on U87/NL1 $\alpha$ /CL1 $\beta$  human glioma xenograft in mice.** The tumor growth patterns of mice during the course of treatment. Significant prolongation of tumor doubling times in M-TMCP and D-TMCP treated groups (4.86 and 5.19 days, respectively), as compared to vehicle-treated control mice (doubling time of 3.88 days). Daily treatment of mice with ACF resulted in a less dramatic inhibition of tumor growth (doubling time of 4.42 days). Volume mean  $\pm$  SEM (n = 8) is shown.



Treatment	Equation	log <sub>10</sub> tumor cell kill
Control	$Y = 0.09272 * X + 0.8775$	0
ACF	$Y = 0.07087 * X + 1.102$	0.387
M-TMCP	$Y = 0.07989 * X + 0.7836$	0.453
D-TMCP	$Y = 0.08046 * X + 0.7699$	0.45

**Figure 25. Log tumor cell kill of M-TMCP and D-TMCP on U87/NL1 $\alpha$ /CL1 $\beta$  human glioma xenograft in mice.** M-TMCP and D-TMCP treated groups demonstrated higher log tumor cell kill values (0.453 and 0.45, respectively), as compared to ACF-treated mice (0.387). Log<sub>10</sub> (tumor volume in mm<sup>3</sup>)  $\pm$  SEM (n = 8) is shown.

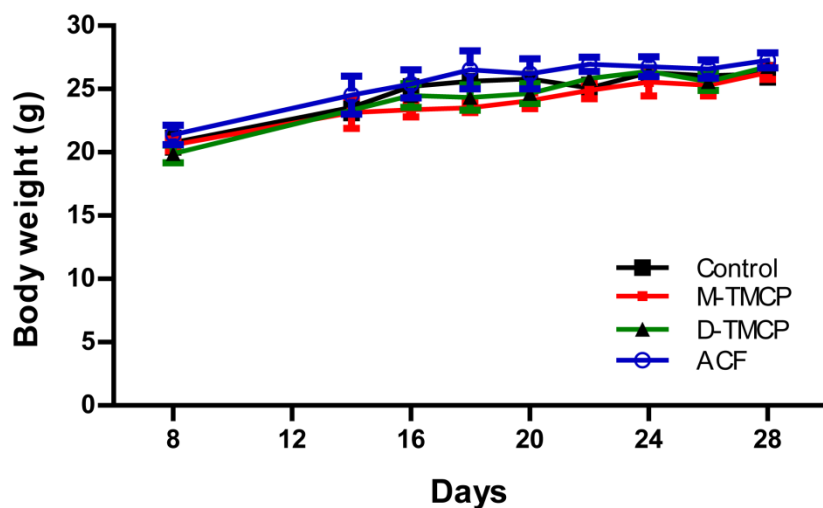


**Figure 26. No loss in body weights of U87/NL1 $\alpha$ /CL1 $\beta$  xenograft-bearing mice treated with HIF-1 dimerization inhibitors.** Weights of the tumor xenograft bearing mice treated with vehicle (black), ACF (red), M-TMCP (Blue) or D-TMCP (Green) were measured throughout the experiment. Mean  $\pm$  SEM (n = 6) is shown.

## 6.2 Effects of M-TMCP and D-TMCP Treatment on Tumor Vascularization, Proliferation, and Apoptosis *in vivo*

To determine the ability of M-TMCP and D-TMCP on tumor prognosis, mice bearing U87/NL1 $\alpha$ /CL1 $\beta$  xenograft were treated with vehicle, ACF, M-TMCP and D-TMCP for 14 days. After the last dose, tumor samples were collected and evaluated by immunohistochemical analysis. At the end of the 14th day treatment, immunohistochemical analysis of U87/NL1 $\alpha$ /CL1 $\beta$  tumor tissue samples demonstrated significant differences in microvascular morphology, tumor cell proliferative activity and apoptosis in treated groups versus control group. Tumors in the vehicle-treated control group had characteristically high levels of VEGF and GLUT-1 expression, abnormally increased microvascular morphology and density (CD34+), high proliferative activity (high Ki67 labeling index) and low percentage of Annexin V+ apoptotic cells (**Fig. 27**). Notably, in control tumors the expression of VEGF and GLUT-1 were observed in avascular and apparently hypo- or non-perfused microvessels, whereas no expression of VEGF and GLUT-1 were observed within 120-150  $\mu$ m around well perfused microvessels (**Fig. 28, 29**). In contrast, the expression of VEGF and GLUT-1 were markedly decreased in ACF, M-TMCP, D-TMCP -treated tumors (**Fig. 27A**), along with a statistically significant reduction in the number, size, and branching of CD34+ microvessels (**Fig. 27B**), decreased in tumor cell proliferation (**Fig. 27C**), and increased percentage of apoptotic cells (**Fig. 27D; Fig. 30**). These IHC results suggested that our identified HIF-1 dimerization inhibitors hit their therapeutic target by suppressing HIF-1 dependent signaling pathway associated with reduced tumor vascularization, cellular invasiveness and modified metabolic micro-environment.

**Figure 27. M-TMCP and D-TMCP reduced tumor vascularization, modified metabolic micro-environment, inhibited cellular invasiveness, and induced cellular apoptosis.** Mice with approximately 100mm<sup>3</sup> U87/NL1 $\alpha$ /CL1 $\beta$  cells xenografts were treated for 14 days and euthanized on day 28. A) Tumor samples were collected after the last treatment and analyzed by immunohistochemistry for VEGF, GLUT-1, CD34, Ki67 and Annexin V. Scale bar: 200  $\mu$ m. B) Total pixel area of VEGF in different treatment. Significantly suppression of VEGF expression were observed in ACF, M-TMCP and D-TMCP treated tumor samples C) Inhibitor treatment decreased cellular proliferation determined by Ki67, resulting in the tumor growth retardation in xenograft models. D) All tumor samples treated with the inhibitors demonstrated significantly higher apoptotic index comparing to control samples. The stained area of CD34 and Ki67 in 20 fields was quantified under  $\times$  400 magnifications (n = 3, each treatment). The stained area of Annexin V in 5 fields was quantified under  $\times$  800 magnifications (n = 3, each treatment). \*, P < 0.05; \*\*\*, P < 0.005 vs. control (two-way ANOVA with Bonferroni correction)

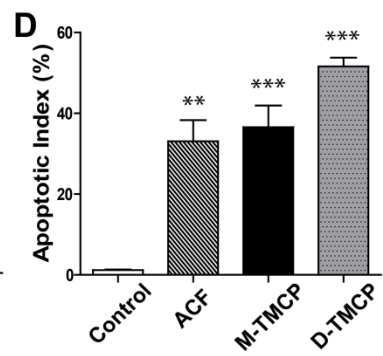
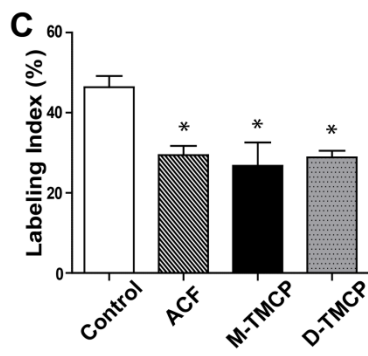
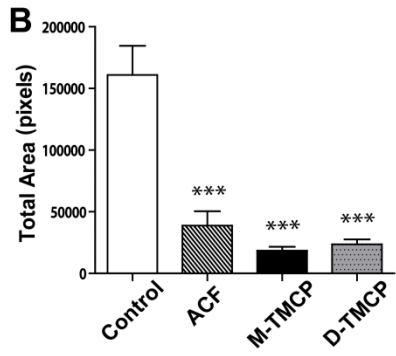
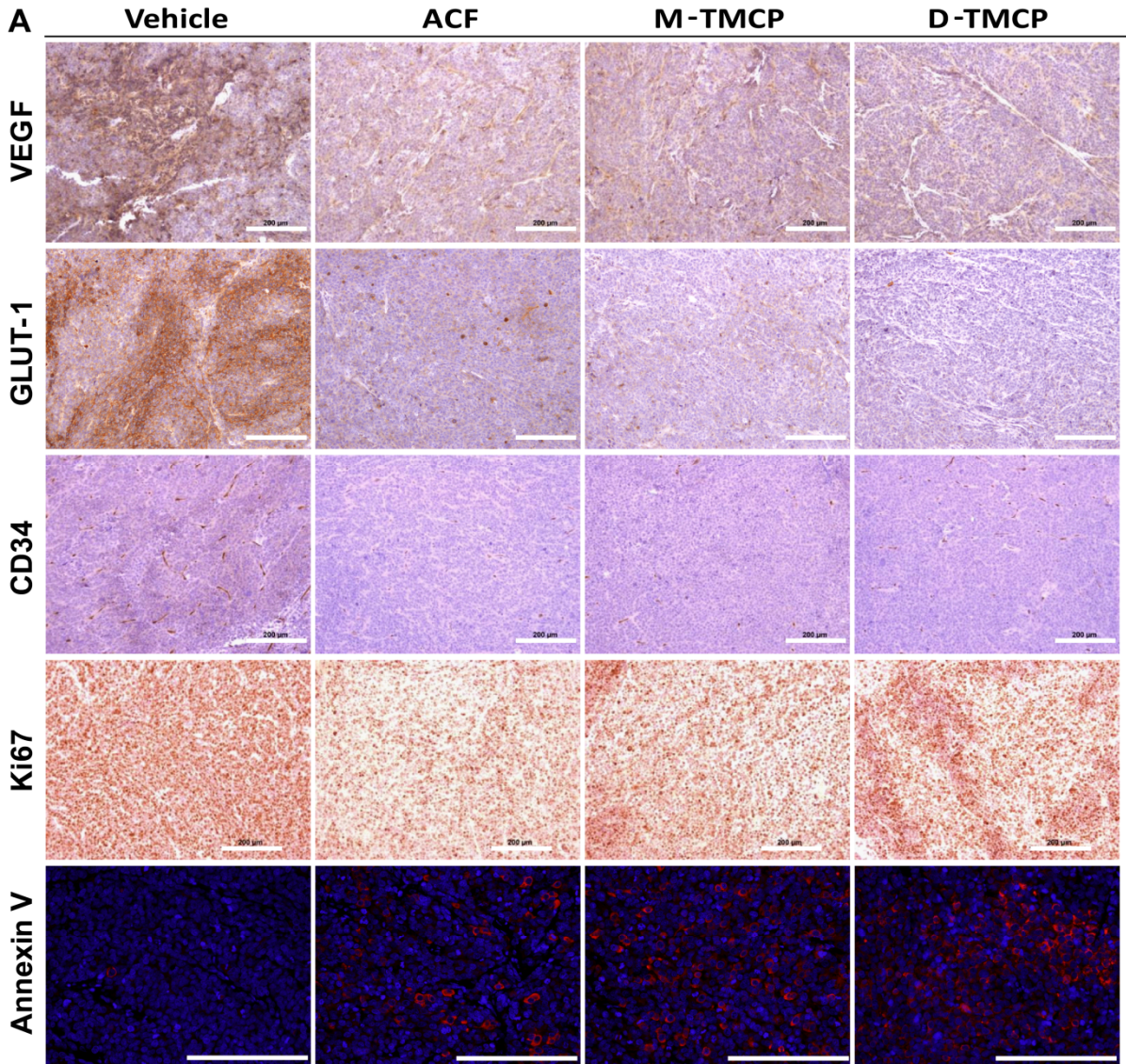


**Figure 28. Immunofluorescent staining for evaluating expression of VEGF (Green) with associated tumor vascular structure (CD34+; Red) in U87/NL1 $\alpha$ /CL1 $\beta$  tumors.** Mice bearing U87/NL1 $\alpha$ /CL1 $\beta$  xenograft were treated with vehicle, ACF, M-TMCP and D-TMCP (2 mg/kg in 3%DMSO in saline; 150  $\mu$ l i.p.) for 14 days. After the last dose, tumor samples were collected and evaluated by immunohistochemical analysis. In control tumors, the expression of VEGF was observed in avascular and apparently hypo- or non-perfused microvessels, whereas much lesser expression of VEGF was observed within 120-150  $\mu$ m around well perfused microvessels. In addition, the expression of VEGF was markedly decreased in ACF, M-TMCP, D-TMCP -treated tumors along with a statistically significant reduction in the number, size, and branching of CD34+ microvessels. Scale bar: 100  $\mu$ m.

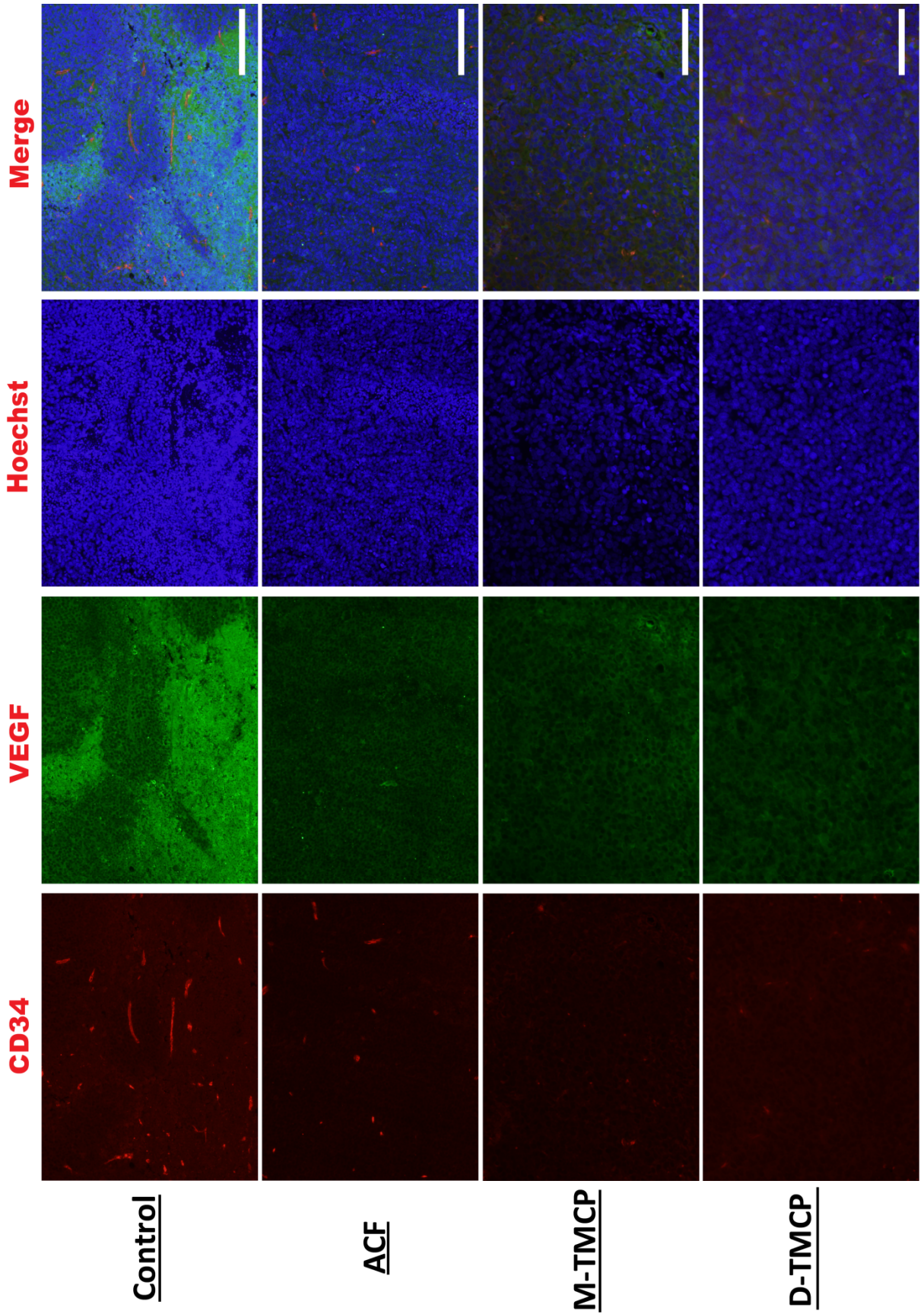




**Figure 29. Immunofluorescent staining for evaluating expression of GLUT-1 (Green) with associated tumor vascular structure (CD34+; Red) in U87/NL1 $\alpha$ /CL1 $\beta$  tumors.** Mice bearing U87/NL1 $\alpha$ /CL1 $\beta$  xenografts were treated with vehicle, ACF, M-TMCP and D-TMCP (2 mg/kg in 3%DMSO in saline; 150  $\mu$ l i.p.) for 14 days. After the last dose, tumor samples were collected and evaluated by immunohistochemical analysis. The expression of GLUT-1 was markedly decreased in ACF, M-TMCP, D-TMCP -treated tumors. In addition, the expression of GLUT-1 was often observed in avascular area. Scale bar: 100  $\mu$ m.

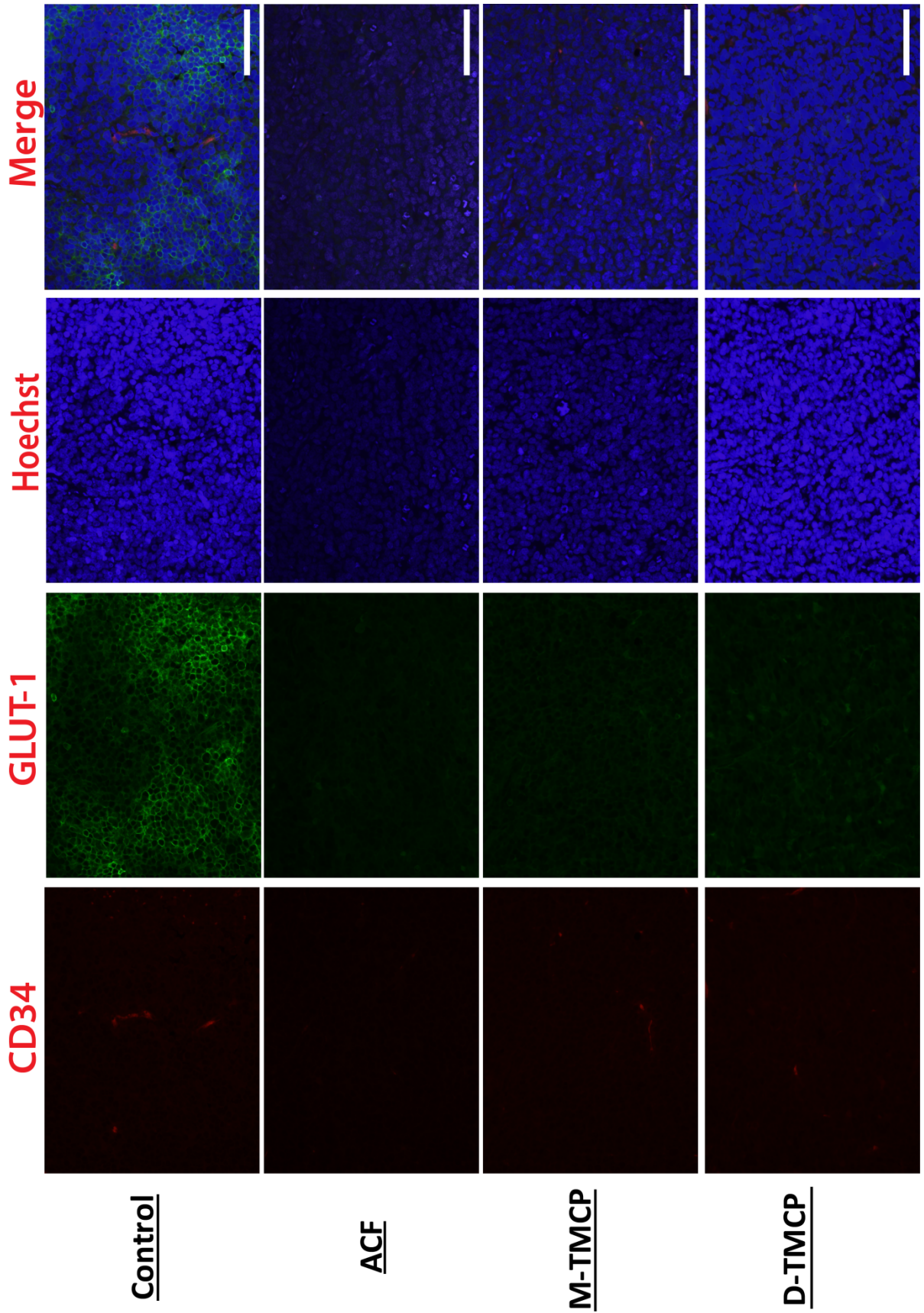
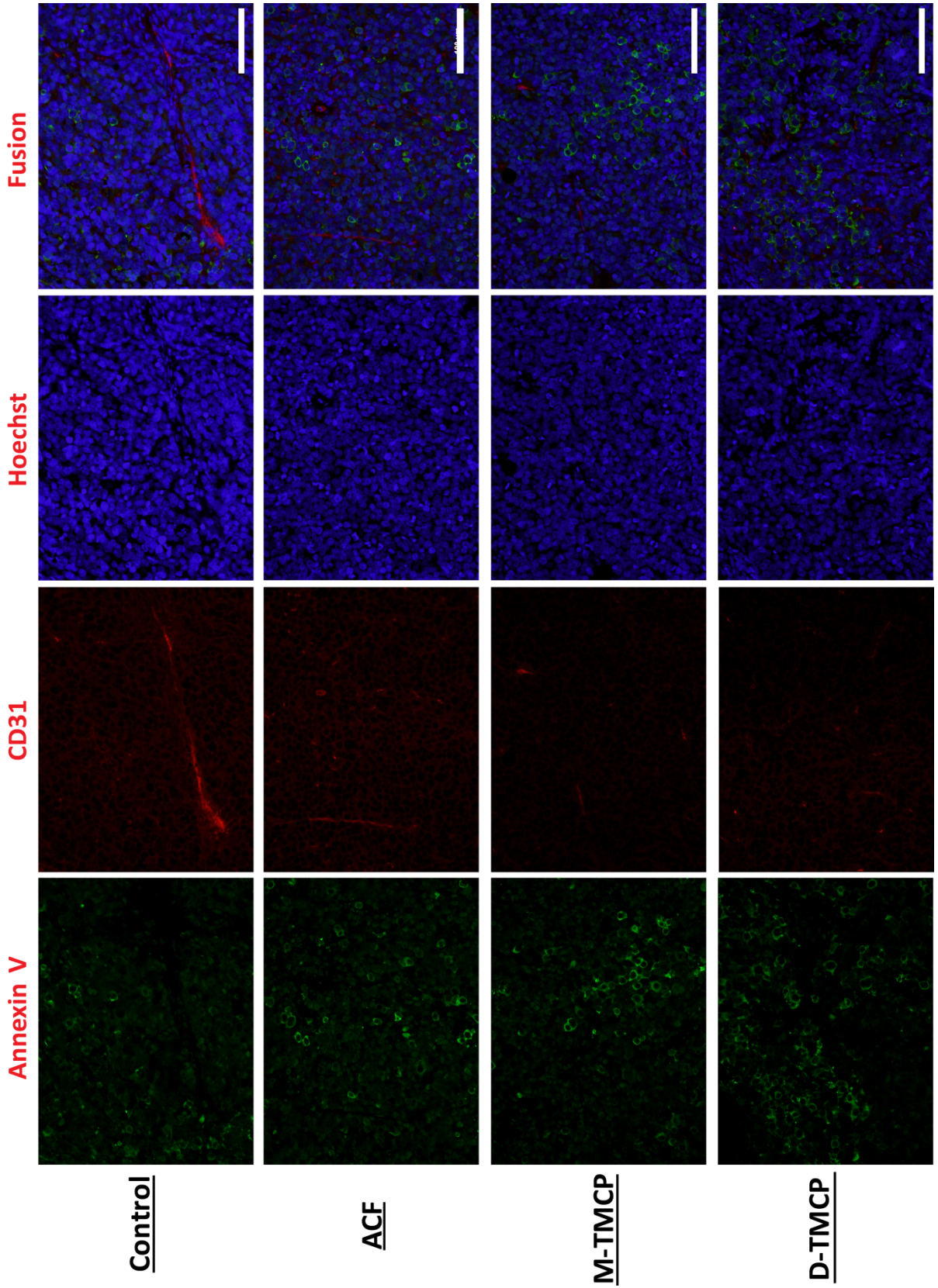


**Figure 30. Immunofluorescent staining for evaluating expression of Annexin V (Green) with associated tumor vascular structure (CD31+; Red) in U87/NL1 $\alpha$ /CL1 $\beta$  tumor.** Mice bearing U87/NL1 $\alpha$ /CL1 $\beta$  xenograft were treated with vehicle, ACF, M-TMCP and D-TMCP (2 mg/kg in 3%DMSO in saline; 150  $\mu$ l i.p.) for 14 days. After the last dose, tumor samples were collected and evaluated by immunohistochemical analysis. The percentage of apoptotic cells (Annexin V positive) was slightly increased in ACF, M-TMCP, D-TMCP - treated tumors verse control, along with a statistically significant reduction in the number, size, and branching of CD34+ microvessels. Scale bar: 100  $\mu$ m.



### **6.3 Assessment of systemic toxicity after chronic administration of D-TMCP *in vivo***

To examine whether the administration of D-TMCP caused drug-induced organ toxicity in nude mice, a separate group of normal mice were treated for three weeks with daily administration of 0, 1, 2, 5, or 10 mg/kg of D-TMCP (in 3%DMSO in saline; 150  $\mu$ l i.p.). All different dosage treatments of D-TMCP did not cause any notable histological changes in brain, heart, lung, liver, spleen, pancreas, kidney, and testis (**Fig. 31 and 32**), suggesting that D-TMCP was well tolerated in mice at doses up to 10 mg/kg.

**Figure 31. No physiological changes observed after repeated D-TMCP treatment, ranging from 1 to 10 mg/kg, for up to 21 days.** Histology analysis of organs from nude mice after 21 days of repeated D-TMCP treatment. After mice were sacrificed, their major organs were collected and fixed in formalin and paraffin-embedded. No abnormalities in the tissue physiology were observed under the microscope in the H&E sections (400× magnification). Scale bar: 200 µm.

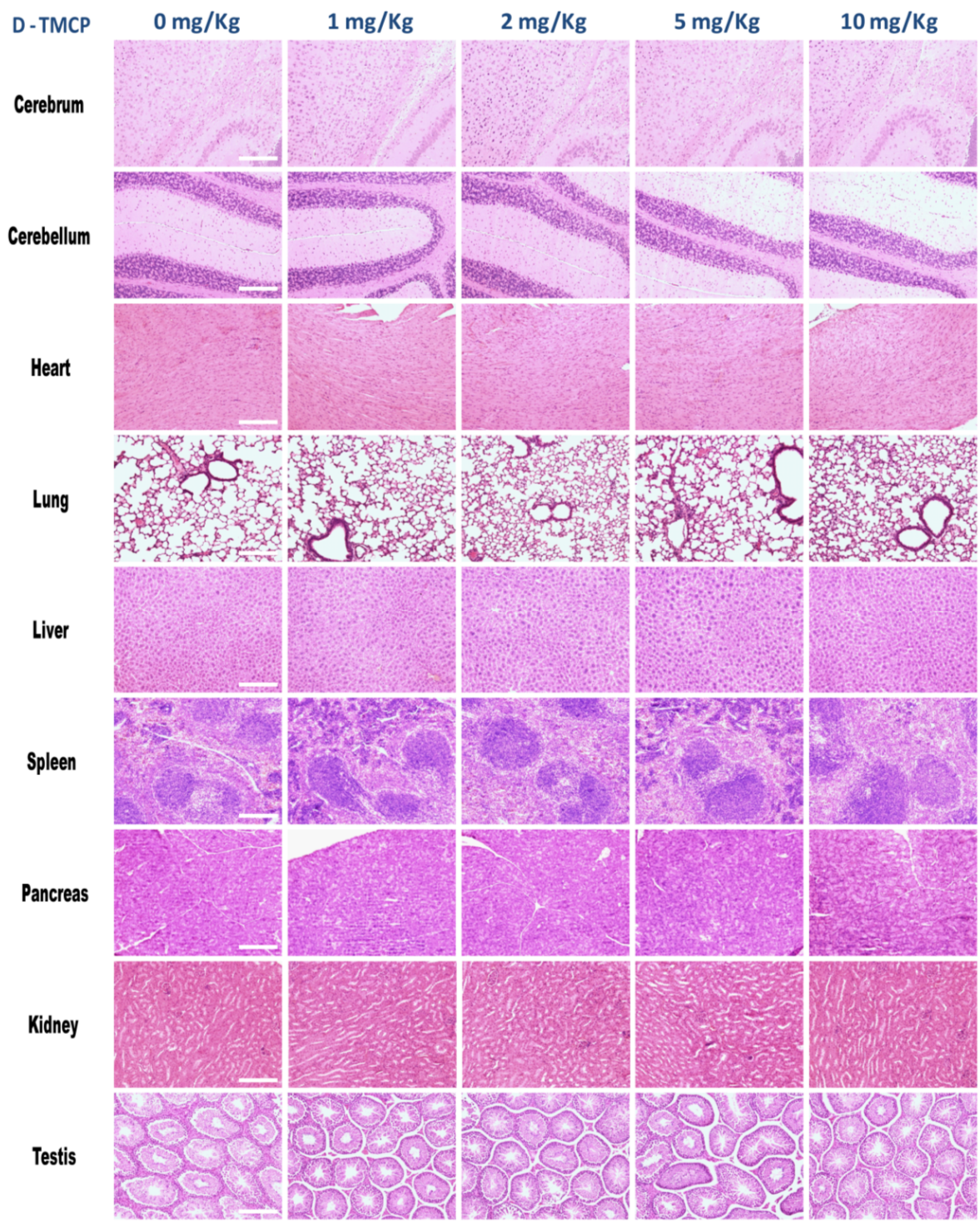
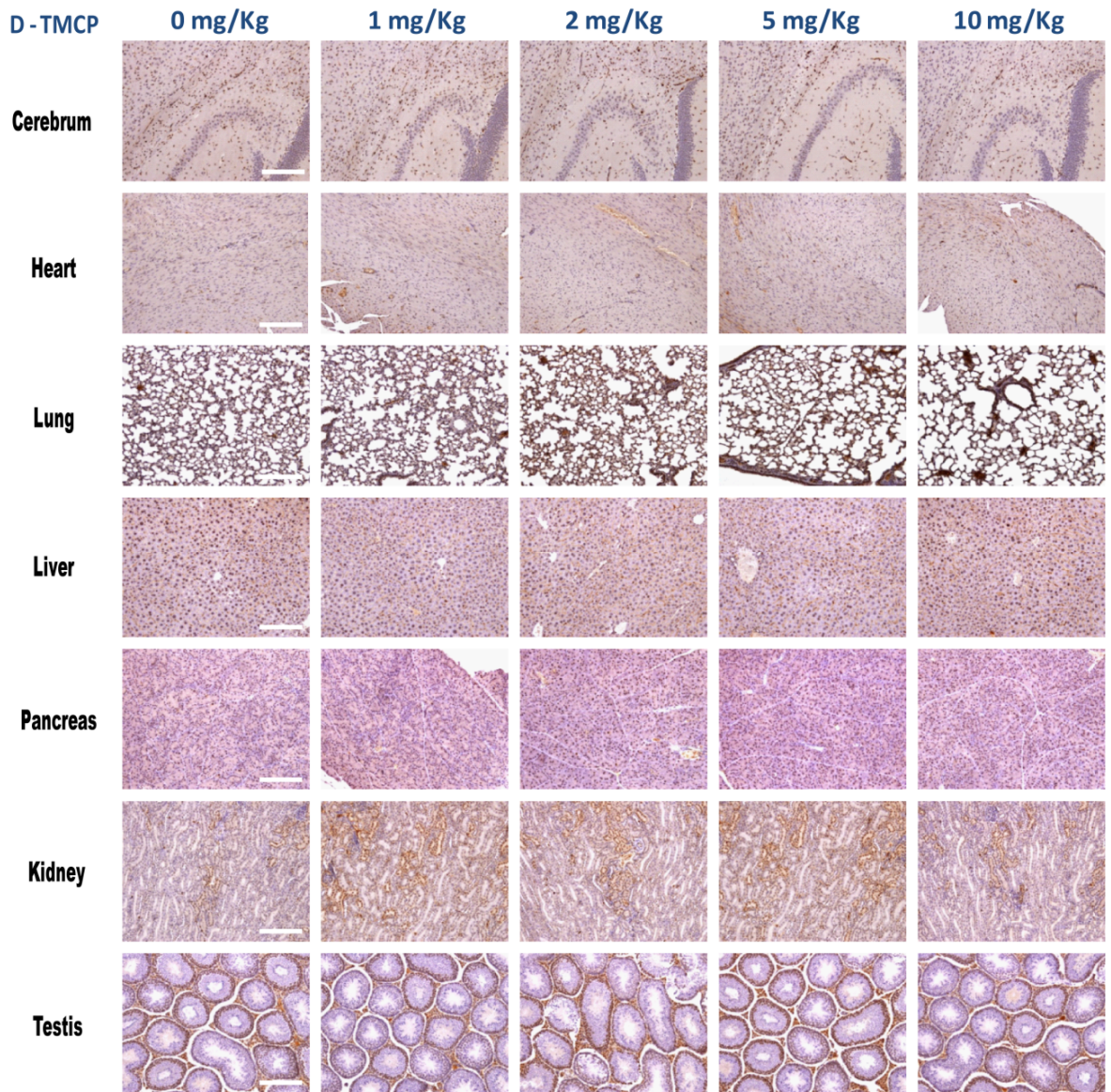


**Figure 32. No abnormal cellular proliferation observed after repeated D-TMCP treatment, ranging from 1 to 10 mg/kg, for up to 21 days.** Histology analysis of organs from nude mice after 21 days of repeated D-TMCP treatment. Mice major organs were collected, fixed in formalin, paraffin-embedded and stained with Ki67 IHC. The expression of Ki67 between each group was similar. No abnormal cellular proliferation was observed. Scale bar: 200  $\mu$ m.





## Chapter 7: Summary and Discussion

HIF-1 participates in energy metabolism, angiogenesis, and proliferation in tumors. Enhanced HIF-1 expression is a common feature of most solid tumors and often leads to poor clinical outcomes. Targeting HIF-1 has long been recognized as an effective yet challenging therapeutic strategy for cancer. Despite efforts have been made to identify small molecule inhibitors that target HIF-1 pathway, the strategies reported so far were mostly used *in vitro* yeast two-hybrid-like or cell-based reporter assays (Mahon et al., 2001, Bex et al., 2007, Li et al., 2008, Cockman et al., 2006, Schwartz et al., 2009, Tan et al., 2005, Narita et al., 2009, Semenza, 2007a, Mooring et al., 2011, Lee et al., 2009). The major drawback of *in vitro* yeast two-hybrid-like assays is the possibility of identifying biologically irrelevant interactions that may never occur *in vivo*, while the cell-based HIF-1-targeted assays offer the advantage of recapitulating relevant signaling *in vivo*. Most of the currently used cell-based HIF-1 assays utilize DNA constructs containing reporter genes under the control of multiple copies of HREs, usually the promoter region of VEGF. The binding of HIF-1 to HREs transactivates its downstream reporter gene, such as fluorescent or luciferase protein. This type of reporter design provides only the final result of HIF-1 transcriptional activity, with no information about the mechanisms of action. Therefore, in the present study, an exclusive HIF-1-targeted screening system was designed focusing on specific protein-protein interaction domains (PAS-AB) in HIF-1 $\alpha$  and HIF-1 $\beta$  to identify only selective inhibitors of HIF-1 $\alpha/\beta$  dimerization. The orientation of reporter vector was also determined to optimize the complementation assay for enhanced induction of HIF-1 $\alpha/\beta$  dimerization. Moreover, the HIF-1 $\alpha/\beta$  dimerization cell-based reporter system was established via lentiviral transduction instead of commonly used transient transfection, in which the level of gene expression decreases quickly over time. This stably transduced U87/NL1 $\alpha$ /CL1 $\beta$  cells can provide robust and quantifiable results in live cells or animal in near real time.

Although HIF-1 $\alpha$ /HIF-1 $\beta$  and HIF-2 $\alpha$ /HIF-1 $\beta$  share some similar properties, recent studies have suggested that they demonstrate distinct characteristics for both isoforms (Loboda et al., 2012, Loboda et al., 2010, Ratcliffe, 2007, Hu et al., 2003). For example, in regulation of angiogenesis, HIF-1 $\alpha$ /HIF-1 $\beta$  and HIF-2 $\alpha$ /HIF-1 $\beta$  may exert counteractive influences on angiogenic mediators. In hypoxia, HIF-1 $\alpha$ /HIF-1 $\beta$  and HIF-2 $\alpha$ /HIF-1 $\beta$  regulate VEGF expression in the same manner (Jones et al., 2001). However, while HIF-1 $\alpha$  decreases interleukin-8 (IL-8) expression, the overexpression of HIF-2 $\alpha$  results in increase of IL-8 (Florczyk et al., 2011, Loboda et al., 2009). The relationships between HIF-1 $\alpha$  and HIF-2 $\alpha$  in regulating different signal pathways remain to be explored further. These paradoxical effects of HIF-1 $\alpha$  and HIF-2 $\alpha$  in cancer may influence therapeutic approaches in developing HIF-1 targeted drugs. The discovery of HIF-1 $\alpha$  was earlier than HIF-2 $\alpha$ , and intensive investigation have led to better understanding of HIF-1 $\alpha$ /HIF-1 $\beta$  in cellular signaling network and pathological situations. Therefore, the design of current reporter system specifically aimed to identify the inhibitors of HIF-1 $\alpha$ /HIF-1 $\beta$  heterodimers. However, HIF-1 $\alpha$  and HIF-2 $\alpha$  share a high degree of homology. There is still a possibility that inhibitors identified using this HIF-1 $\alpha$ /HIF-1 $\beta$  reporter system may also disrupt the formation and function of HIF-2 $\alpha$ /HIF-1 $\beta$  heterodimer.

There is an increasing interest in identification of small molecular inhibitors that target protein-protein interactions that are essential for stabilization and formation of the HIF-1 $\alpha$ /HIF-1 $\beta$  heterodimer. Although several studies have demonstrated that some compound pose significant inhibitory activities in cell free assays, many failed during cell-based assays because of their poor pharmacokinetic properties, such as cell membrane permeability or absorption (Park et al., 2006a, Koh et al., 2008, Mooring et al., 2011, Yewalkar et al., 2010). Herein, this newly developed high-throughput system was designed to screen potential HIF-1 $\alpha$ / $\beta$  inhibitors in live cells so that cell permeability or absorption of

inhibitors would be reflected in the  $IC_{50}$  value. Using a cell based assay, Lee et al (2009) previously have identified acriflavine (ACF), a mixture 3,6-diamino-10-methylacridinium chloride and 3,6-diaminoacridine, as an inhibitor of HIF-1 $\alpha$ / $\beta$  dimerization and transcriptional activity (Lee et al., 2009). The high potency of ACF was confirmed using the newly developed reporter system in the initial screen of HIF-1 inhibitory compound library. However, this study was based on a mixture of two compounds. As a result, it was not clear which of these two compounds is responsible for the potency. To this end, the utilization of structure–activity relationships led to the discovery of a mono- and di-substituted 3,6-diaminoacridine analogues that have significant inhibition of the HIF-1 $\alpha$ /HIF-1 $\beta$  heterodimeric interaction. The functionalization at the 3,6-position of the diaminoacridine to assess potency was critical for understanding the structure-activity relationships in this series and for identifying compounds with improved pharmacodynamic profiles.

The PAS domain in HIF-1 $\alpha$  or HIF-1 $\beta$  can be sub-categorized into PAS-A and PAS-B subdomains, both of which contribute to the heterodimerization. Card et al. demonstrated that a point mutation in the PAS-B subdomain of HIF-2 $\alpha$  can disrupt HIF-2 $\alpha$ /HIF-1 $\beta$  heterodimer formation *in vitro*, and further attenuate hypoxia transcriptional responses in living cells. This result suggested the possibility of disrupting HIF-1 heterodimerization by partially blocking a single PAS subdomain. In Lee et al. study, it was showed that ACF binds to the PAS-B subdomain of HIF-1 $\alpha$ , thereby disrupting HIF-1 $\alpha$ / $\beta$  dimerization and leading to inhibition of HIF-1 transcriptional activity. Therefore, it is most likely that M-TMCP and D-TMCP also bind to the PAS domain of HIF-1 $\alpha$ , based on their similarity in chemical structure with ACF. In such case, M-TMCP or D-TMCP binds with stabilized HIF-1 $\alpha$  only in hypoxic regions, which also introduces an opportunity to use M-TMCP or D-TMCP as HIF-1 $\alpha$  targeted hypoxia imaging agent.

Treatment with M-TMCP or D-TMCP for two weeks resulted in a significant inhibition of tumor growth. The balance between cell proliferation and cell death determines the growth dynamics of tumor tissue. The decrease in tumor cell proliferation (Ki67+ labeling index) and the increase in the number of apoptotic cells, as compared to control, explain the tumor shrinkage observed in all three treatment groups. In addition, M-TMCP or D-TMCP demonstrated significant antitumor activity that was associated with the decrease of VEGF and GLUT-1 expression in *in vivo* U87 human glioma mice models. These changes were paralleled by the downregulation of pro-tumorigenic genes involved in HIF-1 signaling network observed in the qRT-PCR arrays. Early decreases in BLI signals from the xenograft tumors treated with M-TMCP and D-TMCP indicated that our reporter system promptly detect HIF-1 $\alpha/\beta$  disruption in tumors, which preceded the retardation of tumor growth.

Some concerns may be raised about whether the identified HIF-1 inhibitors are too cytotoxic to serve as drug leads. In this study, D-TMCP inhibited HIF-1 activity at concentrations that did not affect proliferation or survival of the cells. Daily administration of 1-10 mg/kg D-TMCP in nude mice for 21 days did not result in distinct changes in the morphology or function of major vital organs. Although acridine analogs are known for antimicrobial activity (Wainwright, 2001, Wainwright, 2000) and even some anti-tumor activity (Patel et al., 2010), for many years their potential roles as anti-cancer drugs have not been fully explored. Herein, this study clarified their mechanism of action at the transcription level and provided evidence for antitumor efficacy of acridine derivatives in *in vivo* small animal tumor models. However, to move the inhibitors into clinical trials, additional preclinical studies are still required.

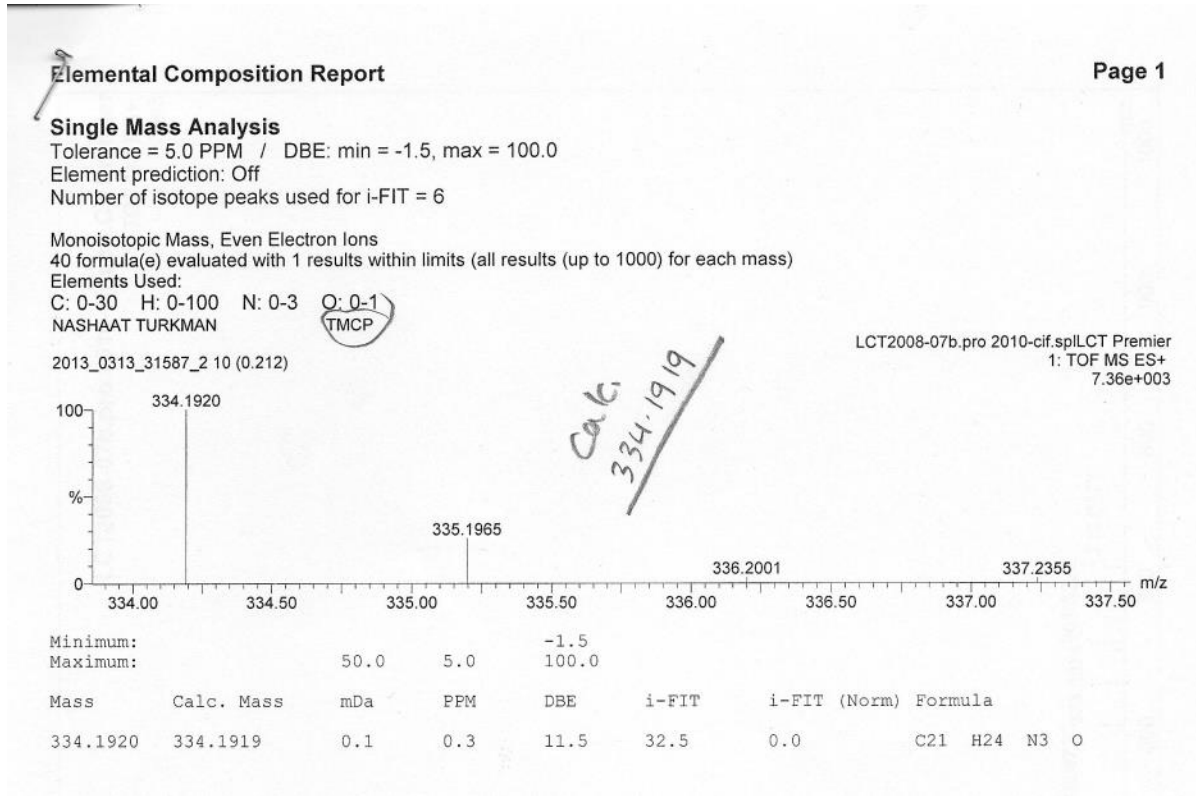
In conclusion, a novel methodology was developed for exploring selective HIF-1 $\alpha/\beta$  dimerization inhibitors *in cellulo* and *in vivo*. Using this HIF-1 $\alpha/\beta$  heterodimerization screening system, the structure-activity relationship of acridine analogues was established,

which provides valuable information for future optimizing HIF-1 $\alpha$ / $\beta$  inhibitor from chemical libraries. Moreover, the most promising drug candidates, M-TMCP and D-TMCP, exhibit significant antitumor efficacy with no physiological toxicity and show great clinical potential as a dual therapeutic and diagnostic agent. The identification of selective HIF-1 $\alpha$ / $\beta$  inhibitors is not only beneficial for therapeutic implications, but also as an analytic tool to further explore the role of HIF-1 $\alpha$ / $\beta$  in human cancers.

## Chapter 8: Future Direction

In the future, the therapeutic potential of M-TMCP or D-TMCP will be further evaluated using different animal models. In addition, we will investigate whether the combination of M-TMCP or D-TMCP with other treatments (e.g. chemotherapy, radiotherapy, or immunotherapy) may be more effective in achieving tumor remission and increasing survival rate. On the other aspect, M-TMCP or D-TMCP will be labeled with different radionuclides, such as  $^{18}\text{F}$  or  $^{188}\text{Re}$ , to explore the possibility of developing new HIF-1 $\alpha$  imaging agent. After isotopic labeling, their efficacy will need to be re-evaluated. If successful, this HIF-1 $\alpha$  imaging agent can serve as a hypoxia indicator to evaluate the treatment response of anti-cancer drugs or radiation therapy. In the meantime, more compound libraries will be explored using this high content HIF-1 $\alpha$ / $\beta$  dimerization screening system to identify potential drug leads.

# Appendix





# Elemental Composition Report

## Single Mass Analysis

Tolerance = 5.0 PPM / DBE: min = -1.5, max = 100.0

Element prediction: Off

Number of isotope peaks used for i-FIT = 6

Monoisotopic Mass, Even Electron Ions

59 formula(e) evaluated with 2 results within limits (all results (up to 1000) for each mass)

Elements Used:

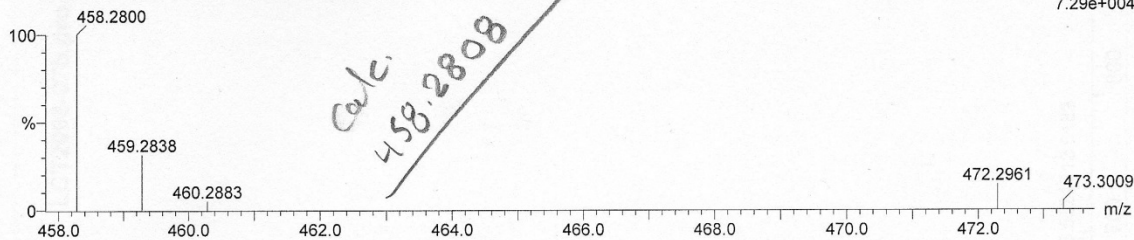
C: 0-30 H: 0-100 N: 0-3 O: 0-2 <sup>23</sup>Na: 0-1

NASHAAT TURKMAN

DTMCP

LCT2008-07b.pro 2010-cif.splLCT Premier  
1: TOF MS ES+  
7.29e+004

2013\_0313\_3159 16 (0.334) Cm (16:35-1:8x2.000)



Minimum: 50.0 5.0 -1.5  
Maximum: 100.0

Mass	Calc. Mass	mDa	PPM	DBE	i-FIT	i-FIT (Norm)	Formula
458.2800	458.2808	-0.8	-1.7	13.5	48.6	0.4	C29 H36 N3 O2
	458.2783	1.7	3.7	10.5	49.4	1.2	C27 H37 N3 O2 <sup>23</sup> Na

## Bibliography

- ARKIN, A., ROSS, J. & MCADAMS, H. H. 1998. Stochastic kinetic analysis of developmental pathway bifurcation in phage lambda-infected *Escherichia coli* cells. *Genetics*, 149, 1633-48.
- BARDOS, J. I. & ASHCROFT, M. 2005. Negative and positive regulation of HIF-1: a complex network. *Biochim Biophys Acta*, 1755, 107-20.
- BEX, C., KNAUTH, K., DAMBACHER, S. & BUCHBERGER, A. 2007. A yeast two-hybrid system reconstituting substrate recognition of the von Hippel-Lindau tumor suppressor protein. *Nucleic Acids Res*, 35, e142.
- BHATTACHARYYA, S. & TOBACMAN, J. K. 2012. Hypoxia reduces arylsulfatase B activity and silencing arylsulfatase B replicates and mediates the effects of hypoxia. *Plos One*, 7, e33250.
- BISSERY, M. C., GUENARD, D., GUERITTE-VOEGELEIN, F. & LAVELLE, F. 1991. Experimental antitumor activity of taxotere (RP 56976, NSC 628503), a taxol analogue. *Cancer Res*, 51, 4845-52.
- BRISTOW, R. G. & HILL, R. P. 2008. Hypoxia and metabolism. Hypoxia, DNA repair and genetic instability. *Nat Rev Cancer*, 8, 180-92.
- CARMELIET, P., DOR, Y., HERBERT, J. M., FUKUMURA, D., BRUSSELMANS, K., DEWERCHIN, M., NEEMAN, M., BONO, F., ABRAMOVITCH, R., MAXWELL, P., KOCH, C. J., RATCLIFFE, P., MOONS, L., JAIN, R. K., COLLEN, D. & KESHERT, E. 1998. Role of HIF-1alpha in hypoxia-mediated apoptosis, cell proliferation and tumour angiogenesis. *Nature*, 394, 485-90.
- CHAPMAN, J. D. 1984. The detection and measurement of hypoxic cells in solid tumors. *Cancer*, 54, 2441-9.

CHEN, S. & SANG, N. 2011. Histone deacetylase inhibitors: the epigenetic therapeutics that repress hypoxia-inducible factors. *J Biomed Biotechnol*, 2011, 197946.

COCKMAN, M. E., LANCASTER, D. E., STOLZE, I. P., HEWITSON, K. S., MCDONOUGH, M. A., COLEMAN, M. L., COLES, C. H., YU, X., HAY, R. T., LEY, S. C., PUGH, C. W., OLDHAM, N. J., MASSON, N., SCHOFIELD, C. J. & RATCLIFFE, P. J. 2006. Posttranslational hydroxylation of ankyrin repeats in I $\kappa$ B proteins by the hypoxia-inducible factor (HIF) asparaginyl hydroxylase, factor inhibiting HIF (FIH). *Proc Natl Acad Sci U S A*, 103, 14767-72.

CORMIER-REGARD, S., NGUYEN, S. V. & CLAYCOMB, W. C. 1998. Adrenomedullin gene expression is developmentally regulated and induced by hypoxia in rat ventricular cardiac myocytes. *Journal of Biological Chemistry*, 273, 17787-17792.

DE WET, J. R., WOOD, K. V., DELUCA, M., HELINSKI, D. R. & SUBRAMANI, S. 1987. Firefly luciferase gene: structure and expression in mammalian cells. *Mol Cell Biol*, 7, 725-37.

DELUCA, M. & MCELROY, W. D. 1974. Kinetics of the firefly luciferase catalyzed reactions. *Biochemistry*, 13, 921-5.

DENKO, N. C. 2008. Hypoxia, HIF1 and glucose metabolism in the solid tumour. *Nat Rev Cancer*, 8, 705-13.

DRUTEL, G., KATHMANN, M., HERON, A., SCHWARTZ, J. C. & ARRANG, J. M. 1996. Cloning and selective expression in brain and kidney of ARNT2 homologous to the Ah receptor nuclear translocator (ARNT). *Biochem Biophys Res Commun*, 225, 333-9.

DRYSDALE, M. J., BROUGH, P. A., MASSEY, A., JENSEN, M. R. & SCHOEPFER, J. 2006. Targeting Hsp90 for the treatment of cancer. *Curr Opin Drug Discov Devel*, 9, 483-95.

ELVIDGE, G. P., GLENNY, L., APPELHOFF, R. J., RATCLIFFE, P. J., RAGOUSSIS, J. & GLEADLE, J. M. 2006. Concordant regulation of gene expression by hypoxia and 2-

oxoglutarate-dependent dioxygenase inhibition: the role of HIF-1alpha, HIF-2alpha, and other pathways. *J Biol Chem*, 281, 15215-26.

FLORCZYK, U., CZAUDERNA, S., STACHURSKA, A., TERTIL, M., NOWAK, W., KOZAKOWSKA, M., POELLINGER, L., JOZKOWICZ, A., LOBODA, A. & DULAK, J. 2011. Opposite effects of HIF-1alpha and HIF-2alpha on the regulation of IL-8 expression in endothelial cells. *Free Radic Biol Med*, 51, 1882-92.

GARAYOA, M., MARTINEZ, A., LEE, S., PIO, R., AN, W. G., NECKERS, L., TREPEL, J., MONTUENGA, L. M., RYAN, H., JOHNSON, R., GASSMANN, M. & CUTTITTA, F. 2000. Hypoxia-inducible factor-1 (HIF-1) up-regulates adrenomedullin expression in human tumor cell lines during oxygen deprivation: a possible promotion mechanism of carcinogenesis. *Mol Endocrinol*, 14, 848-62.

GODA, N., RYAN, H. E., KHADIVI, B., MCNULTY, W., RICKERT, R. C. & JOHNSON, R. S. 2003. Hypoxia-inducible factor 1alpha is essential for cell cycle arrest during hypoxia. *Mol Cell Biol*, 23, 359-69.

GOLDBERG, M. A., DUNNING, S. P. & BUNN, H. F. 1988. Regulation of the erythropoietin gene: evidence that the oxygen sensor is a heme protein. *Science*, 242, 1412-5.

GREENBERGER, L. M., HORAK, I. D., FILPULA, D., SAPRA, P., WESTERGAARD, M., FRYDENLUND, H. F., ALBAEK, C., SCHRODER, H. & ORUM, H. 2008. A RNA antagonist of hypoxia-inducible factor-1alpha, EZN-2968, inhibits tumor cell growth. *Mol Cancer Ther*, 7, 3598-608.

GRUNBAUM, Z., FREAUFF, S. J., KROHN, K. A., WILBUR, D. S., MAGEE, S. & RASEY, J. S. 1987. Synthesis and characterization of congeners of misonidazole for imaging hypoxia. *J Nucl Med*, 28, 68-75.

HANAHAN, D. & WEINBERG, R. A. 2000. The hallmarks of cancer. *Cell*, 100, 57-70.

HANAHAN, D. & WEINBERG, R. A. 2011. Hallmarks of cancer: the next generation. *Cell*, 144, 646-74.

HANZE, J., EUL, B. G., SAVAI, R., KRICK, S., GOYAL, P., GRIMMINGER, F., SEEGER, W. & ROSE, F. 2003. RNA interference for HIF-1alpha inhibits its downstream signalling and affects cellular proliferation. *Biochem Biophys Res Commun*, 312, 571-7.

HARRISON, L. B., CHADHA, M., HILL, R. J., HU, K. & SHASHA, D. 2002. Impact of tumor hypoxia and anemia on radiation therapy outcomes. *Oncologist*, 7, 492-508.

HASSAN, S., LARYEA, D., MAHTEME, H., FELTH, J., FRYKNAS, M., FAYAD, W., LINDER, S., RICKARDSON, L., GULLBO, J., GRAF, W., PAHLMAN, L., GLIMELIUS, B., LARSSON, R. & NYGREN, P. 2011. Novel activity of acriflavine against colorectal cancer tumor cells. *Cancer Sci*, 102, 2206-13.

HIGGINS, D. F., KIMURA, K., BERNHARDT, W. M., SHRIMANKER, N., AKAI, Y., HOHENSTEIN, B., SAITO, Y., JOHNSON, R. S., KRETZLER, M., COHEN, C. D., ECKARDT, K. U., IWANO, M. & HAASE, V. H. 2007. Hypoxia promotes fibrogenesis in vivo via HIF-1 stimulation of epithelial-to-mesenchymal transition. *J Clin Invest*, 117, 3810-20.

HIROTA, K. & SEMENZA, G. L. 2006. Regulation of angiogenesis by hypoxia-inducible factor 1. *Critical Reviews in Oncology/Hematology*, 59, 15-26.

HU, C. J., WANG, L. Y., CHODOSH, L. A., KEITH, B. & SIMON, M. C. 2003. Differential roles of hypoxia-inducible factor 1alpha (HIF-1alpha) and HIF-2alpha in hypoxic gene regulation. *Mol Cell Biol*, 23, 9361-74.

HUDSON, C. C., LIU, M., CHIANG, G. G., OTTERNESS, D. M., LOOMIS, D. C., KAPER, F., GIACCIA, A. J. & ABRAHAM, R. T. 2002. Regulation of hypoxia-inducible factor 1alpha expression and function by the mammalian target of rapamycin. *Mol Cell Biol*, 22, 7004-14.

ISAACS, J. S., JUNG, Y. J., MIMNAUGH, E. G., MARTINEZ, A., CUTTITTA, F. & NECKERS, L. M. 2002. Hsp90 regulates a von Hippel Lindau-independent hypoxia-inducible factor-1 alpha-degradative pathway. *J Biol Chem*, 277, 29936-44.

IYER, N. V., KOTCH, L. E., AGANI, F., LEUNG, S. W., LAUGHNER, E., WENGER, R. H., GASSMANN, M., GEARHART, J. D., LAWLER, A. M., YU, A. Y. & SEMENZA, G. L. 1998. Cellular and developmental control of O<sub>2</sub> homeostasis by hypoxia-inducible factor 1 alpha. *Genes Dev*, 12, 149-62.

JIANG, B. H., JIANG, G., ZHENG, J. Z., LU, Z., HUNTER, T. & VOGT, P. K. 2001. Phosphatidylinositol 3-kinase signaling controls levels of hypoxia-inducible factor 1. *Cell Growth Differ*, 12, 363-9.

JIANG, G., LI, T., QIU, Y., RUI, Y., CHEN, W. & LOU, Y. 2007. RNA interference for HIF-1alpha inhibits foam cells formation in vitro. *Eur J Pharmacol*, 562, 183-90.

JING, S. W., WANG, Y. D., CHEN, L. Q., SANG, M. X., ZHENG, M. M., SUN, G. G., LIU, Q., CHENG, Y. J. & YANG, C. R. 2013. Hypoxia suppresses E-cadherin and enhances matrix metalloproteinase-2 expression favoring esophageal carcinoma migration and invasion via hypoxia inducible factor-1 alpha activation. *Dis Esophagus*, 26, 75-83.

JONES, A., FUJIYAMA, C., BLANCHE, C., MOORE, J. W., FUGGLE, S., CRANSTON, D., BICKNELL, R. & HARRIS, A. L. 2001. Relation of vascular endothelial growth factor production to expression and regulation of hypoxia-inducible factor-1 alpha and hypoxia-inducible factor-2 alpha in human bladder tumors and cell lines. *Clin Cancer Res*, 7, 1263-72.

JONES, D. T. & HARRIS, A. L. 2006. Identification of novel small-molecule inhibitors of hypoxia-inducible factor-1 transactivation and DNA binding. *Mol Cancer Ther*, 5, 2193-202.

JORDAN, B. F. & SONVEAUX, P. 2012. Targeting tumor perfusion and oxygenation to improve the outcome of anticancer therapy. *Front Pharmacol*, 3, 94.

KALUZ, S., KALUZOVA, M. & STANBRIDGE, E. J. 2006. Proteasomal inhibition attenuates transcriptional activity of hypoxia-inducible factor 1 (HIF-1) via specific effect on the HIF-1alpha C-terminal activation domain. *Mol Cell Biol*, 26, 5895-907.

KENNETH, N. S. & ROCHA, S. 2008. Regulation of gene expression by hypoxia. *Biochem J*, 414, 19-29.

KESSLER, J., HAHNEL, A., WICHMANN, H., ROT, S., KAPPLER, M., BACHE, M. & VORDERMARK, D. 2010. HIF-1alpha inhibition by siRNA or chetomin in human malignant glioma cells: effects on hypoxic radioresistance and monitoring via CA9 expression. *BMC Cancer*, 10, 605.

KIM, S. G., KIM, C. W., AHN, E. T., LEE, K. Y., HONG, E. K., YOO, B. I. & HAN, Y. B. 1997. Enhanced anti-tumour effects of acriflavine in combination with guanosine in mice. *J Pharm Pharmacol*, 49, 216-22.

KOH, M. Y., SPIVAK-KROIZMAN, T., VENTURINI, S., WELSH, S., WILLIAMS, R. R., KIRKPATRICK, D. L. & POWIS, G. 2008. Molecular mechanisms for the activity of PX-478, an antitumor inhibitor of the hypoxia-inducible factor-1alpha. *Mol Cancer Ther*, 7, 90-100.

KONG, D., PARK, E. J., STEPHEN, A. G., CALVANI, M., CARDELLINA, J. H., MONKS, A., FISHER, R. J., SHOEMAKER, R. H. & MELILLO, G. 2005. Echinomycin, a small-molecule inhibitor of hypoxia-inducible factor-1 DNA-binding activity. *Cancer Res*, 65, 9047-55.

KOOP, E. A., VAN LAAR, T., VAN WICHEN, D. F., DE WEGER, R. A., WALL, E. & VAN DIEST, P. J. 2009. Expression of BNIP3 in invasive breast cancer: correlations with the hypoxic response and clinicopathological features. *BMC Cancer*, 9, 175.

KOSHIJI, M., KAGEYAMA, Y., PETE, E. A., HORIKAWA, I., BARRETT, J. C. & HUANG, L. E. 2004. HIF-1alpha induces cell cycle arrest by functionally counteracting Myc. *EMBO J*, 23, 1949-56.

KRISHNAMACHARY, B., ZAGZAG, D., NAGASAWA, H., RAINEY, K., OKUYAMA, H., BAEK, J. H. & SEMENZA, G. L. 2006. Hypoxia-inducible factor-1-dependent repression of E-cadherin in von Hippel-Lindau tumor suppressor-null renal cell carcinoma mediated by TCF3, ZFHX1A, and ZFHX1B. *Cancer Res*, 66, 2725-31.

KROHN, K. A., LINK, J. M. & MASON, R. P. 2008. Molecular imaging of hypoxia. *J Nucl Med*, 49 Suppl 2, 129S-48S.

KULSHRESHTHA, R., FERRACIN, M., WOJCIK, S. E., GARZON, R., ALDER, H., AGOSTO-PEREZ, F. J., DAVULURI, R., LIU, C. G., CROCE, C. M., NEGRINI, M., CALIN, G. A. & IVAN, M. 2007. A microRNA signature of hypoxia. *Mol Cell Biol*, 27, 1859-67.

LEE, K., ZHANG, H., QIAN, D. Z., REY, S., LIU, J. O. & SEMENZA, G. L. 2009. Acriflavine inhibits HIF-1 dimerization, tumor growth, and vascularization. *Proceedings of the National Academy of Sciences*, 106, 17910-17915.

LEE, S. T. & SCOTT, A. M. 2007. Hypoxia positron emission tomography imaging with <sup>18</sup>F-fluoromisonidazole. *Semin Nucl Med*, 37, 451-61.

LEHNINGER, A. L., NELSON, D. L. & COX, M. M. 2013. *Lehninger principles of biochemistry*, New York, W.H. Freeman.

LEMAIRE, L., BASTIAT, G., FRANCONI, F., LAUTRAM, N., DUONG THI DAN, T., GARCION, E., SAULNIER, P. & BENOIT, J. P. 2013. Perfluorocarbon-loaded lipid nanocapsules as oxygen sensors for tumor tissue pO<sub>2</sub> assessment. *Eur J Pharm Biopharm*.

LI, S. H., SHIN, D. H., CHUN, Y. S., LEE, M. K., KIM, M. S. & PARK, J. W. 2008. A novel mode of action of YC-1 in HIF inhibition: stimulation of FIH-dependent p300 dissociation from HIF-1{α}. *Mol Cancer Ther*, 7, 3729-38.

LIAO, H. Y., WANG, G. P., GU, L. J., HUANG, S. H., CHEN, X. L., LI, Y. & CAI, S. W. 2012. HIF-1α siRNA and cisplatin in combination suppress tumor growth in a nude



mice model of esophageal squamous cell carcinoma. *Asian Pac J Cancer Prev*, 13, 473-7.

LIU, A. M., QU, W. W., LIU, X. & QU, C. K. 2012. Chromosomal instability in in vitro cultured mouse hematopoietic cells associated with oxidative stress. *Am J Blood Res*, 2, 71-6.

LOBODA, A., JOZKOWICZ, A. & DULAK, J. 2010. HIF-1 and HIF-2 transcription factors--similar but not identical. *Mol Cells*, 29, 435-42.

LOBODA, A., JOZKOWICZ, A. & DULAK, J. 2012. HIF-1 versus HIF-2--is one more important than the other? *Vascul Pharmacol*, 56, 245-51.

LOBODA, A., STACHURSKA, A., FLORCZYK, U., RUDNICKA, D., JAZWA, A., WEGRZYN, J., KOZAKOWSKA, M., STALINSKA, K., POELLINGER, L., LEVONEN, A. L., YLA-HERTTUALA, S., JOZKOWICZ, A. & DULAK, J. 2009. HIF-1 induction attenuates Nrf2-dependent IL-8 expression in human endothelial cells. *Antioxid Redox Signal*, 11, 1501-17.

LOIACONO, L. A. & SHAPIRO, D. S. 2010. Detection of hypoxia at the cellular level. *Crit Care Clin*, 26, 409-21, table of contents.

LUKER, K. E., SMITH, M. C., LUKER, G. D., GAMMON, S. T., PIWNICA-WORMS, H. & PIWNICA-WORMS, D. 2004. Kinetics of regulated protein-protein interactions revealed with firefly luciferase complementation imaging in cells and living animals. *Proc Natl Acad Sci U S A*, 101, 12288-93.

MABJEESH, N. J., POST, D. E., WILLARD, M. T., KAUR, B., VAN MEIR, E. G., SIMONS, J. W. & ZHONG, H. 2002. Geldanamycin induces degradation of hypoxia-inducible factor 1alpha protein via the proteasome pathway in prostate cancer cells. *Cancer Res*, 62, 2478-82.

MAHON, P. C., HIROTA, K. & SEMENZA, G. L. 2001. FIH-1: a novel protein that interacts with HIF-1 alpha and VHL to mediate repression of HIF-1 transcriptional activity. *Genes & Development*, 15, 2675-2686.

MAJUMDER, P. K., FEBBO, P. G., BIKOFF, R., BERGER, R., XUE, Q., MCMAHON, L. M., MANOLA, J., BRUGAROLAS, J., MCDONNELL, T. J., GOLUB, T. R., LODA, M., LANE, H. A. & SELLERS, W. R. 2004. mTOR inhibition reverses Akt-dependent prostate intraepithelial neoplasia through regulation of apoptotic and HIF-1-dependent pathways. *Nat Med*, 10, 594-601.

MALTEPE, E., KEITH, B., ARSHAM, A. M., BRORSON, J. R. & SIMON, M. C. 2000. The role of ARNT2 in tumor angiogenesis and the neural response to hypoxia. *Biochem Biophys Res Commun*, 273, 231-8.

MANALO, D. J., ROWAN, A., LAVOIE, T., NATARAJAN, L., KELLY, B. D., YE, S. Q., GARCIA, J. G. & SEMENZA, G. L. 2005. Transcriptional regulation of vascular endothelial cell responses to hypoxia by HIF-1. *Blood*, 105, 659-69.

MARTIN, G. V., CALDWELL, J. H., GRAHAM, M. M., GRIERSON, J. R., KROLL, K., COWAN, M. J., LEWELLEN, T. K., RASEY, J. S., CASCIARI, J. J. & KROHN, K. A. 1992. Noninvasive detection of hypoxic myocardium using fluorine-18-fluoromisonidazole and positron emission tomography. *J Nucl Med*, 33, 2202-8.

MASON, R. P., ZHAO, D., PACHECO-TORRES, J., CUI, W., KODIBAGKAR, V. D., GULAKA, P. K., HAO, G., THORPE, P., HAHN, E. W. & PESCHKE, P. 2010. Multimodality imaging of hypoxia in preclinical settings. *Q J Nucl Med Mol Imaging*, 54, 259-80.

MELILLO, G. 2006. Inhibiting Hypoxia-Inducible Factor 1 for Cancer Therapy. *Molecular Cancer Research*, 4, 601-605.

MOORING, S. R., JIN, H., DEVI, N. S., JABBAR, A. A., KALUZ, S., LIU, Y., VAN MEIR, E. G. & WANG, B. 2011. Design and Synthesis of Novel Small-Molecule Inhibitors of the Hypoxia Inducible Factor Pathway. *Journal of Medicinal Chemistry*, 54, 8471-8489.

NARITA, T., YIN, S., GELIN, C. F., MORENO, C. S., YEPES, M., NICOLAOU, K. C. & VAN MEIR, E. G. 2009. Identification of a Novel Small Molecule HIF-1 Translation Inhibitor. *Clinical Cancer Research*, 15, 6128-6136.

NUNN, J. F. 1993. *Nunn's applied respiratory physiology*, Oxford ; Boston, Butterworth-Heinemann.

O'DONOGHUE, J. A., ZANZONICO, P., PUGACHEV, A., WEN, B., SMITH-JONES, P., CAI, S., BURNAZI, E., FINN, R. D., BURGMAN, P., RUAN, S., LEWIS, J. S., WELCH, M. J., LING, C. C. & HUMM, J. L. 2005. Assessment of regional tumor hypoxia using 18F-fluoromisonidazole and <sup>64</sup>Cu(II)-diacetyl-bis(N4-methylthiosemicarbazone) positron emission tomography: Comparative study featuring microPET imaging, Po<sub>2</sub> probe measurement, autoradiography, and fluorescent microscopy in the R3327-AT and FaDu rat tumor models. *Int J Radiat Oncol Biol Phys*, 61, 1493-502.

OLENYUK, B. Z., ZHANG, G. J., KLCO, J. M., NICKOLS, N. G., KAELIN, W. G., JR. & DERVAN, P. B. 2004. Inhibition of vascular endothelial growth factor with a sequence-specific hypoxia response element antagonist. *Proc Natl Acad Sci U S A*, 101, 16768-73.

PARK, E. J., KONG, D., FISHER, R., CARDELLINA, J., SHOEMAKER, R. H. & MELILLO, G. 2006a. Targeting the PAS-A domain of HIF-1 alpha for development of small molecule inhibitors of HIF-1. *Cell Cycle*, 5, 1847-1853.

PARK, E. J., KONG, D., FISHER, R., CARDELLINA, J., SHOEMAKER, R. H. & MELILLO, G. 2006b. Targeting the PAS-A domain of HIF-1alpha for development of small molecule inhibitors of HIF-1. *Cell Cycle*, 5, 1847-53.

PATEL, M. M., MALI, M. D. & PATEL, S. K. 2010. Bernthsen synthesis, antimicrobial activities and cytotoxicity of acridine derivatives. *Bioorg Med Chem Lett*, 20, 6324-6.

PAYEN, E., BETTAN, M., HENRI, A., TOMKIEWITCZ, E., HOUQUE, A., KUZNIAK, I., ZUBER, J., SCHERMAN, D. & BEUZARD, Y. 2001. Oxygen tension and a pharmacological switch in the regulation of transgene expression for gene therapy. *J Gene Med*, 3, 498-504.

PIRES, I. M., BENCOKOVA, Z., MILANI, M., FOLKES, L. K., LI, J. L., STRATFORD, M. R., HARRIS, A. L. & HAMMOND, E. M. 2010. Effects of acute versus chronic hypoxia on DNA damage responses and genomic instability. *Cancer Res*, 70, 925-35.

PORTER, J. R., GE, J., LEE, J., NORMANT, E. & WEST, K. 2009. Ansamycin inhibitors of Hsp90: nature's prototype for anti-chaperone therapy. *Curr Top Med Chem*, 9, 1386-418.

POWELL, W. H. & HAHN, M. E. 2002. Identification and functional characterization of hypoxia-inducible factor 2alpha from the estuarine teleost, *Fundulus heteroclitus*: interaction of HIF-2alpha with two ARNT2 splice variants. *J Exp Zool*, 294, 17-29.

RAPISARDA, A., URANCHIMEG, B., SCUDIERO, D. A., SELBY, M., SAUSVILLE, E. A., SHOEMAKER, R. H. & MELILLO, G. 2002. Identification of small molecule inhibitors of hypoxia-inducible factor 1 transcriptional activation pathway. *Cancer Res*, 62, 4316-24.

RATCLIFFE, P. J. 2007. HIF-1 and HIF-2: working alone or together in hypoxia? *J Clin Invest*, 117, 862-5.

RIDDLE, S. R., AHMAD, A., AHMAD, S., DEEB, S. S., MALKKI, M., SCHNEIDER, B. K., ALLEN, C. B. & WHITE, C. W. 2000. Hypoxia induces hexokinase II gene expression in human lung cell line A549. *Am J Physiol Lung Cell Mol Physiol*, 278, L407-16.

ROUWKEMA, J., RIVRON, N. C. & VAN BLITTERSWIJK, C. A. 2008. Vascularization in tissue engineering. *Trends Biotechnol*, 26, 434-41.

RYAN, H. E., LO, J. & JOHNSON, R. S. 1998. HIF-1 alpha is required for solid tumor formation and embryonic vascularization. *Embo Journal*, 17, 3005-3015.

SALERNO, S., DA SETTIMO, F., TALIANI, S., SIMORINI, F., LA MOTTA, C., FORNACIARI, G. & MARINI, A. M. 2010. Recent advances in the development of dual topoisomerase I and II inhibitors as anticancer drugs. *Curr Med Chem*, 17, 4270-90.

SCHWARTZ, D. L., BANKSON, J., BIDAUT, L., HE, Y., WILLIAMS, R., LEMOS, R., THITAI, A. K., OH, J., VOLGIN, A., SOGHOMONYAN, S., YEH, H. H., NISHII, R., MUKHOPADHAY, U., ALAUDDIN, M., MUSHKUDIANI, I., KUNO, N., KRISHNAN, S., BORNMAN, W., LAI, S. Y., POWIS, G., HAZLE, J. & GELOVANI, J. 2011. HIF-1-dependent stromal adaptation to ischemia mediates in vivo tumor radiation resistance. *Mol Cancer Res*, 9, 259-70.

SCHWARTZ, D. L., POWIS, G., THITAI-KUMAR, A., HE, Y., BANKSON, J., WILLIAMS, R., LEMOS, R., OH, J., VOLGIN, A., SOGHOMONYAN, S., NISHII, R., ALAUDDIN, M., MUKHOPADHAY, U., PENG, Z., BORNMANN, W. & GELOVANI, J. 2009. The selective hypoxia inducible factor-1 inhibitor PX-478 provides in vivo radiosensitization through tumor stromal effects. *Mol Cancer Ther*, 8, 947-58.

SEMENZA, G. L. 2001. Hypoxia-inducible factor 1: oxygen homeostasis and disease pathophysiology. *Trends Mol Med*, 7, 345-50.

SEMENZA, G. L. 2006. Development of novel therapeutic strategies that target HIF-1. *Expert Opin Ther Targets*, 10, 267-80.

SEMENZA, G. L. 2007a. Evaluation of HIF-1 inhibitors as anticancer agents. *Drug Discovery Today*, 12, 853-859.

SEMENZA, G. L. 2007b. Hypoxia-inducible factor 1 (HIF-1) pathway. *Sci STKE*, 2007, cm8.

SEMENZA, G. L., AGANI, F., BOOTH, G., FORSYTHE, J., IYER, N., JIANG, B. H., LEUNG, S., ROE, R., WIENER, C. & YU, A. 1997. Structural and functional analysis of hypoxia-inducible factor 1. *Kidney Int*, 51, 553-5.

- SEMENZA, G. L., NEJFELT, M. K., CHI, S. M. & ANTONARAKIS, S. E. 1991. Hypoxia-inducible nuclear factors bind to an enhancer element located 3' to the human erythropoietin gene. *Proc Natl Acad Sci U S A*, 88, 5680-4.
- SEMENZA, G. L., ROTH, P. H., FANG, H. M. & WANG, G. L. 1994. Transcriptional regulation of genes encoding glycolytic enzymes by hypoxia-inducible factor 1. *Journal of Biological Chemistry*, 269, 23757-63.
- SERGANOVA, I., DOUBROVIN, M., VIDER, J., PONOMAREV, V., SOGHOMONYAN, S., BERESTEN, T., AGEYEVA, L., SERGANOV, A., CAI, S., BALATONI, J., BLASBERG, R. & GELOVANI, J. 2004. Molecular imaging of temporal dynamics and spatial heterogeneity of hypoxia-inducible factor-1 signal transduction activity in tumors in living mice. *Cancer Res*, 64, 6101-8.
- SERGANOVA, I., HUMM, J., LING, C. & BLASBERG, R. 2006. Tumor hypoxia imaging. *Clin Cancer Res*, 12, 5260-4.
- SONG, I.-S., WANG, A.-G., YOON, S. Y., KIM, J.-M., KIM, J. H., LEE, D.-S. & KIM, N.-S. 2009. Regulation of glucose metabolism-related genes and VEGF by HIF-1 $\alpha$  and HIF-1 $\beta$ , but not HIF-2 $\alpha$ , in gastric cancer. *Experimental and Molecular Medicine*, 41, 51.
- SONG, S., KWON, O. S. & CHUNG, Y. B. 2005. Pharmacokinetics and metabolism of acriflavine in rats following intravenous or intramuscular administration of AG60, a mixture of acriflavine and guanosine, a potential antitumour agent. *Xenobiotica*, 35, 755-73.
- STOLL, G., BASSE-LUSEBRINK, T., WEISE, G. & JAKOB, P. 2012. Visualization of inflammation using (19) F-magnetic resonance imaging and perfluorocarbons. *Wiley Interdiscip Rev Nanomed Nanobiotechnol*, 4, 438-47.
- SUMIYOSHI, Y., KAKEJI, Y., EGASHIRA, A., MIZOKAMI, K., ORITA, H. & MAEHARA, Y. 2006. Overexpression of hypoxia-inducible factor 1 alpha and p53 is a marker for an unfavorable prognosis in gastric cancer. *Clinical Cancer Research*, 12, 5112-5117.

SUN, X., NIU, G., CHAN, N., SHEN, B. & CHEN, X. 2011. Tumor hypoxia imaging. *Mol Imaging Biol*, 13, 399-410.

SUNG, H. J., MA, W., STAROST, M. F., LAGO, C. U., LIM, P. K., SACK, M. N., KANG, J. G., WANG, P. Y. & HWANG, P. M. 2011. Ambient oxygen promotes tumorigenesis. *PLoS One*, 6, e19785.

TACCHINI, L., DANSI, P., MATTEUCCI, E. & DESIDERIO, M. A. 2001. Hepatocyte growth factor signalling stimulates hypoxia inducible factor-1 (HIF-1) activity in HepG2 hepatoma cells. *Carcinogenesis*, 22, 1363-71.

TAN, C., DE NORONHA, R. G., ROECKER, A. J., PYRZYNSKA, B., KHWAJA, F., ZHANG, Z., ZHANG, H., TENG, Q., NICHOLSON, A. C., GIANNAKAKOU, P., ZHOU, W., OLSON, J. J., PEREIRA, M. M., NICOLAOU, K. C. & VAN MEIR, E. G. 2005. Identification of a novel small-molecule inhibitor of the hypoxia-inducible factor 1 pathway. *Cancer Res*, 65, 605-12.

TATUM, J. L., KELLOFF, G. J., GILLIES, R. J., ARBEIT, J. M., BROWN, J. M., CHAO, K. S., CHAPMAN, J. D., ECKELMAN, W. C., FYLES, A. W., GIACCIA, A. J., HILL, R. P., KOCH, C. J., KRISHNA, M. C., KROHN, K. A., LEWIS, J. S., MASON, R. P., MELILLO, G., PADHANI, A. R., POWIS, G., RAJENDRAN, J. G., REBA, R., ROBINSON, S. P., SEMENZA, G. L., SWARTZ, H. M., VAUPEL, P., YANG, D., CROFT, B., HOFFMAN, J., LIU, G., STONE, H. & SULLIVAN, D. 2006. Hypoxia: importance in tumor biology, noninvasive measurement by imaging, and value of its measurement in the management of cancer therapy. *Int J Radiat Biol*, 82, 699-757.

THOMAS, G. V., TRAN, C., MELLINGHOFF, I. K., WELSBIE, D. S., CHAN, E., FUEGER, B., CZERNIN, J. & SAWYERS, C. L. 2006. Hypoxia-inducible factor determines sensitivity to inhibitors of mTOR in kidney cancer. *Nat Med*, 12, 122-7.

THOMLINSON, R. H. & GRAY, L. H. 1955. The histological structure of some human lung cancers and the possible implications for radiotherapy. *Br J Cancer*, 9, 539-49.

- VAN DYKE, M. M. & DERVAN, P. B. 1984. Echinomycin binding sites on DNA. *Science*, 225, 1122-7.
- VANDERKOOI, J. M., ERECINSKA, M. & SILVER, I. A. 1991. Oxygen in mammalian tissue: methods of measurement and affinities of various reactions. *Am J Physiol*, 260, C1131-50.
- VAUPEL, P. 2004. The role of hypoxia-induced factors in tumor progression. *Oncologist*, 9 Suppl 5, 10-7.
- VIVIANI, V. R., OEHLMEYER, T. L., ARNOLDI, F. G. & BROCHETTO-BRAGA, M. R. 2005. A new firefly luciferase with bimodal spectrum: identification of structural determinants of spectral pH-sensitivity in firefly luciferases. *Photochem Photobiol*, 81, 843-8.
- VOLM, M. & KOOMAGI, R. 2000. Hypoxia-inducible factor (HIF-1) and its relationship to apoptosis and proliferation in lung cancer. *Anticancer Res*, 20, 1527-33.
- WAINWRIGHT, M. 2000. Methylene blue derivatives--suitable photoantimicrobials for blood product disinfection? *Int J Antimicrob Agents*, 16, 381-94.
- WAINWRIGHT, M. 2001. Acridine - a neglected antibacterial chromophore. *Journal of Antimicrobial Chemotherapy*, 47, 1-13.
- WELSH, S. J. & POWIS, G. 2003. Hypoxia inducible factor as a cancer drug target. *Curr Cancer Drug Targets*, 3, 391-405.
- WOOD, S. M., WIESENER, M. S., YEATES, K. M., OKADA, N., PUGH, C. W., MAXWELL, P. H. & RATCLIFFE, P. J. 1998. Selection and analysis of a mutant cell line defective in the hypoxia-inducible factor-1 alpha-subunit (HIF-1alpha). Characterization of hif-1alpha-dependent and -independent hypoxia-inducible gene expression. *Journal of Biological Chemistry*, 273, 8360-8.
- XIA, Y., CHOI, H. K. & LEE, K. 2012. Recent advances in hypoxia-inducible factor (HIF)-1 inhibitors. *Eur J Med Chem*, 49, 24-40.



YEO, E. J., RYU, J. H., CHO, Y. S., CHUN, Y. S., HUANG, L. E., KIM, M. S. & PARK, J. W. 2006. Amphotericin B blunts erythropoietin response to hypoxia by reinforcing FIH-mediated repression of HIF-1. *Blood*, 107, 916-23.

YEWALKAR, N., DEORE, V., PADGAONKAR, A., MANOHAR, S., SAHU, B., KUMAR, P., JALOTA-BADHWAR, A., JOSHI, K. S., SHARMA, S. & KUMAR, S. 2010. Development of novel inhibitors targeting HIF-1 $\alpha$  towards anticancer drug discovery. *Bioorganic & Medicinal Chemistry Letters*, 20, 6426-6429.

YU, E. Z., LI, Y. Y., LIU, X. H., KAGAN, E. & MCCARRON, R. M. 2004. Antiapoptotic action of hypoxia-inducible factor-1 alpha in human endothelial cells. *Lab Invest*, 84, 553-61.

YUN, Z., MAECKER, H. L., JOHNSON, R. S. & GIACCIA, A. J. 2002. Inhibition of PPAR gamma 2 gene expression by the HIF-1-regulated gene DEC1/Stra13: a mechanism for regulation of adipogenesis by hypoxia. *Dev Cell*, 2, 331-41.

ZHANG, H., WONG, C. C., WEI, H., GILKES, D. M., KORANGATH, P., CHATURVEDI, P., SCHITO, L., CHEN, J., KRISHNAMACHARY, B., WINNARD, P. T., JR., RAMAN, V., ZHEN, L., MITZNER, W. A., SUKUMAR, S. & SEMENZA, G. L. 2012. HIF-1-dependent expression of angiopoietin-like 4 and L1CAM mediates vascular metastasis of hypoxic breast cancer cells to the lungs. *Oncogene*, 31, 1757-70.

ZHANG, Q., ZHANG, Z. F., RAO, J. Y., SATO, J. D., BROWN, J., MESSADI, D. V. & LE, A. D. 2004. Treatment with siRNA and antisense oligonucleotides targeted to HIF-1alpha induced apoptosis in human tongue squamous cell carcinomas. *Int J Cancer*, 111, 849-57.

ZHONG, H., DE MARZO, A. M., LAUGHNER, E., LIM, M., HILTON, D. A., ZAGZAG, D., BUECHLER, P., ISAACS, W. B., SEMENZA, G. L. & SIMONS, J. W. 1999. Overexpression of hypoxia-inducible factor 1 alpha in common human cancers and their metastases. *Cancer Research*, 59, 5830-5835.

ZIELLO, J. E., JOVIN, I. S. & HUANG, Y. 2007. Hypoxia-Inducible Factor (HIF)-1 regulatory pathway and its potential for therapeutic intervention in malignancy and ischemia. *Yale J Biol Med*, 80, 51-60.

ZOU, J., LI, P., LU, F., LIU, N., DAI, J., YE, J., QU, X., SUN, X., MA, D., PARK, J. & JI, C. 2013. Notch1 is required for hypoxia-induced proliferation, invasion and chemoresistance of T-cell acute lymphoblastic leukemia cells. *J Hematol Oncol*, 6, 3.

## Curriculum Vitae

**Yun-Chen Chiang, M.S., B.S.**

*Date of Birth:* Jun 12 1986

*Cell:* 1-281-536-6039

*Email:* [yunchen.chiang@gmail.com](mailto:yunchen.chiang@gmail.com)

### **EDUCATION AND EMPLOYMENT**

- Sep 2009 – Jul 2013     **Ph.D. and Graduate Research Assistant,**  
*Graduate School of Biomedical Sciences, University of Texas  
Health Science Center at Houston and University of Texas M.D.  
Anderson Cancer Center, Houston, U.S.A*
- Sep 2008 – Jun 2009     **M.S.,** *Institute of Biomedical Engineering, National Taiwan  
University, Taipei, Taiwan*
- May 2006 – Jun 2009     **Undergraduate Research Assistant,**  
*Functional and Micro-Magnetic Resonance Imaging Center,  
Institute of Biomedical Sciences, Academia Sinica, Taipei, Taiwan*
- Sep 2004 – Jun 2008     **B.S.,** *Department of Life Science, National Taiwan University,  
Taipei, Taiwan*

### **PEER-REVIEW PUBLICATIONS**

- [1] **Chiang YC**, Turkman N, Rabinovich B, Young D, Volgin A, Najjar AM, Gelovani J G., "Development of HIF-1 $\alpha$ /HIF-1 $\beta$  heterodimerization inhibitors using a novel bioluminescence reporter assay system for in vitro high throughput screening," Proceedings of the National Academy of Sciences. (Submitted)
- [2] Shih YY\*, **Chiang YC\***, Shyu BC, Jaw FS, Chen JC, Duong TQ and Chang C, "Endogenous opioid-dopamine neurotransmission underlie negative fMRI signals," [Exp Neurol](#). 2012 Apr; 234(2):382–388. (\* denotes equal contribution)
- [3] Shih YY, Chen CC, Shyu BC, Lin ZJ, **Chiang YC**, Jaw FS, Chen YY, and Chang C, "A new scenario for negative functional magnetic resonance imaging signals: endogenous neurotransmission," [J Neurosci](#) 2009 Mar;29(10):3036-44. **Highlighted in "This Week in The Journal" in the [J Neurosci](#), 2009 29(10):i and Research Highlight in the [Nat Rev Neurosci](#), 2009 10(5):316.**
- [4] Shih YY\*, **Chiang YC\***, Chen JC, Huang CH, Chen YY, Liu RS, Chang C, and Jaw FS, "Brain nociceptive imaging in rats using 18f-fluorodeoxyglucose small-animal positron emission tomography," [Neuroscience](#), 2008 Sep 9;155(4):1221-6. (\* denotes equal contribution)

- [5] Chen CM, Shih YY, Siow TY, **Chiang YC**, Chang C, and Jaw FS, "Antinociceptive Effect of Morphine in  $\alpha$ -chloralose and Isoflurane Anesthetized Rats Using BOLD fMRI," *Biomed. Eng. Appl. Basis Comm.*, vol. 20, pp. 39–46, 2008.1

## **CONFERENCE ABSTRACTS/PRESENTATIONS**

- [1] **Chiang YC**, Turkman N, Rabinovich B, Volgin A, Najjar AM and Gelovani J G, "A novel reporter system for bioluminescence imaging of HIF-1 $\alpha$ / $\beta$  heterodimerization : *in vitro* screening and *in vivo* evaluation of novel inhibitors," *the 1st Annual International Meeting of The Society of Molecular Imaging of Thailand: "From Preclinical Research to clinical Application" Co-Organized by WMIS, ESMI and FASMI, Bangkok, Thailand, 2012 (Oral and Young Scientists Award Candidate)*
- [2] **Chiang YC**, Rabinovich B, and Gelovani J G, "The development of histone methylation sensing reporter *in vitro* and *in vivo*," *the 1st Annual International Meeting of The Society of Molecular Imaging of Thailand: "From Preclinical Research to clinical Application" Co-Organized by WMIS, ESMI and FASMI, Bangkok, Thailand, 2012 (Young Scientists Award Winner)*
- [3] **Chiang YC**, Turkman N, Rabinovich B, Volgin A, Najjar AM and Gelovani J G, "Molecular Imaging of HIF1 $\alpha$ / $\beta$  heterodimerization *in vitro* and *in vivo*," *World Molecular Imaging Congress, San Diego, USA, 2011 (Oral)*
- [4] **Chiang YC**, Najjar AM, Rabinovich B, Volgin A and Gelovani J G, "High throughput screening system for HIF-1 inhibitors *in vitro* and *in vivo*," *World Molecular Imaging Congress, Kyoto, Japan, 2010 (Oral)*
- [5] Shih YY, Huang CH, **Chiang YC**, Chen CC, Chen YY, Jaw FS, Shyu BC, and Chang C, "Vasoconstriction in the caudate-putamen following nociceptive stimuli: role of dopamine D2 receptor," *World Molecular Imaging Congress, Nice, France, 2008*
- [6] **Chiang YC**, Shih YY, Shyu BC, Huang CH, Chen CC, Chen YY, Jaw FS, and Chang C, "Vasoconstriction in the caudate-putamen following nociceptive stimuli: role of opioid receptor," *World Molecular Imaging Congress, Nice, France, 2008*
- [7] Wong WC, Shih YY, **Chiang YC**, Huang CH, Chang C, and Jaw FS, "Quantitative mechanical stimulator for fMRI and microPET studies," *Proc. Intl. Soc. Mag. Reson. Med., Toronto, Canada, 2008*
- [8] **Chiang YC**, Ho CH, Wang HC, and Lo CF, "Proteomic analysis of differentially expressed proteins in *Litopenaeus Vannamei* hepatopancreas cells after white spot syndrome virus Infection," *Annual Conference of Taiwan Society of Biochemistry and Molecular Biology, 2007.*
- [9] Shih YY, **Chiang YC**, Chen JC, Chang C, Liu RS, and Jaw FS, "Imaging brain glucose metabolism of hindpaw tactile stimulation in rats," in *Joint Molecular Imaging Conference 2007, Rhode Island, USA, 2007.*

- [10] **Chiang YC**, Shih YY, Chen JC, Liu RS, and Jaw FS, "Expression of formalin-induced nociceptive responses and pain-inhibited mechanism in rat brain using FDG-microPET," in *Joint Molecular Imaging Conference 2007 Rhode Island, USA*, 2007.
- [11] Shih YY, **Chiang YC**, Chen JC, Chang C, and Jaw FS, "Brain nociceptive imaging in rats using FDG-micorPET," in *54th Annual Meeting of the Society of Nuclear Medicine, Washington DC, USA*, 2007.

### **HONORS & AWARDS**

- [1] **ACAP Student Poster Award**, *the Association of Chinese American Professionals, Houston, 2013*
- [2] **Young Scientists Awards Candidate and Winner**, *the 1st Annual International Meeting of The Society of Molecular Imaging of Thailand: "From Preclinical Research to clinical Application" Co-Organized by WMIS, ESMI and FASMI, Bangkok, Thailand, 2012*
- [3] **Student Travel Stipend Award**, *World Molecular Imaging Congress, San Diego, USA, 2011*
- [4] **Student Travel Award**, *Graduate School of Biomedical Sciences, University of Texas Health Science Center at Houston, 2011*
- [5] **Student Travel Award**, *Graduate School of Biomedical Sciences, University of Texas Health Science Center at Houston, 2010*
- [6] **Student Travel Stipend Award**, *World Molecular Imaging Congress, Nice, France, 2008*
- [7] **Suma Cum Laude, Honor Graduate in the Department of Life Science's**, *National Taiwan University, 2008*
- [8] **Student Stipend Award**, *Foundation for the Advancement of Outstanding Scholarship , 2007*
- [9] **The President's Award for Academic outstanding student** , *National Taiwan University, 2006*
- [10] **Ying Yun-Gun Memorial Fellowship for Academic Excellent Students**, *2006*
- [11] **Poster Creativity Award**, *Wu Chien-Shiung Educational Foundation, 2005*
- [12] **Osheroff' Award for outstanding scientific creativity**, *Wu Chien-Shiung Educational Foundation, 2004*

### **NEWS, REPORTS, & HIGHLIGHTS**

- [1] "A new scenario for negative functional magnetic resonance imaging signals:

endogenous neurotransmission", selected as Research Highlight in the **Nature Review Neuroscience**, 2009 10(5):316.

- [2] "Brain nociceptive imaging in rats using FDG-microPET", listed in the Highlights Lecture of *54th Annual Meeting of the Society of Nuclear Medicine*, Washington DC, USA, 2007